An Investigation on Micro Cutting Mechanics: Modelling, Simulations and Experimental Case Studies

A thesis submitted in partial fulfilment of the requirements of Brunel University for the degree of Doctor of Philosophy

by

Worapong Sawangsri

School of Engineering and Design, Brunel University

June 2014

Abstract

Micro cutting is becoming increasingly important since miniature and micro components/products have become more and more demanded in precision engineering applications and consumer goods in a daily life. Meanwhile, it has not been thoroughly investigated yet. Scientific understanding of the fundamentals in micro cutting mechanics and physics is vital for micro manufacturing of micro or miniature components and products. Consequently, the scientific investigation on micro cutting mechanics is critically needed, particularly on its key fundamental aspects on which a systematic approach and key enabling technologies are developed for micro manufacturing. Therefore, three key fundamental aspects of micro cutting mechanics have been identified for this PhD project and a comprehensive systematic research has been performed through both theoretical and experiment-based investigations.

The three aspects of micro cutting mechanics mainly include dynamic stiffness investigation, innovative micro cutting force modelling, and the study on micro cutting heat, temperature and their partitioned distribution. All experiment-based investigations are undertaken on a diamond turning machine test rig supported with a fast tool servo (FTS) using different reconfigured experimental setups. The finite element (FE)-based analysis is conducted to further support the in-depth analysis on the micro cutting phenomena especially the modelling and simulation of micro cutting force and temperature. Accordingly, both micro cutting force modelling and micro cutting temperature are investigated using modelling and simulation supported by well-designed experimental cutting trials and validations.

The investigation on dynamic stiffness in the micro cutting system is focused on its effects on the micro cutting process and its control strategies. The burrs formation and machining accuracy are explored in relation with control of the dynamic stiffness. Furthermore, the control algorithm for dynamic stiffness is

developed accordingly in order to minimise burrs formation and stabilize the micro cutting accuracy.

The micro cutting force modelling is performed based on specific cutting force, i.e. modelling the cutting force at the unit cutting length or area as coined as the amplitude aspect of the proposed cutting force modelling. The cutting force against a dynamically varied cutting time interval is proposed as the spatial aspect of the cutting force formulation. The amplitude aspect can provide the insight into the micro cutting phenomena particularly in relation with the chip formation and size-effects. The spatial aspect, using a on the wavelet transform (WT) technique and standard deviation analysis can render the dynamic behaviour of the micro cutting force, particularly representing the dynamic effects of the cutting process and its correlation with tool wear.

The micro cutting temperature is investigated to formulate the scientific understanding of cutting temperature, heat and their partitioned distribution particularly at the tool-workpiece-chip interface zone in ultraprecision and micro cutting using a diamond cutting tool. The contribution to knowledge at this aspect is to represent the partitioned cutting heat in the micro cutting process and their different behaviours compared to the conventional metal cutting.

The scientific approach to modelling micro cutting application (MMCA), i.e. based on modelling-simulation combined with experimental validation, is further evaluated and validated to illustrate the overall benefits of this research investigation through micro cutting of single crystal silicon (for ultraprecision machining of large-sized infrared devices). This approach is established in light of combining all the three aspects of the above investigation on micro cutting mechanics. The research results show the approach can lead to industrial scale advantages for ultraprecision and micro cutting but driven by the scientific understanding of micro manufacturing technology. The systematic investigation on dynamic stiffness control, micro cutting force modelling, micro cutting heat and temperature and their integrated approach can contribute well to the future micro cutting applications.

Acknowledgements

First and foremost, I would like to express my gratitude to my supervisor, Professor Kai Cheng for his valuable recommendations, guidance, motivations, encourages and support throughout this research process.

I am grateful to the Faculty of Engineering, Kasetsart University in Thailand for my sponsorship support to my PhD study. The thanks are also extended to Brunel University for all the support for my PhD study.

The special thanks are due to my colleagues, Professor Feng Jiao, Dr. Chao Wang, Dr. Rasidi Ibrahim, Dr. Saiful Anwar Bin Che Ghani, Dr Timothy Minton, Dr. Haitao Li, Dr. Jianfei Sun and Mr. Diego Amerio, for their valuable discussions in many regards on my research work. Special thanks are also to the Brunel technician staff, particularly Mr. Paul Yates for his always helpful assistance.

I am also thankful to my beloved family, my father who passed away but always inspiring me on my mind; my mother and sisters who encourage and always standby me throughout this research study.

Finally, with highly regard to God who is unconditional love forever. He is always my excellent supporter, who always loves, inspires, encourages, motivates, and strengthens me.

Table of Contents

Abbreviations

AR   Autoregressive

CMP   Chemo-mechanical polishing

CNC   Computer numerical control

CT   Cycle time

CWT   Continuous wavelet transform

DAQ   Data acquisition

dbN   Daubechies wavelets

DOC   Depth of cut

DWT   Discrete wavelet transform

FEM   Finite element method

FTP   Fast tool positioning

FTS   Fast tool servo

HTHP   High temperature high pressure

MD   Molecular dynamics

MEMS   Micro electro-mechanical systems

MMCA   Modelling of micro cutting application

MS   Multiscale simulation

PI   Proportional-integral

RMS   Root mean square

RMT   Reconfigurable machine tool

SCD   Single crystal diamond

SOM   Self-organising map

SPDT   Single point diamond turning

STFT   Short-Time Fourier Transform

TCM   Tool condition monitoring

WT   Wavelet transform

Nomenclature

A	Initial yield stress (MPa)
A_j	Approximation coefficient
a_p	Depth of cut (µm)
B	Hardening modulus (MPa)
C	Strain rate dependency coefficient
c	Specific heat (J/kg°C)
D	Damage evolution of material
D_j	Detail coefficient
$\mathrm{dT_D, dT_W, dT_C, dT_T}$	Ranges of temperature (°C) across material in diamond tool, workpiece, chip, and tool tip respectively
d_1	Initial failure strain
d_2	Exponential factor
d_3	Triaxiality factor
d_4	Strain rate factor
d_5	Temperature factor
E	Young's modulus (Gpa)
F	Cutting force (N)
F_{sfA}	Specific cutting force at the unit of specific cutting area (N/mm^2)
F_{sfL}	Specific cutting force at the unit of specific contact length (N/mm)
f	Feed rate (mm/min, mm/rev)

k_D, k_W, k_C, k_T Thermal conductivity (W/m°C) in diamond tool, workpiece, chip, and tool tip respectively

L cutting contact length (mm)

M_t, M_w Mesh sizes of tool and workpiece (µm)

m Thermal softening coefficient

n Work-hardening exponent

q_D, q_W, q_C, q_T Conductive heat transfer (W, J/s) in diamond tool, workpiece, chip, and tool tip respectively

$\dot{Q}_g$ Volumetric generation rate

R tool noise radius (mm)

S Raw signal

$\dot{s}$ Tangential velocity component at the chip–tool interface

T_0 Room temperature (K)

T_{melt} Melting temperature (K)

t nominal depth of cut (µm)

V Element volume

V_c Constant surface speed (m/min)

α Rake angles (°)

$\bar{\varepsilon}$ Equivalent plastic strain (mm/mm)

$\dot{\bar{\varepsilon}}$ Plastic strain rate (s^{-1})

$\dot{\bar{\varepsilon}}_0$ Reference strain rate (s^{-1})

$\dot{\bar{\epsilon}}_p$ Effective plastic strain rate

$\Delta \bar{\varepsilon}^{pl}$ Increment of equivalent plastic strain

$\bar{\varepsilon}_f^{pl}$	Strain at failure
μ	Friction coefficient between diamond tool and workpiece's surfaces
ρ	Material density (kg/m^3)
т	Friction stress (MPa)
υ	Poisson's ratio
$\bar{\sigma}$	Equivalent stress (MPa)

List of Figures

List of Tables

Chapter 1 Introduction

1.1 Research background and significances of the project

1.1.1 Research background

Currently, high-accuracy miniaturized components are increasingly in demand for various industries, such as aerospace, biomedical, electronics, environmental, communications and automotive. The miniature parts and micro-products are essential requirements since they are currently providing micro-systems that promise to enhance health care and quality of life. They also aid economic growth in such applications as optical devices, subminiature actuators and sensors, IT micro-components, digital cameras, mobile phones, micro-stents, medical and biomedical products as well as biotechnological or chemical processing equipment (Chae, et al., 2006; Luo, et al., 2005; Alting, et al., 2003). Consequently, the enhancing devices and equipment for various manufacturing industries such as micro-aspheric dies and moulds, precision ball screws, gears and bearings etc. have been significantly increasing in demand, as their size becomes smaller, the required accuracy becomes higher and surface quality becomes much better (Suzuki, et al., 2006).

Due to the essential requirements of these high demand micro-products and miniaturizations, the micro-cutting mechanisms substantially differ from those of conventional cutting. The keys to the scientific understanding of manufacturing systems and methods of producing miniature parts or micro-products are then essential requirements. Thus, the basics of micro-cutting mechanics and physics, which is one of the most challenging areas emerging in the last two decades, are critically needed. Numerous research works have investigated micro-cutting characteristics in particular, including size effects which can influence underlying cutting mechanics in terms of micro cutting force and specific cutting energy (Cheng & Huo, 2013), undeformed chip thickness, chip formation, machined surface generation/finish, tool wear mechanism, etc. They

are still not well understood, especially for some specific issues for which in-depth studies are still indeed required and have not yet been thoroughly investigated. The knowledge contributions in micro/nano-cutting physics and mechanics are still challenging and even some of the aforementioned mechanics have been explored and investigated by a numbers of researchers across the world. Especially, some new and currently interesting issues, which have never been investigated, critically need to be further explored. Thus, in order to develop better innovation in the key issues of manufacturing the current and future technologies of micro-products and miniaturizations, a scientific understanding of the fundamental theoretical micro-cutting mechanics and physics is then needed.

Figure 1.1 Micro-products and miniaturizations in various industries

This research mainly focuses on the basis of fundamentally theoretical investigations into micro-cutting physics and mechanics based on ultra-precision machining, in particular diamond turning. The investigations have been implemented by both modelling and simulation and experimental cutting validations. The micro cutting mechanics are investigated, especially including

dynamic stiffness and its effects on micro-cutting, micro-cutting force modelling and its useful applications, scientific interpretations, and micro-cutting temperature and heat partitioned distribution.

1.1.2 Definition and scope of micro cutting

Micro cutting is kinematically similar to conventional cutting, but fundamentally different from conventional cutting in many aspects. The meaning and scope of the micro cutting may have differences based on experiences and attitudes of people who are involved in micro machining. However, there are a number of features can be used to characterize and define the scope of micro cutting. For instance, the uncut chip thickness, dimensions and accuracy of micro parts or features, cutting tool geometry, underlying cutting mechanics, and application area (Cheng & Huo, 2013).

The uncut chip thickness is the material layer being removed during the cutting process. The current state-of-the-art suggests the uncut chip thickness is less than tens of microns which widely accepted by the micro machining community with regards to the dimensions and accuracy of micro parts or features, miniaturized parts and components may have dimensions ranging from 1-1,000 µm with at least two dimensions which fall into this range. Generally, micro cutting achieves form and dimensional absolute accuracy of better than a few microns or a relative accuracy in the order of 10^{-3}-10^{-5} and surface roughness (Ra) less than 100 nm, respectively.

Regarding the cutting tool geometry, the size and geometry of micro cutting tools determines the limit of size and accuracy of micro features. Even in micro peripheral turning there is no requirement on tool size, but micro turning tools have to be employed for micro-hole boring and face grooving of micro components with a high aspect ratio. Meanwhile, underlying cutting mechanics, scaling down the size of machine tools and cutting tools from conventional macro cutting to micro cutting scales is not simple, but it results in size effects on machining which in turn interacts with and affects cutting mechanics fundamentally.

1.1.3 Micro cutting mechanics, processes and toolings

Diamond turning is a process of mechanical machining of precision elements using lathes or derivative machine tools (e.g. turn-mills, rotary transfers) equipped with natural or synthetic diamond cutting tools. Most single point diamond turnings (SPDTs) are operated using computer numerical control (CNC) machine tools. This makes it user-friendly due to the CNC system also being used in the system operation of conventional machining. The use of diamonds in association with ultra-precision machines can generate precision patterns and precision surfaces on a micro or nano scale. The diamond turning machine is sophisticated equipment that produces the final surface, which typically does not need the traditional polishing operation after diamonding turning. However, surface quality produced by the best diamond turning does not yet match the best conventional polishing practice. Thus, the limits of diamond turning for both figure and surface finish accuracy have not yet been reached (Rhorer & Evans., 1995). These limitations are needed in developing both precision of machining systems and elements and a scientific understanding of micro-cutting physics and mechanics.

Due to the research being experiment-based, the implicated machine tools, equipment and enhancing devices are involved. These require high precision, accuracy, rigidity and repeatability. Important machines and devices have been used in this project, such as a single point diamond turning (SPDT) machine, single crystal diamond cutting tool, fast tool servo (FTS), optical microscope and thermo-imaging camera etc. More details of using machines and devices can be found in the chapters 2,3,4,5 and 6, and appendices.

In order to achieve high dimensional accuracy, precision, repeatability and surface integrity of the process outcomes and subsequent the micro products, the elements of machine system are so important parts to be concerned. They mainly include: air bearing spindles, linear drive motors, high accuracy linear encoder and rotary encoder systems, fast tool servo and slow slide servo etc., which have been developed in order to produce the best micro-parts and products.
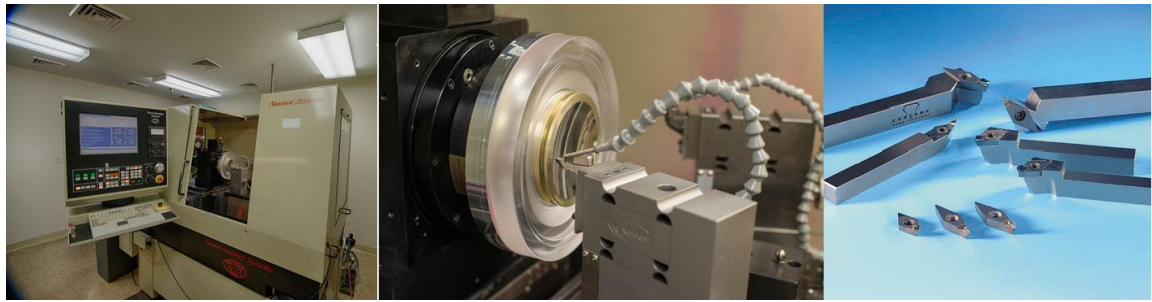
| (a) | (b) | (c) |

Figure 1.2 (a) ultra-precision machine, (b) single point diamond turning (SPDT), and (c) diamond tools (Empire Precision Plastics and Contour Fine Tooling Ltd)

The single crystal diamond with its edge sharpness has the ability to produce an almost optical finish in materials such as aluminium, copper and their alloys. It is often used in the final stages of the manufacturing process to achieve sub-nanometre level surface finishes and sub-micrometre form accuracies of machining dimensions (Davies, et al., 2003).

Some materials wear out the diamond turning tools at a much faster rate than other materials. The reason for this fast wear rate is yet unknown. For example, it is commonly known that ferrous materials rapidly wear out diamond tools while some others have a slower rate. Thus, the consideration of diamond-turnable materials is an essential concern due to the diamond tool being rapidly worn. The selected materials are then important and must not cause wear rates that are too fast by thermal, chemical and mechanical effects. A number of diamond-turnable materials are listed in Table 1.1, which are known by publications (Rhorer & Evans., 1995).

In this research, three different materials are selected to conduct the experimental studies and investigations; two of them are listed in Table 1.1, aluminium alloys and single crystal silicon. Meanwhile, the titanium alloys are not a diamond-turnable material. Silicon is also selected as the silicon based application case study of micro-cutting due to it being considered marginal as tool wear can be high. Even, reasonably large areas of amorphous silicon are

reported to have been successfully machined (Rhorer & Evans., 1995). Thus, the three differences cutting mechanics which have been selected as aforementioned in section 1.1.1 namely include dynamic stiffness, micro cutting force modelling and its applications, and micro cutting temperature and heat partitioned distribution. The investigations based on these three specific materials will be thoroughly investigated, analysed and compared.

Table 1.1 Diamond-turnable Materials

Aluminium	Calcium fluoride	Polymethymethacrylate
Brass	Magnesium fluoride	Polycarbonates
Copper	Cadmium telluride	Polyimide
Beryllium copper	Zinc selenide	
Bronze	Zinc sulphide	
Gold	Gallium arsenide	
Silver	Sodium chloride	
Lead	Calcium chloride	
Platinum	Germanium	
Tin	Strontium fluoride	
Zinc	Sodium fluoride	
Electroless nickel	KDP	
	KTP	
	Silicon	

1.1.4 Challenges in micro-cutting mechanics

Three specific issues have been introduced in the consideration of significant topics in this research project. Thus, the novel micro-cutting force modelling, micro-cutting temperature and heat partitioned distribution, and dynamic stiffness and its effects on burrs formation as well as machining accuracy have been analytically investigated. Finally, the fundamentally theoretical background of these three issues of micro-cutting is proposed, performed and evaluated by both modelling and simulation and experimental cutting validations.

Dynamic stiffness, the proportion of dynamic cutting forces against the dynamic displacements of cutting tools in the micro-cutting process is believed to show different characteristics from static stiffness. This could possibly affect machining accuracies in particular including the micro slot accuracy and the burr formation. Therefore, it is proposed to investigate how dynamic stiffness exists and affects the micro-cutting. Furthermore, the controllable method of dynamic stiffness is considered in order to find solutions for reducing and minimizing micro-form errors and burrs formation. Thus, the schematic algorithm of the hysteresis compensated module is proposed and applied as a technical tool for reducing and controlling the hysteresis effect of the fast tool servo (FTS) in the diamond turning machine. This compensation may help in the reduction of any errors of dynamic cutting tool movements during the cutting process. Case studies of micro-featured forms as well as micro-form accuracies and burrs measurements have been conducted. Also, the comparison between cutting with and without the hysteresis compensation module has been made.

The cutting force is used to represent the cutting process' behaviour and is directly relevant to cutting mechanisms such as surface generation, chip formation, cutting vibration, cutting temperatures and tool wear mechanism etc. However, the cutting force in micro-cutting is different from conventional cutting in both absolute and characteristic aspects. Thus, the micro-cutting force needs to be modelled correctly in order to gain a better understanding of the micro-cutting process behaviour. Also, it would be able to be used in micro-cutting applications, for example tool condition monitoring (TCM). The micro-cutting force modelling is then properly modelled which can better interpret the micro-cutting mechanics such as machined surface generation, chip formation, size effect and cutting temperature, throughout the effects on tool wear etc. In this thesis, the ability to interpret micro-cutting mechanics and physics by using this proposed novel approach is implemented. This innovative cutting force model is employed to cutting tool wear and breakage monitoring as an application case study. Also, this micro-cutting modelling can be further developed with smart cutting tools for smart ultra-precision and micro-machining of high value devices such as infrared optics and titanium-based medical devices (Wang, et al., 2014).

Since, thermal field and cutting temperature in metal machining are recognized as the major factors affecting the tool wear, tool life, machine quality, part dimensional accuracy and residual stresses (Yang, et al., 2011), the scientific understanding of cutting temperature and heat distribution is becoming essential in micro-cutting. In order to gain a better understanding of micro-cutting temperature and thermal effects, the cutting temperature and heat partitioned distribution into the tool-workpiece-chip in micro-cutting is studied in this research project. The micro-cutting temperature, and consequently thermal effects, should be different from those of conventional cutting since a very small depth of cut (DOC) is often taken on the micro-cutting scale. Thus, the micro-cutting temperature and heat partitioned distribution is investigated by both FE-based modelling and simulation with cutting trials as validation. Further discussion of thermal effects on surface integrity and quality, machining accuracy and tool wear is also presented.

1.2 Aim and objectives of the research

The aim of this research is to investigate the fundamentals of micro cutting mechanics and thus achieve scientific understandings of the in-depth micro-cutting physics. The distinct objectives of the research are:

1) To develop a modelling-simulation-experiment based approach to investigate micro cutting mechanics with applications to ultraprecision diamond turning in particular.

2) To investigate dynamic stiffness and its effects on machining accuracy, particularly including micro slot accuracy and micro-burrs formation. The schematic of a controllable method is further proposed to compensate for the characteristic movements of the cutting tool in order to avoid and minimize machining errors and burrs in micro-cutting.

3) To establish novel cutting force modelling using specific cutting forces, for example, the specific cutting force at the unit length or area, and against short-cutting time. This modelling approach would allow a better interpretation of the micro-cutting mechanics and physics, such as chip formation, size-effect and tool wear etc., phenomena in micro-cutting at

small amounts of absolute cutting force in particular. The novel approach is further applied in tool condition monitoring (TCM) as an application case study.

4) To further explore the scientific understandings of the tool-workpiece-chip temperature and heat partitioned distribution in micro-cutting. Further discussions of thermal effects on machined surface quality, machining accuracy and tool wear are also given.

1.3 Chapter plan of the thesis

The thesis consists of eight chapters. The comprehensive details of the thesis are illustrated as in Figure 1.3, which also illustrates the underlying philosophy of the chapters and their logic flow.
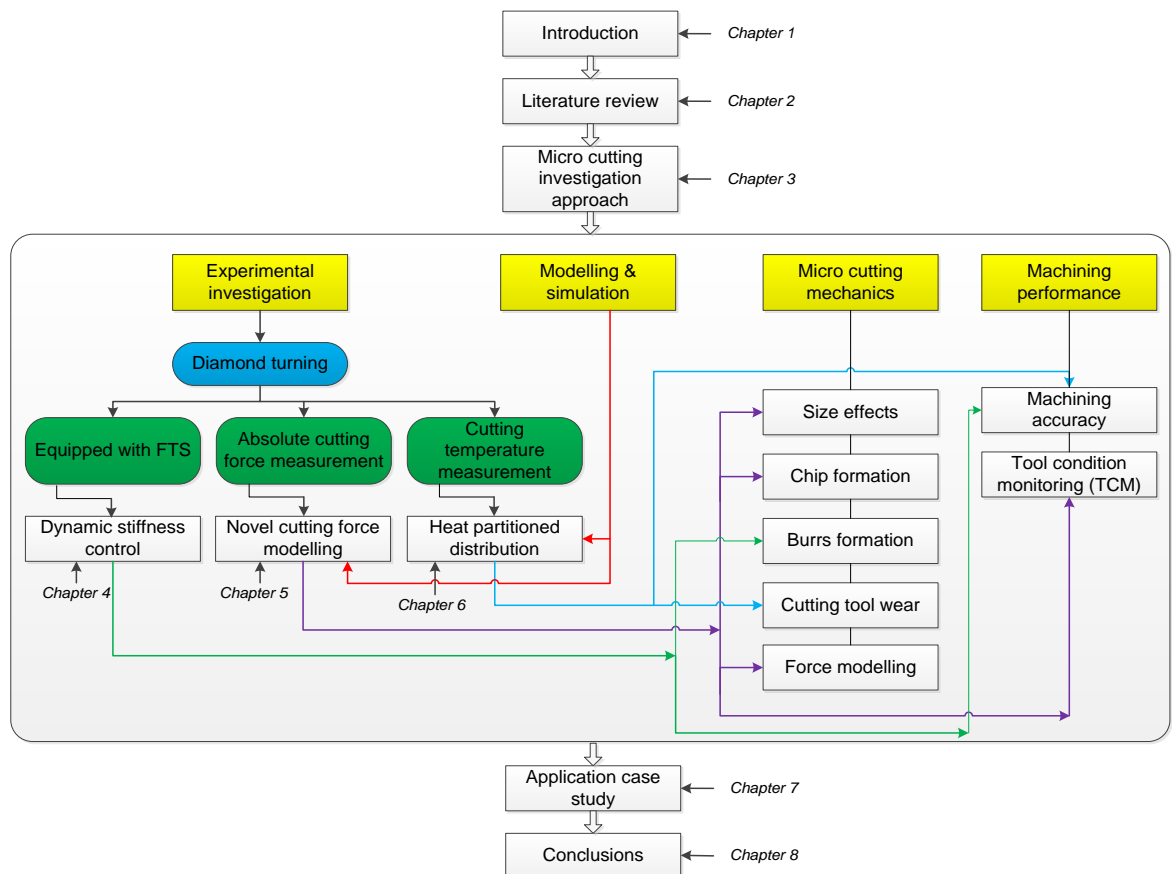
Figure 1.3 Chapter plan of the thesis

Chapter 1 introduces the research background and importance of the research including micro-cutting mechanics and physics challenges, relevant machine tools and equipment, aims and objectives, and structure of the thesis.

Chapter 2 reviews state-of-the-art and relevant fundamental theoretical backgrounds of the micro-cutting mechanics and physics, and the ultra-precision turning machine and its components. Also, the modelling and FE-based simulation of micro/nano-cutting are reviewed. The knowledge gaps identified are also described.

Chapter 3 explains the formulation of the research approach to micro-cutting, in particular the experimental setups and procedures, and technological and theoretical analysis. The modelling and simulation method is also elucidated.

Chapter 4 investigates and identifies dynamic stiffness, particularly in ultra-precision diamond turning and its effects on the machining accuracy, especially including micro-forms accuracy and burrs formation. Also, it proposes the schematic algorithm of a hysteresis compensated module for maintaining the machining accuracies and minimizing the machining errors and burrs in micro-cutting.

Chapter 5 proposes the cutting force modelling using specific cutting force at the unit length and area. The novel modelling approach is presented in two aspects, namely amplitude and special aspects. This innovative modelling can better interpret the micro-cutting mechanics and physics especially on chip formation, size effect and cutting tool wear characteristics in micro-cutting. The spatial aspect correlation with detection of tool wear is also analysed as an application study.

Chapter 6 analyses the partitioned distribution of cutting heat and temperature into the tool, workpiece, and chip of micro-cutting. The modelling and FE-based simulation of tool-workpiece-chip temperature has been developed. The experimental validations are also implemented and verified. The discussions on

comparisons between simulation and experimental results, and also thermal effects in micro-cutting are further given.

Chapter 7 emphasizes a case study applied to micro-cutting of single crystal silicon. The three interests of cutting, mechanics and physics of single crystal silicon, and its inherent natures, are further analysed and discussed.

Chapter 8 draws conclusions arising from this research investigation. Further recommendations for future work are also provided.

Chapter 2 Literature Review

2.1 Introduction

Micro cutting mechanics and physics play an important role in helping micro product designers and manufacturers understand well the intrinsic nature of micro machining which are crucial basis of theoretical fabrications of miniature parts and components, and micro products. Due to the fact that they are quite different cutting scales from those aspects of conventional cutting, and consequent scientific theoretical backgrounds and methodologies of cutting behaviors. Thus, the scientific understandings of micro cutting mechanics and physics are highly necessary since the micro products tend to be dramatically increasing in demand in widespread industrial sections. This chapter, the thorough backgrounds and literatures of micro cutting mechanics are reviewed firstly. The introduction of ultra-precision machines especially in single point diamond turning (SPDT) is reviewed. The following topics; diamond cutting tools and fast tool servo (FTS) are also introduced. The modelling and simulation techniques and procedures are given in brief. Finally, the knowledge gap identifications of three special issues of currently unclear on scientific understandings of micro cutting mechanics and physics are discussed with regards to how these issues are significant in micro cutting and critical needed to study in this research.

2.2 Micro cutting mechanics

The characteristics and inherent phenomena of the micro cutting mechanics are quite different from those in conventional cutting (Chae, et al., 2006; Liu, et al., 2004). This part explores the cores of the cutting mechanics and physics by emphasising some of the significant issues presented by numerous studies. Thus, the currently scientific understandings of micro cutting such as micro cutting force modelling, undeformed chip thickness, ductile and brittle transition, size-effects, micro cutting temperature, etc., are discussed.

2.2.1 Micro cutting force and size-effect

The micro cutting force is very small when compared with conventional cutting. It is 1,000 times downscaled from the normal cutting force in conventional cutting. Its characteristics are consequently quite different from those of conventional cutting. For instance, the ploughing or rubbing force is dominant in the cutting process rather than shearing force. The ploughing force is always caused by a significant amount of frictional interaction due to the effective rake angle of the tool becoming negative (Manjunathaiah & Endres, 2000). Particularly, when the undeformed chip thickness is smaller than cutting edge radius i.e., magnitude of thrust force is greater than cutting force. The trend of cutting force is non-linearly increasing when smaller undeformed chip thickness is applied. However, the undeformed chip thickness becomes greater than the cutting edge radius; magnitude of cutting force would be inversely larger than thrust force. Cutting and thrust forces are also linearly increased with the increase of the undeformed chip thickness for which the thrust force increases at a much slower rate than the cutting force. In summary, the trend of cutting and thrust forces are quite similar to those of conventional cutting when undeformed chip thickness is much greater than cutting edge radius (Ikawa, et al., 1991; Lucca, et al., 1993; Ng, et al., 2006). Meanwhile, it is quite a different characteristic when undeformed chip thickness becomes smaller than the cutting edge radius.

Regarding the size effect, the size effect results from the small ratio of undeformed chip thickness to tool edge radius, consequently the material removal and chip formation mechanisms are dominated. The corresponding cutting, ploughing, and slipping phenomenon depend on this ratio. Thus, the cutting process is influenced, for instance its effects on the decreasing quality of surface finish and surface integrity. This is due to the fact that scales of machining, such as depth of cut or undeformed chip thickness is comparable to the cutting tool edge radius, i.e. the depth of cut is the same order of edge radius, then the effective rake angle may become highly negative. Thus, non-linearly thrust force is increasing and dominating the cutting process (Cheng & Huo, 2013; Dornfeld, et al., 2006). In other words, the size effect can be

characterised by non-linear increases in the specific cutting energy, i.e. energy per unit volume when undeformed chip thickness is decreasing. This effect especially occurs at the micro cutting level (Liu & Melkote, 2007). Due to a small change in the depth of cut which can significantly influence the cutting process. Thus, numerous studies have been investigating what amounts of the ratio are, and what the corresponding to the size effect, e.g., specific cutting energy and consequent surface roughness would be. The contribution to knowledge of the size effects still need to be explored to optimise between the cutting parameters and the tool parameters so that the best machined surfaces will be achieved.

2.2.2 Chip formation and minimum chip thickness

In micro cutting, chips may not be formed if undeformed chip thickness is smaller than a minimum chip thickness. The definition of minimum chip thickness is the smallest magnitude of uncut chip thickness which a chip can be stably formed. This concept has been studied in order to understand the minimum requirement of depth of cut to ensure proper cutting and avoid ploughing and the sliding of the cutting tool. Especially, an investigation of the minimum chip thickness is very important in order to achieve more accurate machining. In conventional cutting, there are no concerns about the tool edge radius effects because it is so small compared to the depth of cut of a few millimetres. In ultraprecision cutting, the effective negative rake angle is always applied due to the effects of edge radius (Chae, et al., 2006), and then just a portion of the tool edge is occupied. This can, significantly, cause ploughing and a poor surface, or sometimes burnishing and a shiny surface, depending on the depth of cut (Son, et al., 2005).The states of minimum chip thickness can be explained according to the scale of the undeformed chip thickness being considered. In Figure 2.1, the chip starts to be formed when undeformed chip thickness is approximately equivalent to the minimum chip thickness (figure 2.1(b)). In other words, the chip removed is smaller than the desired depth of cut because the cutting process is still dominated by elastic spring-back of machined material which depends on the elastic deformation property of each material (figure 2.1(b)). When the undeformed chip thickness increases until larger than the minimum chip thickness, the chip can be removed with a total

magnitude of the desired depth of cut (figure 2.1(c)). However, no chip can be formed when the undeformed chip thickness is smaller than the minimum chip thickness because of the tool edge radius effect (as shown in figure 2.1(a)). In addition, below the minimum depth of cut, no material removal will occur (Dornfeld, et al., 2006).
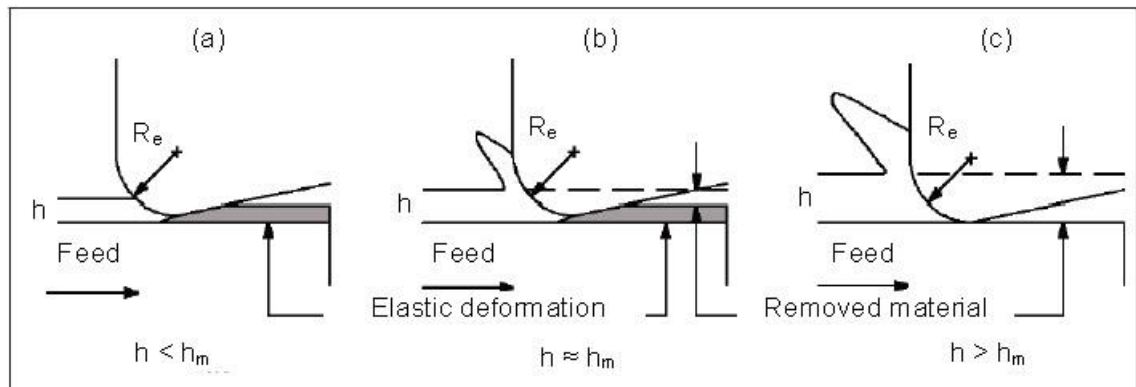
Figure 2.1 Characteristics of the minimum chip thickness: (a) no chip formed, (b) removed chip is smaller than desired DOC, (c) removed chip is equal to desired DOC (François, et al., 2009)

From a practical point of view, the minimum chip thickness is a measure of the extreme machining accuracy attainable because the machined surface roughness is mainly attributed to the ploughing/rubbing process when the uncut chip thickness is less than the minimum chip thickness. Due to this minimum chip thickness effect, the micro machining process is affected by two mechanisms. One is chip removal and the second is the ploughing/rubbing process. The extent of ploughing/rubbing and the nature of the micro-deformation during ploughing/rubbing contribute significantly to increased cutting forces, burr formation, and increased surface roughness. Thus, the scientific understanding of minimum chip thickness is essential for optimising and selecting appropriate machining conditions (Liu, et al., 2006).

2.2.3 Brittle-ductile transition

Generally, in conventional cutting, machining brittle materials at the high depth of cut (DOC) tends to cause excessive surface and subsurface cracking. To overcome this, machining in a ductile mode at a sufficiently small depth of cut

15

has been proposed by many researchers. For instance, Bifano et al (Bifano, et al., 1991) found that when machining brittle materials with a below critical depth of cut, brittle materials can be machined in a ductile regime with a consequently good surface finish and no surface pitting or cracking. Since the chip thickness in micro machining can be of the order of the critical depth of cut, micro machining can serve as a novel means of fabricating unique features in brittle materials. Thus, the definition of ductile mode cutting which can be achieved under certain chip formation conditions. It has been found that cutting brittle materials, such as tungsten carbide and silicon wafer, ductile mode chip formation can be achieved when the undeformed chip thickness is less than the tool cutting edge radius and tool cutting edge radius is small enough (Arefin, et al., 2007). This should meet the requirements of many fabrication industries of brittle materials which is widely used in parts or components of several micro products such as optical devices, electronic devices and radioactive equipment in nuclear plants, etc. Therefore, the investigation and study on the upper bound of cutting tool edge radius for ductile mode cutting is essentially needed for each material. Also it can help manufacturers to improve production rates while the surface finish remains of high quality.

2.2.4 Micro cutting temperature

The cutting temperature in micro cutting could be quite low in comparison with that in conventional cutting due to the small scales of cutting, and low cutting energy as well as the high thermal conductivity of both diamond and work materials such as aluminium and copper (Ikawa, et al., 1991). However, the micro cutting temperature cannot be neglected because a small temperature rise to the order of 10 K in a tool may cause an expansion of the tool shank and in turn, the deterioration of the machining accuracy. Also tool breakage and wear can be affected by small temperatures and even damaged in micro size. Moreover, there is considerable evidence in which temperature plays a significant role in chemical damage on diamond cutting tools. Thus, cutting temperature and generated heat in micromachining need to be understood and more research is needed urgently on the cutting temperature and its effect on diamond tool wear. Some pieces of research are concerned with the cutting

temperature, thermal effects on the micro cutting process and correspondingly the tool wear, quality of machined surfaces, and machining accuracy. For instance, Shimada et al (Shimada, et al., 1992) presented the possibility of the analysis of cutting temperature using molecular dynamics analysis to introduce a suitable scaling on the gradient in thermal fields which is caused by the thermal conductivity of the work materials. However, the micro cutting temperature and its partitioned heat distribution are quite a complicated system of characteristics and so many factors have influence. Thus, micro cutting temperature is still challenging to investigate at very small scales of machining (a few micrometres down to nanometres) especially based on real experimental case studies for instance, in particular ultraprecision and diamond turning.

2.2.5 Tool wear and burrs in micro cutting

Micro cutting tools used in ultra-precision machining generally have high hardness, for example diamond in micro turning. The high hardness plays an important role in reducing the wear rate, and enables machinability on hard and ceramic materials (Cheng & Huo, 2013). However, tool wear and breakage are factors of major concern especially when machining hard and difficult to cut materials due to size effects which cause the stress level in a tool edge to exceed the strength of diamond, oxidation, graphitization, diffusion, carbide formation, and material phase in-homogeneities and the slender geometry for the solid micro tools promote tool wear (Ikawa, et al., 1991), the cutting temperature is also a critical factor in influencing tool wear in micro cutting. Moreover, most workpiece materials do not fall into the class of ideal materials for micro manufacture and hence, unpredictable tool life and premature tool breakage before any degrees of severe cold occur. Therefore, a challenge for tool condition monitoring in micro machines is critically needed. Since micro machining is a knowledge-based application and needs proper selection of tooling, machine tools, cutting conditions and cutting strategies. The diamond tool wear especially in single point diamond turning (SPDT) and tool condition monitoring (TCM) have been studied by numerous researchers. For example, Bornet et al., (Born & Goodman, 2001) proposed the influence of significant cutting parameters on the tool wear by using experimental design techniques

relative to experimentation of diamond turning on large single-crystal silicon optics. They also presented a preliminary model that may be used to predict tool wear over the parameter space investigated. Brinksmeier et al (Brinksmeier, et al., 2006) presented a thermo-chemical process for modifying the chemical composition of the subsurface zone to avoid chemical reactions between the carbon of the diamond tool and the iron of the workpiece, and correspondingly excessive chemical tool wear when machined steel alloys. As a result, the diamond tool wear was reduced by more than three orders of magnitude. Schefferet al (Scheffer & Heyns, 2001) implemented a monitoring system utilising simultaneous vibration and strain measurements on the tool tip which investigated for wear of synthetic diamond tools, and wear measurements were taken in the manufacturing plant. Consequently the self-organising map (SOM) which is a type of neural network was developed to identify the tool state.

The burrs formation is one of significant issues in micro machining due to the burr being very difficult to remove and, more importantly, burr removal can seriously damage the workpiece. Also conventional de-burring operations cannot be easily applied to micro-burrs due to the small size of parts. In addition, de-burring may introduce dimensional errors and residual stresses in the component (Lee & Dornfeld, 2005). These problems are highly dependent on burr size and type, and are becoming more critical. Therefore, the prevention of burrs formation at the first state of machining, which is the best solution, is critical. Otherwise, if this is not possible, the minimising of burr formation is needed. In order to minimise burr formation, it is critical to understand the basic mechanisms involved in burr formation and the relationship between the cutting parameters and burr formation. A number of research works have been conducted into burr formation minimisation approach. For instance, Lee et al (Lee & Dornfeld, 2005) investigated the size and type of burr that is created in stainless steel 304 as a function of machining variables in order to help illuminate the micro-burr formation mechanisms. The relationship between micro-burr formation and tool wear was also investigated by implementing tungsten–carbide micro-mills to cut holes. Aramcharoen et al (Aramcharoen & Mativenga, 2009) also investigated the size effect in micro milling of H13

hardened tool steel which was observed by studying the effect of the ratio of undeformed chip thickness to the cutting edge radius on process performance. They found that how this ratio drives the specific cutting force, surface finish and burr formation in micro-scale machining. This ratio can lead to optimum micro-scale machining conditions for obtaining the best surface finish and minimising burr size. However, a few studies have been focusing on burr formation in diamond turning which is an important issue especially in miniature parts or components manufacturing and mass production is required. For instance, Nishiguchi (Nishiguchi, et al., 1988) examined the relationship between tool setting angle, i.e., the setup of angle in a plane of cutting edge and workpiece surface, cutting force and machined surface roughness of diamond turning on Al-Mg alloy, for the purpose of determining the reason for the deterioration of the machined surface roughness compared with the geometrical surface roughness. They found that burrs generated at the tool setting angle of less than -0.1° which caused the deterioration of the machined surface roughness.

2.3 Ultraprecision turning machines

The ultra-precision turning machine has been devolved and used over the last 50 years. The ultra-precision machine tool represents a special class of machines that perform at an extreme level of precision. The definition of ultra-high precision turning machines can be given as the ability of machines to generate or conduct the machined surfaces or the features, subsequently appropriate for performing optical functions and mechanical functions respectively. The ultimate surfaces and features from the ultra-precision machine require overall form errors in the order of 0.1 μm/100 mm. (in optical terms, about $\lambda/4$ or better) with surface finish less than 10 nm R_a. Typically, the ultra-precision machines with aerostatic spindles have error motions < 20 nm. Linear slides use oil hydrostatic bearings constructed with an overall geometry < 1μm/1m 10^{-6}or better). Linear measurement encoders have effective resolution < 0.1 nm over 1 m of travel. Spindles and linear slides use minimum influencing brushless DC motors. Control systems are based on DSP and gate array hardware tightly integrated with the measurement and actuator system.

These machines with a special class specification were originally developed to machine optical surfaces by single point diamond cutting tools (Luttrell, July 2010)

2.3.1 Diamond turning machine and its key components

Diamond turning machines are commonly used to manufacture rotational systematic parts of non-ferrous metal, polymers (especially PMMA) and brittle hard materials such as germanium, silicon and others. Furthermore, non-rotational workpieces are being manufactured on ultra-precision lathes using fast tool servo systems or slow-tool functionality as dynamic auxiliary axis in modern ultra-precision machines. The batch size of diamond turned workpieces varies from individual items to several thousand pieces per batch. Probably the most prominent application of high batches being diamond machined is varifocals. Fast tool machining enables the manufacturing of freeform parts for logically varying curvatures on the lens which allows toric lens design and correction of different visual defects of each individual customer (Cheng & Huo, 2013).

The main components defining the accuracy of a machine tool or ultra-precision machines are the materials used for the machine structure elements and the moving components, the used guidance systems, the drive systems for linear and rotary positioning, the measurement systems and, of great influence on the overall performance, the used control systems with the associated amplifiers.

2.3.1.1 Machine base and structure

Due to the characteristically low cutting forces and the aim of highest form accuracy and surface quality even over long machining times, the machine base material has to be thermally very stable. This feature is expressed in a low thermal expansion coefficient and a low specific heat capacity. To improve the surface quality, good damping properties of the base material are needed. These attitudes are best fulfilled using granite or mineral casting as material. Mostly granite is used in the field of ultraprecision machine beds because of its

very low thermal expansion coefficient of 6.5 μm/mK which is 2.5 times less than the one of mineral casting. Additionally, granite with a density of 2.8 kg/dm^3 is beneficial in terms of Eigen frequency and dynamic properties.

Figure 2.2 A current single point diamond turning machine with granite base and slides (Moore Nanotechnology Systems LLC)

2.3.1.2 Drive systems

Two designs of linear direct drives are commercially available; iron core and ironless drives. Different to the ironless motor the iron core motor uses a ferrous base in between the windings. The iron core motor only needs one counter side of magnets leading to a compact design. Ironless motors are built up with two counter facing rows of magnets.

Commonly for ultraprecision machines, ironless direct drives with three phases are used, due to their ability to ensure the highest positioning accuracy and extremely continuous motion which is commonly needed for diamond turning. Intensive investigation into direct drives in combination with air bearings proved possible steps of 10 nm and below depending on the control. In addition, the maximum possible acceleration for ironless motors is higher compared to the iron core ones.
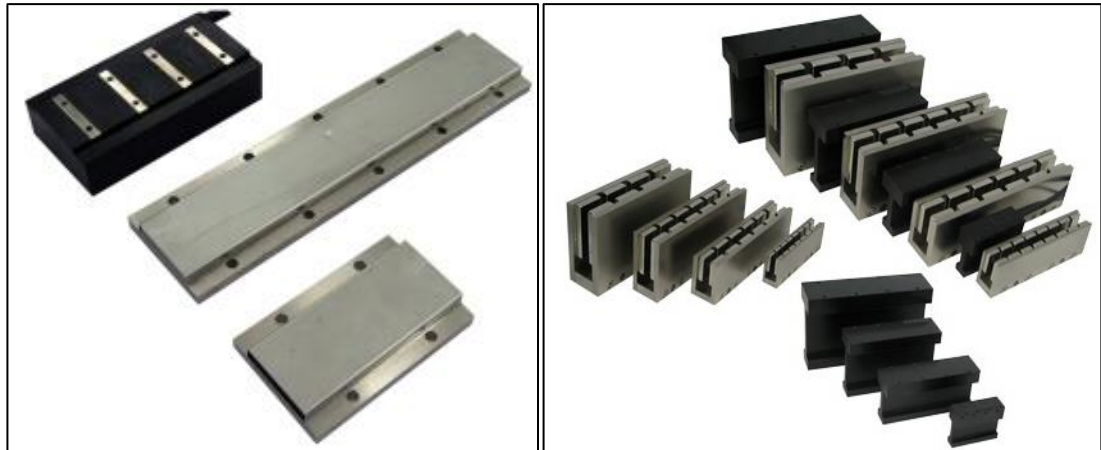
Figure 2.3 Iron core (left) and ironless (right) direct drive brushless linear motors (Motion Control Products Ltd)

Regarding diamond turning, ironless linear motors are state of the art in a machine axis to overcome the cogging-effect. Feedback resolution systems in UP lathes are unexceptional optical encoders and incremental scales. Well-established manufacturers of encoder systems are Haidenhain, Renishaw and Sony offering linear scales down to an optical resolution of 138 nm (Sony) and down to 0.034 nm interpolated resolution (Sony).

Figure 2.4 The high accuracy linear encoder and rotary encoder system (Renishaw plc)

Also due to the high circumferential speed, the spindles usually feature air bearing technology to reduce the heat development in the spindle at high rotational speeds. Nevertheless, high load capacities up to 102 kg (Precitech Heavy duty HD-160 spindle) and highest axial and radial motion accuracy below

12.5 nm (PI 5.5) can be achieved. The damping of the air bearing is again beneficial for the surface quality of the produced workpieces. To allow fast tool servo manufacturing and C-axis functionality, many spindles are equipped with high resolution feedback systems.
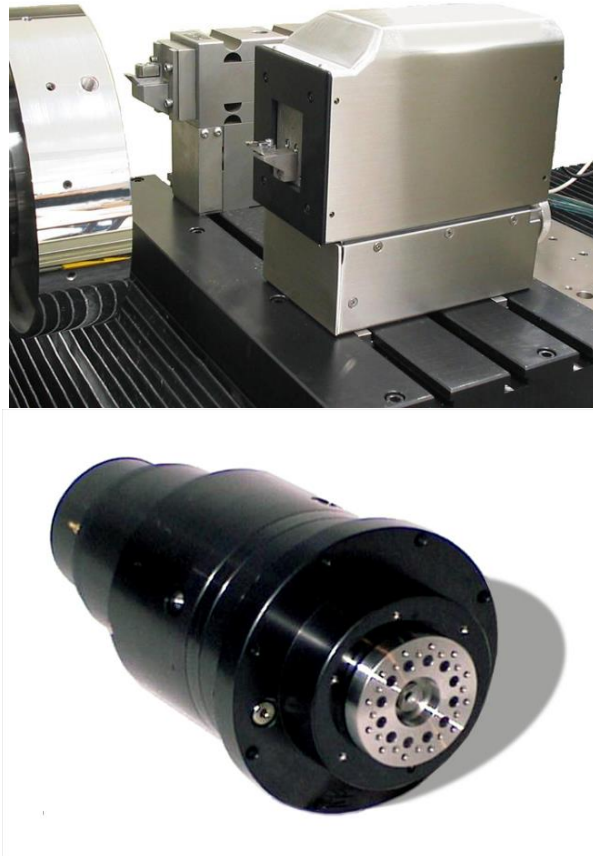
Figure 2.5 Nanotech Fast Tool Servo (NFTS-6000) and C-axis position control of work spindle (Moore Nanotechnology Systems, LLC)

For many ultraprecision machine tools the use of linear direct drives is state of the art. The theoretical stiffness of these drives is infinite, as long as the force is below its maximum force. In addition, In order to gain the necessary position accuracy, the influences of friction and backlash (which will reduce the position resolution), have to be minimised. As a thermal heat source a drive needs to be considered as a disturbing element for the temperature profile in a precision machine system. Such requirements often turn out to be counteracting when detailing a machine's design.

2.3.1.3 Guidance systems

Free of direct mechanical contact are fluid bearings and guideways based on aerostatics or hydrostatics. A thin film of air or oil separates the slide from the guideway and allows for linear or rotary motion in one degree of freedom. The gap for the fluid is in the range of 3 to 10 µm in aerostatic systems and between 7 to 20 µm in hydrostatic ones. In order to preload such a system and to introduce a sufficient stiffness, a wrap-around is needed, usually leading to a fairly large design compared to roller-based systems. Alternatively, magnets are used to preload aerostatic bearings and guideways. For hydrostatic guideways the preloading with largely dimensioned vacuum pockets is known.

Regarding the diamond turning, the equipment of ultra-precision lathes with mainly hydrostatic bearing systems in all linear slides gives straightness of below 0.1 µm/100 mm moving length. The hydrostatic bearings ensure stick-slip free movement for the smallest movements down to the single-digit range of nanometres. Additionally, high stiffness for minimised displacement in the bearing system combined with high damping ensures highest form and surface quality.

2.3.1.4 Control systems and amplifiers

Generally, for the CAD model of the part to be machined, a CAD/CAM system is used for tool path planning providing G-Code for the control system. Geometrically simple parts can be machined directly at the machine with manual G-Code programming or on machine software such as ShopMill (Siemens) or MillPlus (Heidenhain). Some machine control systems are capable of reading polynomial based paths (e.g. Spline, Nurbs), but in a second step they internally break down the polynomial description into discrete points for tool path, velocity and acceleration calculation (Cheng & Huo, 2013).

The density of the planned set points in G-Code is directly proportional to the deterministic accuracy of the part. Using a low density of points for the part's surface description, the machine control interpolates in between, the operator

has little to no influence on this interpolation and therefore cannot control the part's precision. Errors in the range of several microns can easily occur due to unsuited data preparation.

In diamond turning, to ensure the desired accuracy, a control system is needed which handles the high accuracies in short control cycles to guarantee accurate movement along the desired tool paths without interpolation errors and loss of set-point data. The most common control system PMAC is supplied by the manufacturer DeltaTau Data systems Inc. and is used for example in Moore and LT ultra-machines. Precitech machines use a PC-based control system by PDMIA running on QNX real time operating systems. Figure 2.6 illustrates the currently ultraprecision diamond turning machine which was developed with the latest "precision engineered" designs and components, including high stiffness hydrostatic oil bearing slideways, state-of-the-art linear motor drives with sinusoidal drive amplifiers, and an exclusive PI 5.5 10,000 rpm heavy-duty groove compensated air bearing work spindle with liquid cooling for long term thermal stability.

2.3.2 Experimental-based research studies and development of ultra-precision turning machines: the state of the art

There are a number of valuable research studies of experimental-based investigation on micro cutting mechanics and physics by using crystal single-point diamond cutting tool with the ultraprecision machine. For instance, Lu et al (Lu & Yoneyama, 1999) proposed the miniature manufacturing system and a new micro turning system are subjected to investigating the possibility of reduction of reacting forces to a sufficiently low level without deflection of the micro workpiece. Arefin et al (Arefin, et al., 2007) investigated and determined the upper bond of cutting tool edge radius for ductile mode cutting of a brittle material. Single crystalline silicon material has been cut with varieties of cutting tool edge radii in a set of experimentation. Son et al. (Son, et al., 2005) studied the relationship between the friction of a tool-workpiece interface and the minimum cutting thickness in micro cutting. They proposed an ultraprecision cutting model in which the tool edge radius and the friction coefficient are the

principal factors determining the minimum cutting thickness with a continuous chip. It was indicated that a smaller edge radius and a higher friction coefficient result in a smaller cutting depth. The experimental results were also conducted by ultraprecision diamond cutting to verify the proposed model and provide various supporting evidences. Also Lucca et al. (Lucca, et al., 1994) conducted an experimental study of the depth of the plastically deformed layer which results in the orthogonal ultraprecision machining of copper. The commercial diamond turning machine with the orthogonal fly cutting using a flat-nosed single crystal diamond tool was used in the experimental investigation.

Figure 2.6 'Nanotech 450UPL' - Ultra-Precision 2-Axis CNC Diamond Turning Lathe produced by Moore Nanotechnology Systems, LLC

The development of ultraprecision machining over the last decades has been reported by (Chapman, 2004 ; Riemer, 2011). Currently, some major advances in controls, feedback systems, servo drives, and general machine design and construction have evolved to the point where today's ultra-precision machining

systems are more productive, more precise, and lower in price. This adoption of new technologies was utilised in the development of single point diamond turning machines. When combined in a regimented manner, these allow surfaces to be single point diamond turned in many materials such as aluminium, copper, nickel, brass, also crystal materials, e.g. germanium, silicon, etc., to a surface texture often as low as 2 nm RMS.

These enabling machine features include:

- Epoxy granite or natural granite machine bases allow higher thermal and mechanical stability, damping characteristics, lower centre of mass, and design flexibility.

- Hydrostatic oil bearing box-way linear axes, for enhanced damping, smoothness of motion, geometrical accuracy, and wear free operation.

- DC linear motors provide rapid feed rates, smooth, wear-free, and non-influencing motion, and superb longitudinal dynamic stiffness.

- High-speed air bearing spindles allow faster feed rates, therefore reduced cycle times, as well as smooth rotational motion, high load capacity, and stiff aerostatic spindles.

- High-resolution linear scales with resolution of 1 nm and below replacing laser interferometers for nanometric axis position and improved geometrical accuracy.

- Environmental control by air-conditioning of machine housings and customised systems for enhanced vibration isolation.

- Grinding and polishing of diamond tools with well-defined geometry and sub-micron cutting edge waviness.

- High speed PC-based computer numerical controls allowing data exchange and large part programs.

- Advanced drive and feedback devices to improve work piece accuracy.

- Measurement and error compensation systems on machine work pieces to access residual work piece errors.

- Multi-axis machines, fast tool servo and slow slide servo turning for freeform machining.

- Dedicated software for free form machining.

The ultra-precision machine was originally developed based on the commercial applications, and market and industrial requirements. Also the growing markets of precision, optics and micro technologies and systems yield a high potential for engineering tasks in ultra-precision manufacturing. Thus, in the future, the new challenges in developing the ultra-precision machines will continue to be driven by market requirements. Advances in computing technology, and photonics, will likely yield further advances in control and feedback technology that will allow ultra-precision machining technologies to continue to advance in line with market requirements (Chapman, 2004).

2.4 Diamond cutting tools

Diamond is a suitable material for cutting tools due to its excellent mechanical, chemical, thermal and electrical properties. The advantages of diamond cutting tools are, they were used in most of the early micro machining research due to their ultra-high hardness for wear resistance and this enables machinability of hard and ceramic materials. Also ultra-small sharp cutting edge radius could be easily generated which enables smaller undeformed chip thickness to be programmed and hence ultraprecision machining. Diamond tools also have the ability to maintain an extremely sharp cutting edge owing to its mechanical and chemical properties.

Diamonds can be divided into single crystals and poly crystals. Single-crystal diamond (SCD) is the only tool material that can be used for ultraprecision machining, because an extremely sharp cutting edge can only be obtained on SCD. The estimated edge sharpness (cutting edge radius) is at the level of a few nanometres to a few tens of nanometres. According to the source of production, SCD can also be divided into two categories: natural diamond and composite diamond.

With regards to diamond cutting tools being manufactured, diamonds can originate from nature as mono-crystalline diamonds (Gäbler & Pleger, 2010). These mono-crystals can also be obtained from high temperature high pressure (HTHP) synthesis. The HTHP process enables the growing of bigger diamonds

which may be required for heavier cuts and thicker chip dimensions. In selecting diamond cutting tools for micro machining, a key requirement is to select the tool with the smallest edge radius and least edge waviness.

| (a) | (b) |
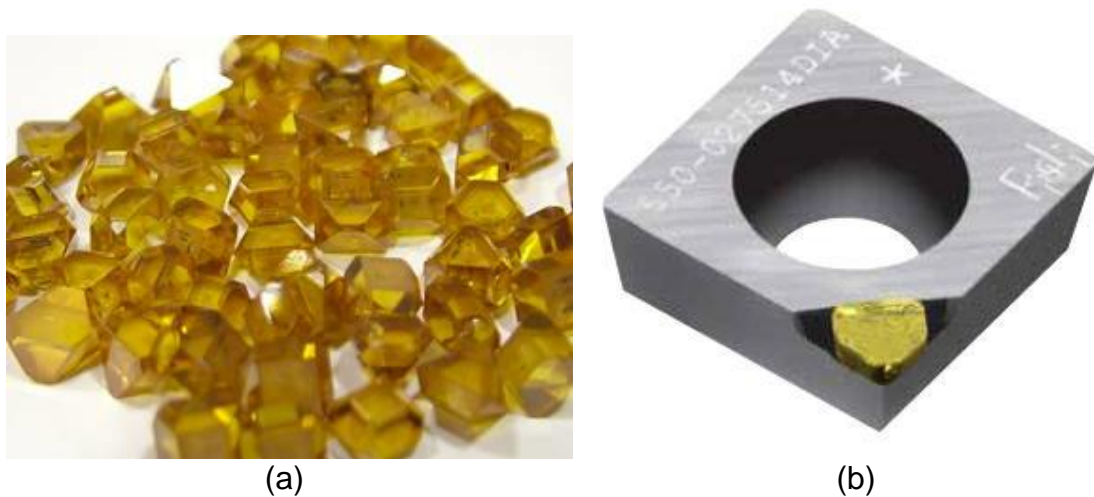
Figure 2.7 Mono-crystalline synthetic diamonds for requiring an ultra-high quality surface finish (© 2013 FiudiSrl): (a) manufactured in HTHP processing (BECKER Diamantwerkzeuge GmbH), (b) inserted with mono-crystalline natural diamond cutting edge

Recently, the composite diamond, i.e., the artificially made SCD, has been commercialised as the cutting tool material for the ultraprecision cutting process in place of the natural diamond (Cheng, 2009).

SCD tools have been used in industry for many years for producing optics and precision components by diamond turning or fly-cutting. Although the cutting edge radius of single point diamond tools can be sharpened down to 20 nm (Miyamoto, et al., 1990) and edge waviness can be controlled to 50 nm or so, the use of single point diamond tools for micro cutting is mainly for simple convex shape micro parts or micro structures, due to a diamond turning tool clearance angle which limits the generation of concave shapes with deep or steep cavities.

Figure 2.8 Single-point diamond tools for ultraprecision machining by Rudrali Hi Tech Tools Pvt. Ltd. (Rao, et al., 2014)

Due to hard and excellent properties of the tools are always required which helping tools can produce high precisions, productivities, and low rates of tool wear etc., particular in machining hard and brittle materials. Thus, diamond is a preferable material for machining of hard materials, materials with inclusions and difficult to cut materials, for glass machining or machining other cutting tool materials such as cemented carbides. Typical processes that use diamond tools are micro turning, milling and drilling as well as grinding (Cheng & Huo, 2013). However, the disadvantages of diamond tools is that they have a very high affinity to iron, micro cutting is mostly limited to the machining of nonferrous materials such as brass, aluminium, copper, and nickel, etc., (Cheng, 2009). Thus, machining hard materials e.g. single crystal silicon, titanium, and other brittle materials by diamond cutting tools have been currently challenging in ultraprecision machining.

Moreover, tool life and tool wear monitoring is one of crucial issues in developing cutting tool geometry. Although, the effective tool condition monitoring TCM systems have been developed by many researchers (Dornfeld, 1990; Chae, et al., 2006) in order to increase diamond cutting tool

performances, but it is still challenging due to diamond tool wear mechanism is quite complicated and difficult to characterise which differs from other cutting tools. Thus, the optimum diamond tool geometries associated with effective (TCM) systems remain in requirements.

The rapid wear rates of diamond tools in ultraprecision machining of brittle materials are another issue which have been widely concerned and challenged. Meanwhile, an excellent mirror-surface finishes of hard or brittle materials are highly required in diamond machining. Thus, diamond tool geometry associated with optimum machining conditions especially in ultraprecision and diamond machining has also been a critical issue in recent years.

Another disadvantage of diamond tools is high production costs due to the expensive laser structuring of the cutting edge and the attachment of the cutting edge element to the substrate material which is not simple in terms of process engineering (Gluche, et al., 2003).

2.5 Fast tool servos (FTS)

The fast tool servo (FTS) has been widely used in ultraprecision in particular machines, since it can be carried out with high accuracy, repeatability and machinability especially for free-form surfaces of miniature parts and micro products. Basically, the FTS associated with the diamond cutting tool is applied to the ultraprecision machines e.g., diamond turning. The fabrications of free-form surfaces and nonrotationally symmetric surfaces by diamond turning is essential required the high accuracy poisoning of cutting tool in the order of nanometre scales of errors, which can possibly be implemented by piezoelectric-driven fast tool servo. Thus, many attempts have been carried out to gain benefits of using the FTS with the highest performances in diamond turning. For instance, Noh et al (Noh, et al., 2009) presented the design, characteristic, evaluation and experiment of a fast tool positioning (FTP) unit driven by a voice coil actuator. Dow et al (Dow, et al., 1991) presented the development of a diamond turning machine with piezoelectric-driven fast tool servo in a laboratory-scale. The developed machine demonstrated the ability of

high-speed features machining such as sine wave, square wave, and ramp-shaped surfaces. In addition, they also implemented testing of this fast too servo on a commercial diamond turning machine. Wei et al (Sze-Wei, et al., 2007) designed and tested the optical performance of a fine tool servo system for global position error compensation which was installed on a miniature ultraprecision lathe. In order to achieve a closed-loop control system with proportional-integral (PI), analogue controller is implemented and tested in the set of experiments. Tian et al (Tian, et al., 2009) proposed the modelling and control of a flexure-based precision mechanism of piezoelectric actuator, which is adopted to improve the static and dynamic performance of the flexure-based mechanism, by focusing on the parallel flexure hinge is optimised to improve the positioning accuracy of the mechanism.

The piezoelectric actuator is a kind of short stroke actuator. It is very promising for applications in the rotary table drive and slideways drive because of its high motion accuracy and wide response bandwidth. Currently, piezoelectric actuators have been applied in the design of the fine tool-positioner in order to obtain a high precision motion of the cutting tool. The piezoelectric actuator combined with mechanical flexure hinges, the so-called fast tool servo (FTS) system, is used for positioning control of the diamond cutting tool. Thus, the FTS plays a significant role in ultraprecision machining especially for achieving of high accuracy, repeatability and machinability for fabrications of micro/nano products. More recently, the FTS system has been introduced for diamond turning components and products with structured, free-form surfaces and non-rationally symmetric surfaces such as laser mirrors, ophthalmic lenses moulds, etc. (Cheng, 2009).

The piezo-actuator based FTS system is designed to perform precision positioning of the tool during a short stroke turning operation and also hold diamond tools. Static deformation of the FTS structure caused by cutting forces during rough and finish machining, must be minimised to reduce the form and dimension error of the workpiece at nanometre scales. Therefore, high stiffness, particularly in the feed direction which affects the machined surface directly, is required. A high first natural frequency is then required in the FTS structure to

prevent resonance vibrations of FTS structure under domination of cutting forces.

On the other hand, the high stiffness of the FTS structure will reduce the effective stroke of the piezo actuator to some extent. For this reason a compromise is made between the high stiffness and actuator stroke reduction.
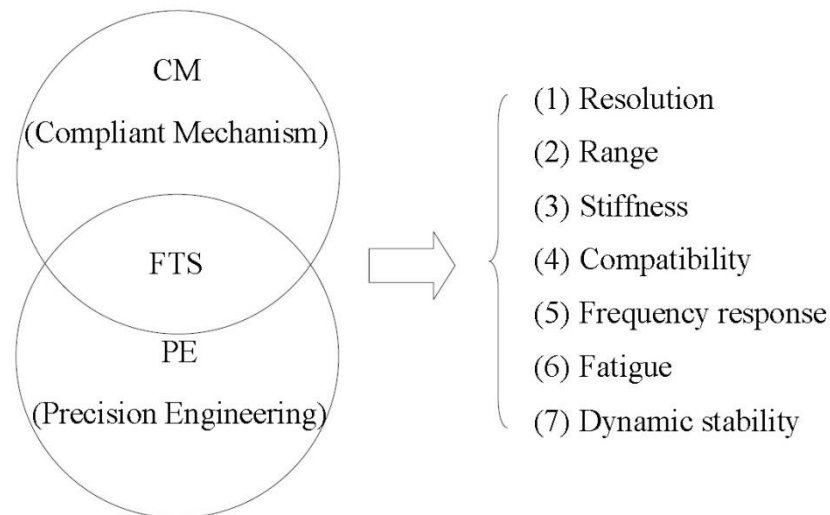
Figure 2.9 FTS being an interdisciplinary subject of CM and PE and its design requirements

A typical FTS consists of four major parts: compliant mechanism (CM) which holds a cutting tool, piezoelectric actuator, displacement sensor and control system. Moreover, design of the FTS should take into account for both compliant mechanism (CM) and precision engineering (PE); due to the FTS is the intersection of CM and PE as shown in Figure 2.9. Thus, based on the understanding of the FTS design, seven critical parameters or issues including resolution, range, stiffness, compatibility, frequency response, fatigue and dynamic stability respectively, should be concerned (Li, et al., 2011).
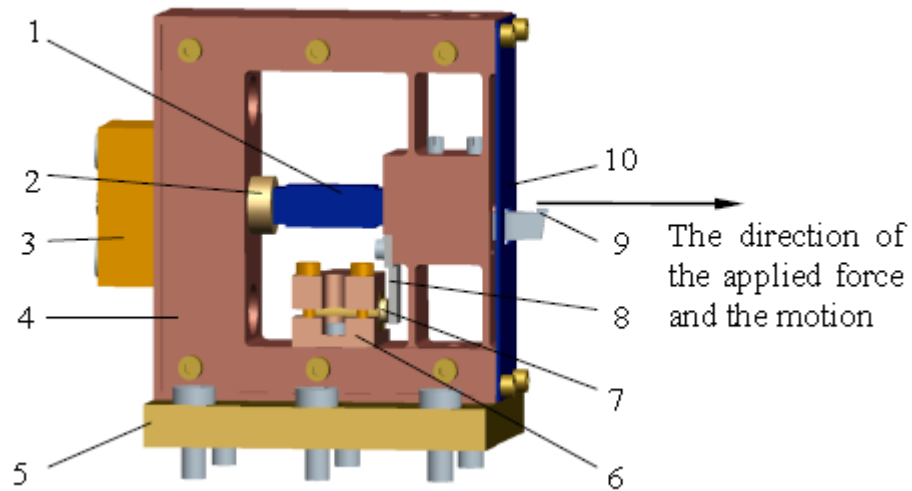
Figure 2.10 A schematic model of the FTS including the main parts: (1) the piezoelectric actuator, (2) the preload screw, (3) the lock screw base, (4) the CM structure, (5) the base, (6) the sensor holder, (7) the sensor, (8) the sensor plate, (9) the cutting tool, and (10) the front cover (Li, et al., 2011).

2.6 Modelling and simulations

Modelling and simulation techniques can illustrate the ability to simulate the micro cutting process behaviours virtually and more accurately. Typically, there have three diferrent methods and consequent objectives mainly included finite element (FE), molecular dynamics (MD), and multiscale simulation (MS) which have been currently used in implementing modelling and simulation of micro cutting (Cheng & Huo, 2013). Table 2.1 presents the comparasons of these three simulation techniques used in modelling and simulation of micro cutting.

Table 2.1 Developments and applications for various simulation techniques (Cheng & Huo, 2013)

Techniques	FE	MD	MS
Simulation scale	Big	Small	Medium
Basic unit	Node	Atom	Atom
Generated time (Approx.)	1940s	1950s	1990s
Basic priciple	Constitutive equation	Potential function and Newton's second law	-
General tools	ANSYS, Abaqus, Deform 3D	Lammps, GROMOS, MDynaMix	QC, MAAD, CADD, CGMD

2.6.1 Modelling and anlysis using finite element method (FEM)

Currently, the FEM is one of the most popular simulation techniques due to it being complementary to experimental approaches as it can overcome some of limitations, if done correctly. Also it can offer a reasonable insight into certain verifiable trends or guidance on empirical research to assist further understandings of the process. However, FEM has been a critical limitation for micro cutting due to it being based on principles of continuum mechanics. Hence, material properties are defined as bulk material properties whereas, in reality, the material behaves discontinuously in many cases of micro machining (Dornfeld, et al., 2006). In most cases of isotropic micro machining, FEM can be an attractive modelling method because the process can be reasonably treated in continuum space. FEM is, therefore, suitable for any materials modelling that are deformed in the ductile regime or the so-called plastic deformation materials. Thus, Johnson-Cook's constitutive material modelling is one of the best choices for numerous attempts to conduct the modelling and simulation of micro machining in particular (Liu, et al., 2006; Lai, et al., 2008; Liu & Melkote, 2005; Özel, 2006) is expressed as the flow stress which is a function of strain,

strain rate and temperature in terms of functional equation below (Liu & Melkote, 2007; Zong, et al., 2007; Zong, et al., 2006).

$$\overline{\sigma} = [A + B(\overline{\varepsilon})^n]\left[1 + C\ln\left(\frac{\dot{\overline{\varepsilon}}}{\dot{\overline{\varepsilon}}_0}\right)\right]\left[1 - \left(\frac{T-T_0}{T_{melt}-T_0}\right)^m\right] \qquad (2.1)$$

Where $\overline{\sigma}$ is the equivalent stress, $\overline{\varepsilon}$ is the equivalent plastic strain, $\dot{\overline{\varepsilon}}$ is the plastic strain rate, $\dot{\overline{\varepsilon}}_0$ is the reference strain rate (1.0 s^{-1}), T_0 is room temperature, T_{melt} is the melting temperature, *A* is the initial yield stress (MPa), *B* is the hardening modulus, *n* is the work-hardening exponent, *C* is the strain rate dependency coefficient (MPa), and *m* is the thermal softening coefficient.

The alternative main flow stress of constitutive models can be found in the comparative table as illustrated in Table 2.2 below

Table 2.2 Summary of main flow stress constitutive models (Wu, 2012)

Material model	Mathematical representations	Material constants
Tabular format	$\overline{\sigma} = \overline{\sigma}(\overline{\varepsilon}, \dot{\overline{\varepsilon}}, T)$	N/A
Oxley (Oxley, 1989)	$\overline{\sigma} = \sigma_1(\overline{\varepsilon})^n$	σ_1, n
Shirakashi and Usui (Shirakashi et al., 1970)	$\overline{\sigma} = A.(\overline{\varepsilon})^n.(\dot{\overline{\varepsilon}})^m[-\lambda(T - T_0)]$	A, m, n, λ
Johnson and Cook (Johnson et al., 1983)	$\overline{\sigma} = [A + B(\overline{\varepsilon})^n]\left[1 + C\ln\left(\frac{\dot{\overline{\varepsilon}}}{\dot{\overline{\varepsilon}}_0}\right)\right]\left[1 - \left(\frac{T - T_0}{T_{melt} - T_0}\right)^m\right]$	A, B, C, m, n
Zerilli and Armstrong (Zerilli et al., 1995)	$\overline{\sigma} = C_0 + C_1.\exp[-C_2 T + C_3 T\ln(\dot{\overline{\varepsilon}})] + C_4\overline{\varepsilon}^{1/2}.\exp[-C_5 T + C_6 T\ln(\dot{\overline{\varepsilon}})]$	$C_0, C_1, C_2, C_3, C_4, C_5$

2.6.2 Molecular dynamics (MD) modelling and analysis

MD simulation is a microscopic approach to analyse the behaviour of a solid model from an atomistic point of view which needs to be well-established for

structure and potential function as the input parameters. It can accommodate micro-material characteristics as well as dislocations, crack propagations, specific cutting energy, etc. It is generally reserved for nanometrical cuts because it requires large computing power and gives only a local representation of the material's behaviour (Shimada, et al., 1993). However, there are three major obstacles in MD modelling. The core part of MD requires good representation of interatomic forces among various combinations of atoms involved in cutting, referred to as a potential. Formulating a potential requires the equivalent of one good Ph.D. level study and thus very few potentials are available. Secondly, since MD calculates interatomic forces among all atoms within a certain boundary, intensive computational power is required. Therefore, many MD studies are limited to a very small space, such as at a nanometer or angstrom level. Thirdly, MD analysis lacks a good representation of continuum behaviour of material. Therefore, most MD simulations clearly state the boundary of application (Dornfeld, et al., 2006).

2.6.3 Multiscale (MS) modelling and analysis

From the aforementioned two modelling and simulation techniques of micromachining, they have their own limitations. If FEM analysis is suitable for continuum scales while MD analysis is better for atomic scales of simulation, Multi-scale modelling technique is emerging to combine both atomic and continuum scales together in order to fill the limited gaps of both techniques. The multi-scale modelling technique is aimed to bridge the length and timescales associated with relevant physical processes, also the ability to perform multi-scale characterisation of a material, i.e., to characterise the structure and its evolution with deformation on different scales (Mohamed, 2006). Thus, the physical parameters gained from micro-scale are conveyed to macro-scale through some equivalent methods, and macro-scale calculations supply some boundary conditions for micro-scale. This not only saves computational time but captures micro deformation mechanisms of objects accurately (Cheng & Huo, 2013).

2.7 Knowledge gaps identified

In this research, the issues that have been of interest and studied were selected in three separate topics. The first is the dynamic stiffness, particularly in single point diamond turning (SPDT) process. This topic focuses on how the dynamic stiffness affects the cutting process and machining accuracies especially in induced machining errors and burrs formation. Further discussions on finding results, its effects on the cutting process, and method of reducing or minimising the effects through experiment-based findings can be found in Chapter 4.The second topic is presented on the micro cutting force modelling instead of using the absolute micro cutting forces for better interpreting the micro cutting mechanics and physics. The modelling approach is introduced in two aspects including amplitude and spatial aspects. The amplitude aspect using specific cutting forces can be used in interpreting the micro cutting mechanics and physics. Meanwhile, the spatial aspect is dynamic analysis of cutting forces against a dynamically varied cutting time interval. The special aspect associated with wavelet transform technique and standard deviation analysis can verify the correlations with detection of diamond tool wear. The model formulation, methodology, the interpretation of the cutting mechanics, the correlation with tool wear detection, and further discussions on benefits of model approach can be found in Chapter 5. The last topic is the scientific understandings of the partitioned distribution of cutting heat and temperature in micro cutting. FE-based simulation on micro cutting temperature is carried out, associated with the experimental validation conducted in SPDT with the same cutting conditions. The analysis on heat partitioned distribution in micro cutting, and further discussions can be found in Chapter 6. In this section, the knowledge gaps identified for these topics are expressed as following described.

2.7.1 Dynamic stiffness in cutting process

The dynamic loads or dynamic cutting forces are always dominating in the realistic cutting process. The machine tool's structures are then dominated by the dynamic excitation loads with a specific amplitude and frequency. The machine tools are subjected to constantly changing deformation of structures.

The definition of dynamic stiffness, in terms of the excitation loads or dynamic cutting forces against the dynamic displacements which possibly affect the dynamic cutting process and consequently the machining accuracies, is attempted in this study. Due to the dynamic stiffness is believed that it exists and effects on burr formation and machining accuracy in micro cutting, a few studies have been done on dynamic stiffness investigation particularly in micro cutting. For instance, Yigit et al (Yigit & Ulsoy, 2002) proposed a systematic procedure to evaluate the dynamic stiffness characteristics of design alternatives for a reconfigurable machine tool (RMT). The results show that joint non-linearities of machine tools may affect dynamic stiffness considerably. Kim et al (Kim, et al., April. 9-11, 2008) presented a case study on dynamic characteristics analysis and dynamic stiffness evaluation of a 5-axis multi-tasking machine tool of ram-head type. The dynamic stiffness of the machine tool was analysed and measured by both finite element method (FEM) and a hydraulic exciter test respectively. The results show that theoretical analysis and exciter testing showed good agreement with each other. Andreas (Archenti, Thesis 2008) presented the model-based identification to evaluate machine tool and machining system stability because high static stiffness is required in order to reduce deformations in machining systems. Meantime, high dynamic stiffness is needed in order to minimise the self-excited and/or forced vibration. However, high static stiffness results often in a low damping system and therefore reduces dynamic stiffness. Thus, a trade-off between the static stiffness and dynamic stiffness needs to be optimised. However, these investigations have been made on the machines used in the macro-machining scales. Meanwhile, Zhou et al (Zhou & Cheng, 2009) established the dynamic cutting process system modelling and proposed the dynamic loop stiffness of the cutting process. The machined surface topography and the origins of surface error are analysed and validated by the preliminary cutting trials.

Currently, there have been no studies presenting clear evidence of relationships of the dynamic stiffness to burr formation and machining accuracies in particular in micro cutting. Thus, the dynamic stiffness is of interest and needs to be clearly investigated and defined, due to it being believed that dynamic stiffness

is influencing the micro cutting process rather than the static stiffness which has previously numerous investigations.

2.7.2 A novel cutting force modelling

Generally, the cutting forces have always been used to predict the cutting mechanism behaviours and cutting performances in particular instances of dynamic cyclic vibration, machined surface roughness, surface generation mechanism, chip formation, even cutting tool wear mechanism, etc. However, the absolute cutting forces in micro cutting are generally quite small down to 0.1-1N scale (Lee & Cheung, 2003) and consequently have totally different characteristics when compared with those of conventional cutting. Thus, this can cause inaccuracy and be difficult to analyse exact behaviours of cutting mechanisms by using absolute values. Thus, accurate and reliable cutting force modelling is needed instead of using absolute cutting force for predicting, analysing and better understanding of micro machining processes and systems. This micro cutting force model should differ from those of general models for macro cutting scales which have been used widely. In addition, the model should clearly depict the intrinsic nature of micro cutting force for better understanding and accurate interpretation of the characteristics of cutting mechanics and physics.

In recent years, a number of research studies have proposed many aims of cutting force modelling particularly in diamond turning. For instance, Lee et al (Lee, et al., 2002) presented the microplasticity model to predict the pattern of cyclic variation of cutting forces in diamond face turning. They used power spectrum analysis to extract the features of the cyclic cutting force patterns and find the relationship between the cyclic variation of cutting forces and the crystallographic orientation of the work materials being cut. Lo-A-Foe et al (Lo-A-Foe, et al., 1988) built up the force relationship model which was implemented numerically to estimate the surface roughness of SPDT with experimental validation. Chae et al (Chae, et al., 2006) investigated the dynamic component of micro cutting forces being mainly due to shearing forces, which is similar to conventional cutting force simulations when the depth of cut

is greater than tool edge radius. However, they summarised that the offset static component between the experiment and the predictions clearly indicated that ploughing forces in micro machining processes cannot be fully expressed by macro cutting models. Also the dynamic component dominated by the ploughing forces has not yet been proved. Kim et al (Kim & Kim, 1995) determined the two effects of micro cutting taking place under 1 µm (or less) depth of cut. One is the effective negative rake angle of the rounded edge of the tool. Another is the friction due to the elastic recovery of the workpiece at the clearance face. The investigation was implemented by analysing and comparing the cutting force per unit width (N/mm) of two orthogonal micro cutting models.

Most monitoring systems developed up to date employ force, acoustic emission and vibration. For example, Dornfeld et al (Dornfeld, 1990) developed a multi-layered perception type neural network for an on-line tool wear monitoring system. They combined the outputs of several sensors (acoustic emission, force and spindle motor current) for monitoring progressive tool wear in a single point turning operation, then conducted signal processing and feature selection for decision making algorithm. Also a new technique, the wavelet transform (WT) analysis has been recently used for tool wear monitoring. Fang (Fang, et al., 2012) proposed the wavelet packet transform helps in identifying the changes in the vibration signals in different frequency bands to detect the tool-edge wear in high-speed turning of Inconel 718. Wang et al (Wang, et al., 1998) also presented a new approach for process monitoring in reconfigurable machining systems based on WT. They proposed the sharp and worn tool can be presented in terms of different intensities of coefficients of the WT for each scale (frequency bandwidth). Despite Rehorn (Rehorn, et al., 2005) stating that the development of tool condition monitoring (TCM) systems have been widely researched in association with several important trends of methodology, few studies have been conducted on diamond tool wear monitoring. Even though a few research works, for instance works of Scheffer et al., (Scheffer & Heyns, 2001) have currently been conducted on diamond tool wear monitoring, it has always been used multiple-sensor approaches e.g., vibrational analysis and accelerometers sensing combined with a kind of neural network which often causes the system to be more complicated and not always user-friendly.

However, they suggested that the wavelet transform analysis feasibly helps in improving the ability of tool breakage detection by less specific training and so is required. In summary, a few studies have been proposed on tool condition monitoring (TCM) particularly in SPDT while it becomes more challenging due to mirror-surfaces of miniature parts and micro products being widely required. The WT analysis has also not been widely used or thoroughly investigated yet in tool wear monitoring systems. Thus, more simply, less sensoring techniques, and a user-friendly version of the TCM for diamond cutting tool is needed.

However, the interpretation of micro cutting mechanics and physics by using the proper micro cutting force modelling instead of general force models at macro scale have not been thoroughly investigated and presented yet. Thus, the modelling approach is represented in terms of the proper micro cutting force model, proposed particularly in two aspects namely amplitude and spatial aspects. The amplitude aspect using the specific cutting force at the unit cutting length and area is presented. This model formulation can better interpret the micro cutting mechanics and physics, particularly in chip formation mechanism and the size effects in micro cutting. The spatial aspect analyses the dynamic forces against a short cutting time interval. The spatial aspect is utilised in application of tool wear monitoring in SPDT by wavelet transform technique associated with standard deviation analysis.

2.7.3 Cutting temperature and heat partitioned distribution in micro cutting

Cutting temperature in micro cutting can play a significant role in influencing the machining performance particularly on the tool wear (Dan & Mathew, 1990), surface generation and integrity, and machining accuracy (Kim, et al., 2012). The heat occurring in micro cutting is a relatively small amount, it cannot be neglected because the temperature concentration is comparably high in the small cutting zone, area or volume. Many research studies are concerned with the cutting temperature's effects on the micro cutting process and correspondingly on the tool wear, quality of machined surfaces, and machining accuracy. For instance, Ikawa et al (Ikawa, et al., 1991) stated that even a small

increment of cutting temperature can cause an expansion of the tool shank and in turn, deterioration of the machining accuracy. Furthermore, it governs the wear rate of a diamond tool, which is fatal to the machined surface roughness. Kim et al (Kim, et al., 2012) proposed the quality of micro cutting features can be maintained by reducing the tool wear and cutting heat generation in the micro cutting process under various cutting lubrication conditions. Moriwaki et al (Moriwaki, et al., 1990) stated that the machining error by cutting heat is not negligible even in micro diamond cutting based on their experimental and theoretical analyses of the thermal deformation of the cutting tool and workpiece due to the cutting heat. Chen et al (Chen, et al., 2013) studied a set of micro cutting experiments carried out and measured the cutting temperature in the micro cutting process with a fast-response high accuracy thermocouple supported with FE modelling and simulation validation. They also claimed that the effect of heat generation needs to be addressed especially when high machining accuracy is required.

Therefore, the micro cutting temperature and heat partitioned distribution is one of the most critical issues of scientific understanding in micro cutting mechanics and physics. In micro cutting, cutting temperature and heat partitioned distribution of diamond tool-workpiece-chip interface and subsequently thermal effects in each component of micro cutting are still not well understood. Thus, a quantitative investigation on cutting temperature and heat partitioned distribution analysis in micro cutting is necessary to contribute to knowledge. The investigation is implemented through the experimental cutting supported with the FE-based model and simulation validation. The extensive discussion on the effects of cutting temperature on the tool wear, surface generation and machining accuracy are also given.

Chapter 3 Formulation of the research approach to micro cutting mechanics

3.1 Introduction

The research project aims to interpret micro cutting mechanics and physics based on experimental investigation. The scientific understandings focus in particular on three main issues comprising experimental investigations carried out on dynamic stiffness, micro cutting force modelling and micro cutting temperature. However, in order to be capable of better interpretation than just experimental investigation, modelling and simulation have also been conducted to investigate micro cutting force modelling and micro cutting temperature before the experimental implementations. Figure 3.1 illustrates the schematic of the research approach to micro cutting mechanics investigation.
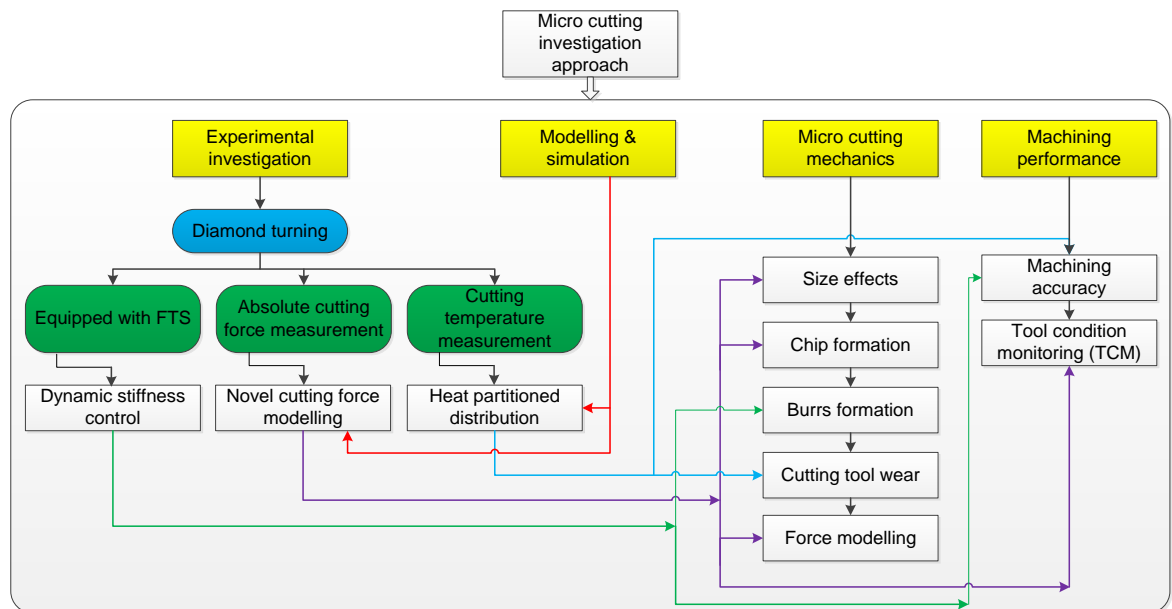
Figure 3.1 The schematic of the research approach to micro cutting mechanics investigation

Single point diamond turning (SPDT) has been carried out in the sets of experiments for all aspects of research approaches. Firstly, diamond turning with and without FTS identified and verified the dynamics stiffness and its effects as well as the controllable method of dynamic stiffness in micro cutting. The controllable method is expected to optimize and minimize unwanted effects, particularly in burr formation and machining accuracy, e.g., micro slot accuracies. Secondly, a novel cutting force modelling has been proposed in order to better interpret micro cutting mechanisms and for use in a tool wear monitoring application. This novel approach has been established based on the measurements of absolute cutting force during the cutting trials. The outcomes of the model are proposed as a method for scientific interpretation particularly of size effect, chip formation and tool wear mechanisms respectively. Finally, micro cutting heat and temperature have been measured and analysed based on cutting experiments. Analyses on the heat partitioned distribution into cutting tool/tool tip, workpiece and chip have been carried out. The thermal effects on machining accuracy, surface quality and tool wear are further analysed and discussed. Modelling and simulation validation of the cutting force modelling approach and micro cutting temperature are also conducted before experimental trials. The schematic procedures and details of these issues are explained. The technical and theoretical analyses are also described in this chapter.

3.2 Experimental set-ups and procedures

Experimental study is essential in this research because the micro cutting investigation requires substantial evidence. Thus, in order to thoroughly investigate the research approach as proposed, proper, reasonable, possible and simple experimental set-ups and methods for measuring results are needed. The experiments can be divided into three sub-topics as follows:

3.2.1 Dynamic stiffness investigation

Because of inherent hysteretic behaviour the piezoelectric actuator in the FTS system is never linear. In other words, the hysteresis between charging and

discharging voltage is never equal. Then, the cutting process always involves error distances of moving tools, i.e., the actual movements of the cutting tool are not the same as the desired movements. Thus, in order to control the actual movements of the cutting tool, the hysteresis compensation module is applied in the cutting experiments (Figure 3.2). The concept of the hysteresis compensation module is a controllable tool using FTS for reducing the hysteresis effects and controlling the tool movement characteristics. Thus, the cutting tool movements and consequent dynamics stiffness are then controlled. This is because the proportion of the dynamic cutting force to the corresponding dynamic displacements is reducing.

The experimental planning of dynamic stiffness investigation is based on comparison of 2 types of cutting, i.e., normal cutting and hysteresis compensated cutting. The hysteresis compensated cutting means machining with controllable tool, the so called hysteresis compensated module, in order for controlling the characteristic movements of the diamond tool during cutting process. Meanwhile, normal cutting means machining without this controllable tool, i.e., the hysteresis effects of the FTS would be involved in the cutting process. The cutting conditions were setup as similar to each other between both types of cutting to perform the three cases study of micro-featured forms. The planning of both cutting types started by setting the zero depth of cut with skimming the workpiece surface by face turning with a small depth of cut. The 3 case studies of micro-featured forms were then performed by cutting on three wafers of aluminium AA 6082-T6 with sizes of 50 mm diameter and 10 mm thickness. Finally, the comparison between normal and hysteresis compensated cutting were implemented in regards to burrs formation and slot accuracy. The schematic algorithm of investigation of dynamic stiffness is illustrated in Figure 3.2. It can be observed that both results of cutting with and without the hysteresis compensation module are compared and analysed. Thus, the main effects of the changing dynamic stiffness due to the changing proportion of cutting forces to dynamic displacements which resulted from the control of characteristic movements of cutting tool can be discussed in two aspects. One is the formation of burrs, and another aspect is the machining accuracy in micro cutting. The Details of the experimental procedures, cutting conditions, including

controllable method and tool, results, concluding remarks and discussions can be found in Chapter 4.
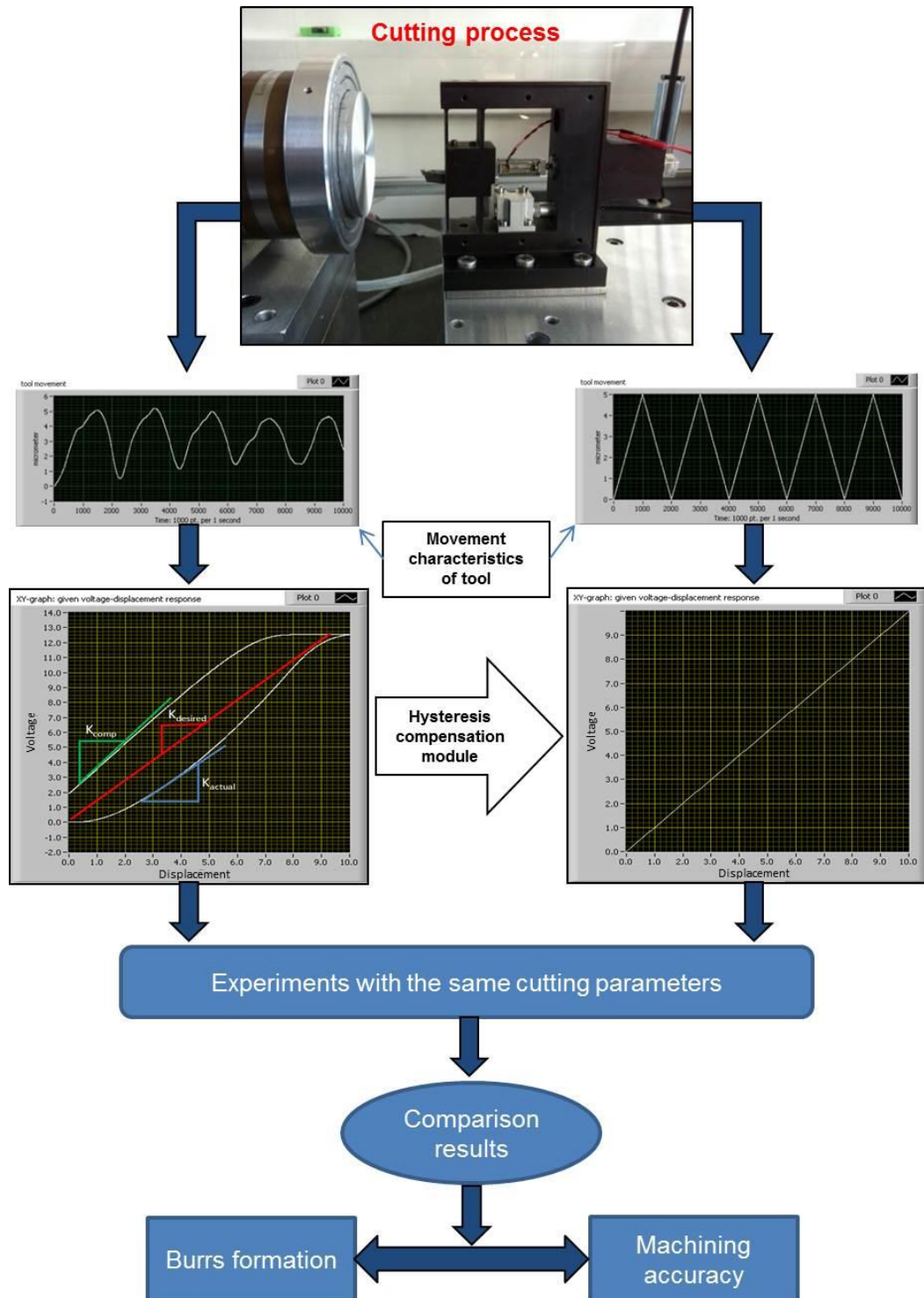
Figure 3.2 Schematic diagram of cutting experiments with and without the hysteresis compensation module for dynamic stiffness investigation

3.2.2 Micro cutting force modelling

The cutting experiments set-up for this novel approach is based on normal cutting with different type of materials, mainly including single-crystal silicon, titanium Ti-6Al-4V, and aluminium AA 6082-T6. A newly reground diamond cutting tool was used in the cutting experiments for all materials. In order to monitor the progress of wear on the cutting tool, each material was needed to cut six times repeatedly under the same cutting conditions.

The experimental planning for micro cutting force modelling investigation is explained. The three selected materials were pre-machined as a wafer with 10 mm thickness and 60 mm of diameter. The selected materials were machined by the same cutting behaviours which first times cutting with small depth of cut for skimming the workpiece surface and setting the zero depth of cut on this skim surface. The main cutting six times repeatedly by the same cutting conditions was performed. The cutting conditions in this experimental investigation are 10 µm depth of cut, 100 m/min constant surface speed, and 5 mm/min feed rate, respectively. The feed and cutting forces were recorded by Labview data acquisition through a DAQ card. The feed and cutting forces data of silicon cutting were selected in implementing the interpretation of the chip formation mechanism in micro cutting. Meanwhile, forces data of all selected materials were analysed the tool wear progress by wavelet transform technique associated with stand deviation analysis. The specific details can be found in Figure 3.3
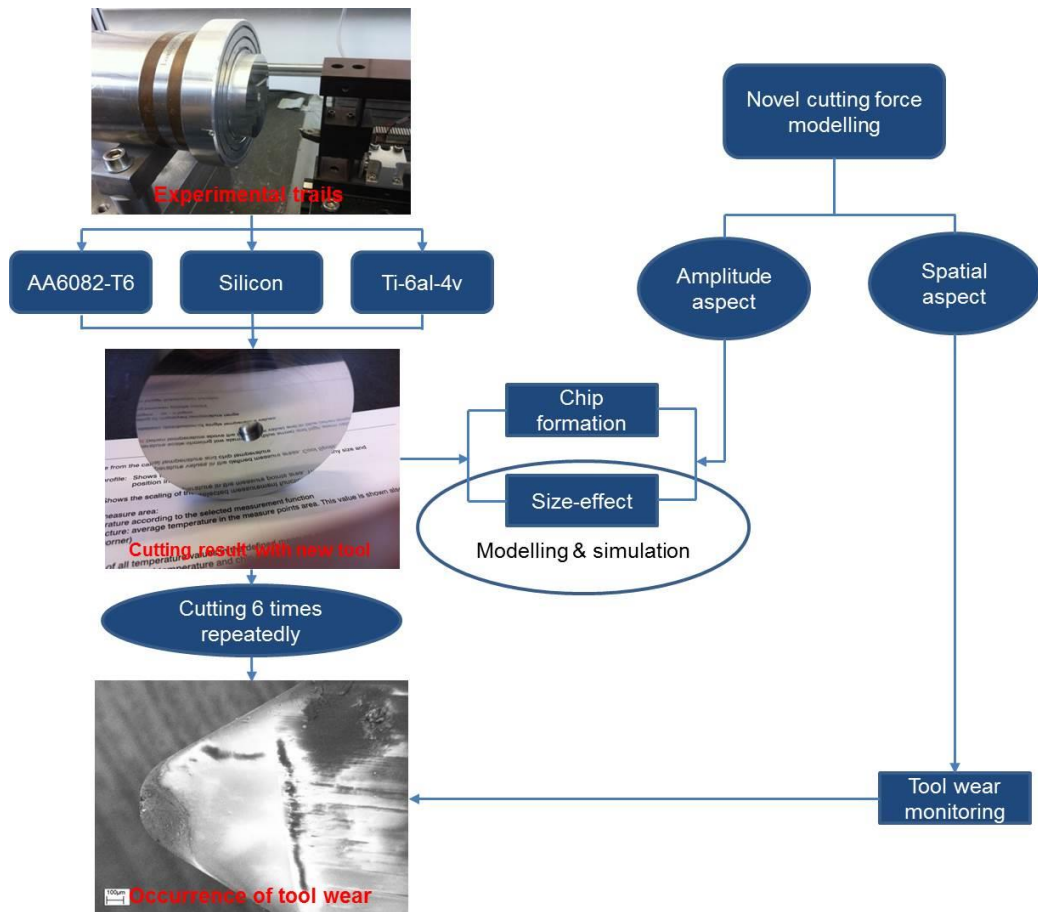
Figure 3.3 The schematic of the novel cutting force modelling approach

Figure 3.3 shows the schematic of the cutting force modelling approach which depicts the corresponding parallel to the cutting experiments. Also, it illustrates how it links to micro cutting mechanism interpretations and application for tool wear monitoring respectively. Modelling and simulation were also implemented to interpret the size effect in micro cutting, and validate the experiments which is a better method of investigating and providing explanations more satisfactory than by using cutting experiments only. The wavelet transform technique is adopted and introduced for tool condition monitoring (TCM) in the cutting force modeling application. The experimental details, results and further discussions are in Chapter 5.

3.2.3 Micro cutting heat and temperature investigation

Modelling and simulation of micro cutting temperature under specific cutting conditions were carried out for cutting aluminium AA6082-T6. Experimental

validations were also conducted under the same cutting conditions. The materials used in this experimental investigation include aluminium AA 6082-T6, titanium Ti-6Al-4V and single crystal silicon.

The experimental planning of micro cutting temperature and heat partitioned distribution investigation was similar to experiments of cutting force modelling approach in previous section. Again, the three selected materials were pre-machined as a wafer with 10 mm thickness and 60 mm of diameter respectively. The thermal imaging camera was installed in front of the cutting scenarios as shown in Figure 3.4. The zero depth of cut was set by face cutting a small depth of cut. Thus, the 3 times cutting repeatedly and continuously by the same cutting conditions were performed. The real time cutting temperature on four specific areas of cutting Ti-6Al-4V associated with three specific areas of cutting AA 6082-T6 and single crystal silicon were then collected by the thermal imaging camera through its specific software. The four specific areas are included the diamond tool, tool tip, workpiece and chip, respectively. However, cutting temperature on chip of aluminium and silicon cutting cannot be captured due to the limitation of the camera. The curve fitting of cutting temperature graphs were implemented in order to reduce the errors and variability from measurements and devices. Finally, the heat partitioned distribution of three selected materials was analysed. The cutting conditions in this experimental setup were used as equal to 10 µm depth of cut, 100 m/min constant surface speed, and 5 mm/min feed rate, respectively. The schematic procedures of micro cutting heat and temperature are depicted in Figure 3.4. The specific details and further discussions on the tool wear, surface generation and machining accuracy are also included in Chapter 6.
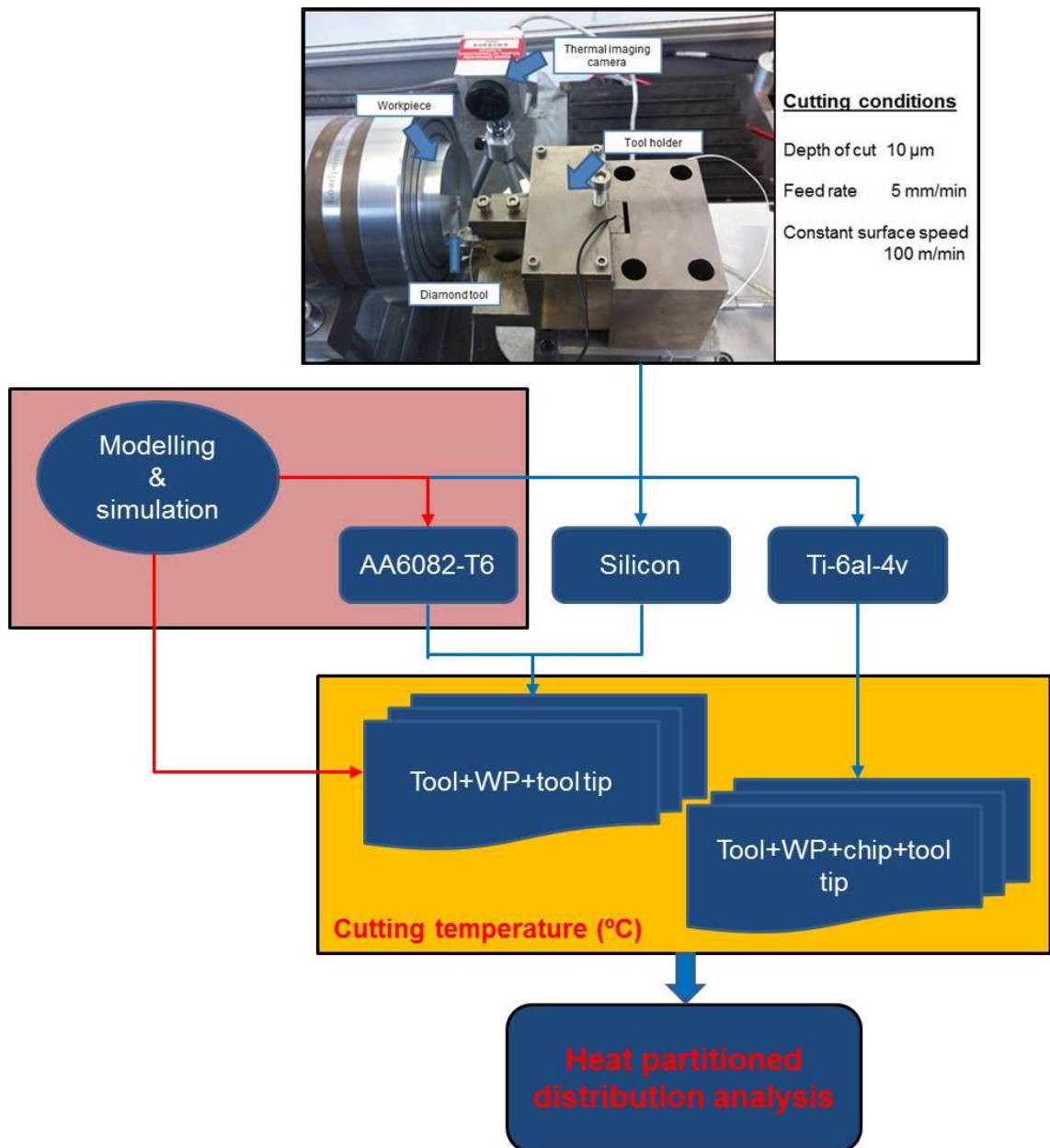
Figure 3.4 Schematic procedures of micro cutting heat and temperature investigation

3.3 Modelling and simulation method: finite element analysis (FEA) in micro cutting

The expected research outcomes of modelling and simulation are based on two main objects. One is the micro cutting force, and the other is the cutting temperature. Thus, the constitutive material modelling of aluminium AA6082-T6 and titanium Ti-6Al-4V are constructed. The chip separation criterion modelling and the differential equation of thermal conduction are applied as input

parameters to the models. The simulation results are consequently presented in two aspects, i.e., the micro cutting force and temperature. The cutting force outcomes are divided into two particular types, and include simulated force results from cutting with a normal rake angle (0º) and varied rake angles and chamfers. The simulation of cutting forces outcomes and its benefits can be found in Chapter 5. Meanwhile, the micro cutting temperature outcomes are subsequently analysed: the micro cutting temperature and heat partitioned distribution validations are detailed in Chapter 6.
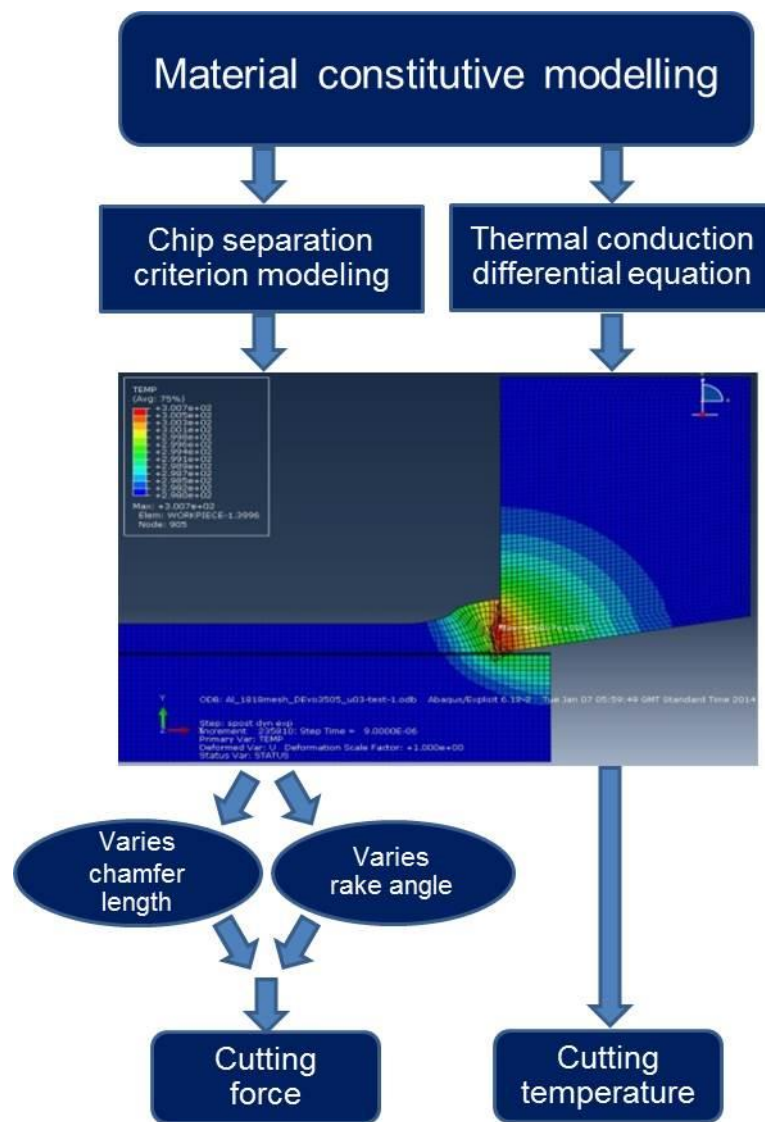
Figure 3.5 Modelling and simulation of micro cutting forces and temperature

The schematic structure of modelling and simulation of micro cutting forces and temperature is illustrated in Figure 3.5.

3.4 Theoretical and technical analysis on the research approach

Relevant methods are required in order to appropriately set out the research findings. Thus, techniques, equipment and theories are applied to analyse specific problems in the research approach. They can be separated into three parts as follows:

(1) Firstly, the microscope Axio Scope.A1 and Zygo NewView 5000 profilometer are used to analyse burr formation and micro slot accuracies respectively. The outcomes from cutting with and without using the hysteresis compensation module are then evaluated and compared.

(2) Secondly, the heat partitioned distribution needs heat transfer analysis particularly in micro cutting. Therefore, the conductive heat transfer is introduced and applied particularly in analysing the generated heat diffusion into tool-workpiece-chip partition.

(3) Finally, the diamond tool wear progressing requires the wavelet transform technique associated with standard deviation analysis in order to detect the tool wear stages in the micro cutting process.

The specific details for each technique or theory can be found in sections 3.4.1-3.4.3

3.4.1 Burrs formation and machining accuracy analysis

Burr formation may be caused by the effects of dynamic stiffness. It is believed that when dynamic stiffness is controlled, burr formation will be limited and minimized. In order to verify the burr formation, it is then investigated using the microscope. Thus, the burr formation of micro cutting with and without using the hysteresis compensation module has been analysed and compared. The microscope Axio Scope.A1 and its technical specifications are shown in Figure 3.6 and Appendix 6 respectively.

Figure 3.6 Microscope Axio Scope.A1 and its features

The dimensional accuracy of micro slot is also believed to be influenced by dynamic stiffness in the cutting process, due to the micro triangle (V-shaped slot) and square slots conducted in the experimental trials. Thus, step height measurements were carried out with the Zygo NewView 5000 profilometer in order to investigate micro slot dimensions. The micro slot accuracies were then assessed and compared between cutting with and without using the hysteresis compensation module. Figure 3.7 depicts the Zygo NewView 5000 profilometer, and its technical data can be found in Appendix 3.
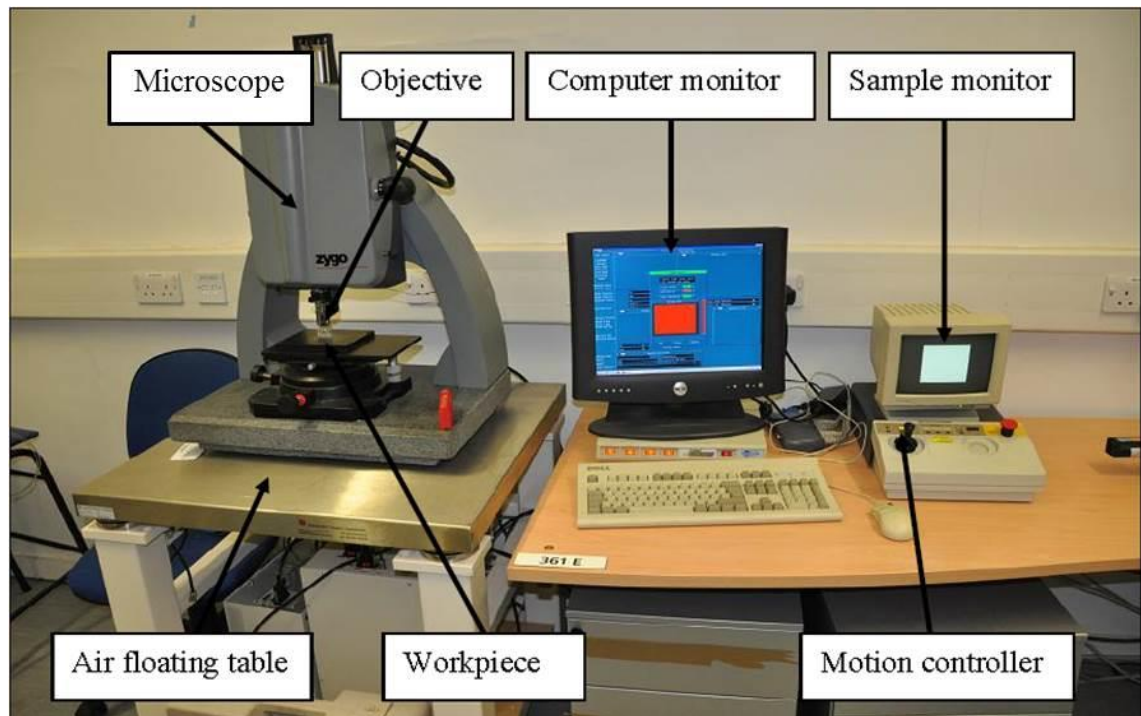
Figure 3.7 Zygo NewView 5000 profilometer and its functions

3.4.2 Heat transfer in micro cutting for tool-workpiece-chip heat partitioned distribution

The conductive heat transfer is applied in consideration of diamond tool-workpiece-chip heat partitioned distribution in micro cutting. Heat conduction (or thermal conduction) is the transfer of internal energy by microscopic diffusion and collisions of particles or quasi-particles within a body between solids due to a temperature gradient. The theoretical background of heat transfer mechanisms can be separated and interpreted in three mechanisms comprising conduction, convection and radiation. Convection heat transfer is energy transport due to bulk fluid motion through gases or liquids from a solid boundary resulting from the fluid motion along the surface. Radiation heat transfer is energy transport due to emission of electromagnetic waves or photons from a surface or volume. Meanwhile, energy transfer by conduction can take place in solids, liquids and gases. Conduction can be thought of as the transfer of energy from the more energetic particles of a substance to adjacent particles that are less energetic due to interactions between particles. The time rate of energy transfer by conduction is quantified macroscopically by Fourier's Law (Moran & Shapiro, 2006; IV & V, 2012;

Sobhan & Peterson, 2008; Volz, 2007). Thus, in micro cutting, the conductive heat transfer through solids is considered to be due to molecular vibration. Based on Fourier's Law, the rate of heat transfer across any plane is normal to the x direction, Q/A $(\dot{Q}_x)$, or the so called heat transfer per unit area (W/m^2). It is proportional to the temperature gradient dT/dx in the x direction where the temperature $T(x)$ varies linearly with position x. The constant of proportionality is called the material thermal conductivity k. Considering the steady state of one-dimensional heat conduction, it can be expressed by the scalar equation

$$q_x = -k\frac{dT}{dx} \qquad \dot{Q}_x = -kA\frac{dT}{dx} \tag{3.1}$$

where the heat flux q depends on a given temperature T and thermal conductivity k. The minus sign is a consequence of energy transfer in the direction of decreasing temperature, $\dot{Q}$ represents the heat flow through a defined cross-sectional area A, thus, integrating the one-dimensional heat flow equation through a material's thickness x gives as:

$$\dot{Q}_x = \int_A q.\,dA \tag{3.2}$$

$$\dot{Q}_x = \frac{kA}{\Delta x}(T_1 - T_2) \tag{3.3}$$

The theoretical background mentioned above is associated with the experimental results of micro cutting temperature. The analyses of heat partitioned distribution of three specific sample materials are implemented and described in details in topic 6.5.

3.4.3 Wavelet transform associated with standard deviation for tool wear monitoring and analysis

Wavelet analysis is a powerful tool in signal processing which represents the next logical step, i.e., a windowing technique with variable-sized regions. Wavelet analysis allows the use of long time intervals that are more precise at low frequency information and shorter periods at high frequency information.
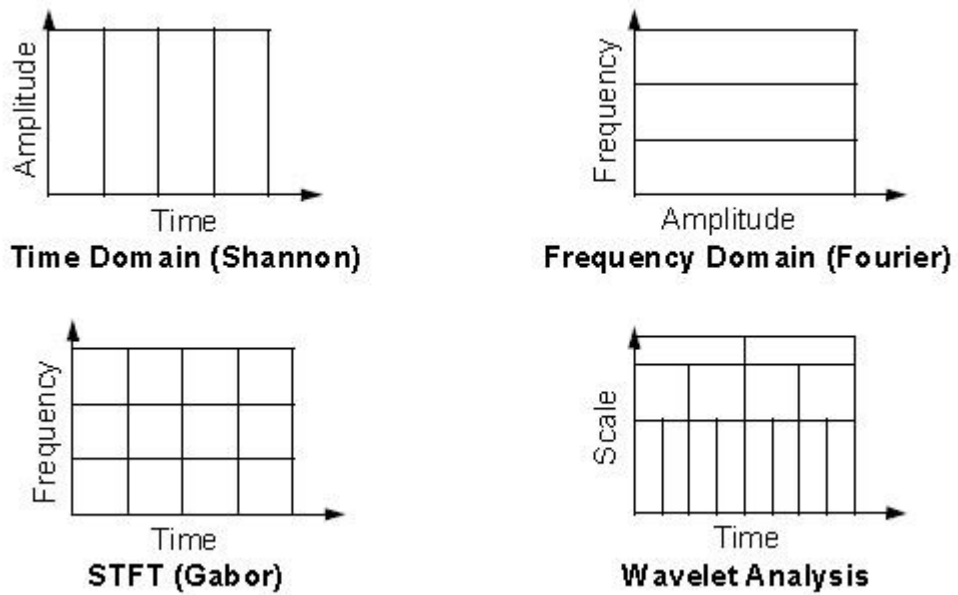
Figure 3.8 The signal processing comparisons in contrast with time-based, frequency-based, STFT and wavelet analysis (Misiti, et al., 2000)

It is noted that wavelet analysis does not use a time-frequency region, but rather a time-scale region. Meanwhile, previous methods including the time domain use the amplitude-time region, while the frequency domain and the Short-Time Fourier Transform (STFT) use frequency-time region respectively (Misiti, et al., 2000). Conventional time-frequency analysis methods such as STFT only provide uniform time and frequency resolutions in the whole time-frequency domain. Consequently, only information with limited precision can be obtained, and that precision is determined by the size of the window (Anon., 2005). Meanwhile, the wavelet transform (WT) uses windows of different lengths for different frequencies. High frequencies are analysed with narrower windows for better time resolution, while at low frequencies wider windows are used for better frequency resolution. Thus, the WT can extract more information in the time domain at different frequency bands (Teti, et al., 2010). In other words, the wavelet can provide fine frequency resolution at low frequencies and fine time resolution at high frequencies, which is impossible when using the methods mentioned previously. That means the wavelet can provide high time resolution and frequency resolution simultaneously.

The basic idea behind signal processing with wavelets is that the signal can be decomposed into its component elements through the use of basic functions. In

the case of wavelet analysis, the basic functions consist of the wavelet scale function, and scaled and shifted versions of the mother wavelet. Unlike in Fourier analysis, the basic function is just sine or cosine waves. A wavelet transform is a popular tool for studying intermittent and localized phenomena in various signals, e.g., cutting force signals for tool wear monitoring and analysis. Owing to the multiresolution ability of a wavelet transform, the noised signals can be separated into several approximation and detail signals (Lin, 2001). The wavelet transform of a signal *f(t)* is defined as the sum of the time of signal *f(t)* multiplied by a scaled and shifted version of the wavelet function *Ψ(t)* (Kwak, 2006; Huang, et al., 2013). Thus, the coefficients *C(a, b)* of the continuous wavelet transform (CWT) of the signal *f(t)* can be expressed as follows:

$$C(a,b) = \int_{-\infty}^{\infty} f(t)a^{-0.5}\Psi(\frac{t-b}{a})\,dt \tag{3.4}$$

where *a* and *b* are the scaling and shifting parameters in the wavelet transform. A family of scaled and shifted wavelets can be produced by varying the parameters *a* and *b*. For the sampled signal *f(k)*, a discrete wavelet transform can be used. The most commonly used discrete wavelet transform is the scaling and shifting of parameters with powers of two, expressed as follows:

$$a = 2^j \tag{3.5}$$

$$b = ka = k2^j \tag{3.6}$$

where *j* is the number of levels in the discrete wavelet transform (DWT). The coefficients *C(a, b)* of the discrete wavelet transform can be divided into two parts, namely, approximation coefficients and detail coefficients. The approximation coefficients (scaling coefficients) are the high scale, low frequency components of the signal $f(k)$, while the detail coefficients (wavelet coefficients) are the low scale, high frequency components of the signal $f(k)$ (Kwak, 2006). The approximation coefficients *(A_j)* and the detail coefficients *(D_j)* of the discrete wavelet transform for the sampled signal $f(k)$ at level *j* can be expressed as follows:

$$A_j = \sum_{n=0}^{\infty} f(n)\, \psi_{j,k}(n) = \sum_{n=0}^{\infty} f(n) \frac{1}{\sqrt{2^j}} \psi\left(\frac{n-k2^j}{2^j}\right) \tag{3.7}$$

$$D_j = \sum_{n=0}^{\infty} f(n)\, \Psi_{j,k}(n) = \sum_{n=0}^{\infty} f(n) \frac{1}{\sqrt{2^j}} \Psi\left(\frac{n-k2^j}{2^j}\right) \tag{3.8}$$

where $\psi_{j,k}(n)$ is the scaling function associated with the wavelet function $\Psi_{j,k}(n)$.

There are a number of well-known wavelets such as Morlet, Haar, Shannon, Symmlets, Coiflets and Daubechies wavelets, etc., in the common family of wavelet mother functions. The most popular are the Daubechies, Symmlets and Coiflets wavelets. These mother wavelets give the best overall performance in respect of the mean squared error between reconstruction signal and original signal, and maximizing the signal-to-noise ratio improvement. However, the performance of the abovementioned wavelet mother functions in extracting the feature sensitive to wear quality may vary according to the mother wavelet properties (Pal, et al., 2011). Thus, in this research project, the Daubechies wavelet was selected in analysing the tool wear states detection.

The wavelet transform associated with the standard deviation analysis is capable of being applied in detecting cutting tool wear states (Huang, et al., 2013). A wavelet transform can decompose signals into different frequency bands in the time domain. Statistical tools such as root mean square (RMS) or standard deviation can then be extracted from the decomposed signal for each frequency band and used as the monitoring feature for tool wear (Li, 2002 ; Xiaoli, et al., 1997). In this research, single crystal silicon is a material of interest for tool wear detection based on wavelet decomposition and analysis of force signals through experimental cutting. In order to analyse the tool wear states, an analysis of standard deviation of cutting force at different wavelet coefficients has been conducted. The schematic procedures of wavelet transform technique as well as standard deviation analysis of tool wear monitoring have been proposed in Figure 3.9. More details and further analysis of tool wear in cutting titanium and aluminium comparable to cutting silicon can be found in Chapter 5.
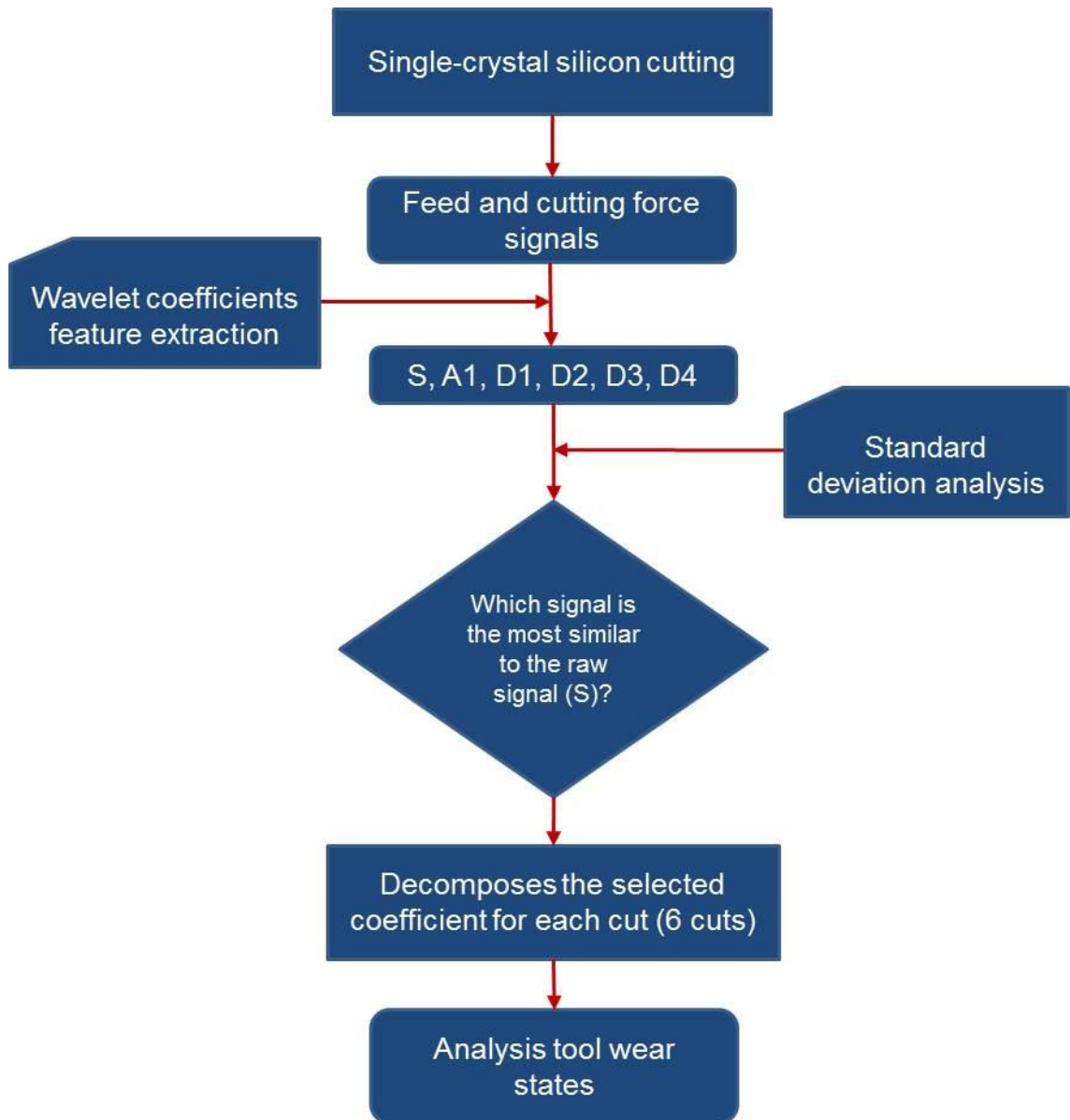
Figure 3.9 Schematic procedure for analysis and monitoring of tool wear status

Chapter 4 Dynamic stiffness and its effects on micro cutting

4.1 Introduction

The dynamic stiffness is one of the latest and most interesting issues that has been proposed for cutting mechanics particular in micro cutting. It is believed that not only static stiffness in the micro cutting process has been concerned and taken into consideration, but also the dynamic stiffness greatly influence and affect the machining performances. This may be caused by the cutting process and is mainly dominated by the dynamic excitation loads or dynamic cutting forces, and consequent directly influence on dynamic displacements of cutting tool which results in cutting performances. Thus, scientific point of view, the dynamic stiffness is quite important to study on its characteristics and effects on the micro machining particularly at both stages of machine design and machining process. Basically, static stiffness in machine tools refers to the performance of structures under the static or quasi-static loads which normally come from gravity and cutting force, etc. Apart from the static loads, machine tools are subjected to constantly changing dynamic forces and the machine tool structure will deform according to the amplitude and frequency of the dynamic excitation loads, which is termed dynamic stiffness (Cheng, 2009).

Although, there have been attempts to investigate the dynamic stiffness, characteristics and benefits, a few previous reports on the dynamic stiffness investigation. However, these attempts almost always investigated conventional cutting. For instance, Yigit et al (Yigit & Ulsoy, 2002) proposed a systematic procedure to evaluate the dynamic stiffness characteristics of design alternatives for a reconfigurable machine tool (RMT). Kim et al (Kim, et al., April. 9-11, 2008) also presented a case study on dynamic characteristics analysis and dynamic stiffness evaluation of a 5-axis multi-tasking machine tool of ram-head type. However, a proper dynamic stiffness definition, effects and benefits

have not been thoroughly determined and investigated yet in micro cutting in particular. Therefore, in this chapter great efforts have been made to investigate the dynamic stiffness in terms of its existences, definitions, characteristics, effects and consequent benefits of study.
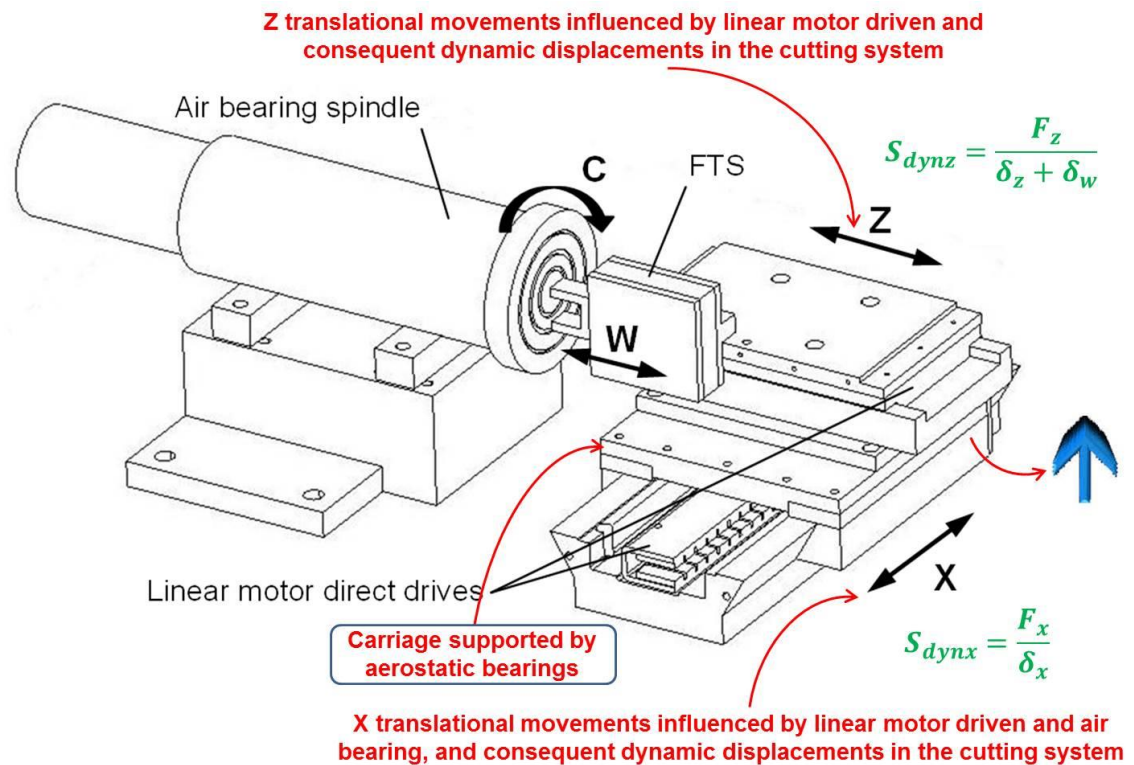
Figure 4.1 The schematic illustrating the dynamic stiffness conception in ultraprecision diamond turning

The conception of dynamic stiffness in ultraprecision diamond turning is illustrated in Figure 4.1. The diamond turning machine uses linear motors direct drive for rendering high precision translational motions. The carriage slideways are supported by aerostatic bearings, which are free from contact friction. Consequently, the dynamic displacements of cutting tool are heavily dominated by dynamic cutting forces during the cutting process. The dynamic stiffness can then be formulated based on the dynamic cutting force against the dynamic displacements but in a truly different dynamic manner.

In order to investigate the dynamic stiffness of the dynamic cutting process, and its influences on the cutting performances in the ultra-precision diamond turning, two cutting methods included normal cutting and cutting with compensated hysteresis module for three case studies on micro-featured slots

were proposed, performed and compared. The interested outcomes of dynamics stiffness are analysed based on the definitions, characteristics, effects on machining performances especially on micro slot accuracies and burrs formation. In addition, the benefits of control and optimisation of the characteristic movements of cutting tool and consequent dynamic stiffness are analysed.

4.2 Experimental cutting setups and trials

In order to implement the three differences of micro-featured slots, one micro triangle slot (V-shaped slot) and two squared slots with different cutting conditions as the three case studies by experiment-based investigation, the ultraprecision machining utilising single point diamond turning (SPDT) equipped with a fast tool servo (FTS) were conducted. The fabrication of each micro-featured slot was designed the cutting time as equal to 20 seconds. The single crystal diamond tool with edge and nose radius is 82.40 nm and 0.302 mm, respectively, which was observed by scanning electron microscope (SEM) as shown in Figure 4.2 is used. A Kistler Type 9256C2 three-component force mini-dynamometer was installed underneath the tool holder in order to measure the cutting forces in three directions. The Micro-epsilon type S600-1 capacitive sensor was also installed inside the FTS to measure the characteristic movements of dynamic cutting tool. The ZYGO NewView 5000 white light interferometer was used for micro slots accuracy monitoring and measurement. Meanwhile, the microscope Axio Scope.A1 was used in burrs formation monitoring. The real-time of dynamic cutting forces and cutting tool movements for both normal and hysteresis compensated cutting of micro-featuring slots were collected through the data acquisition (DAQ) card associated with Labview programming.
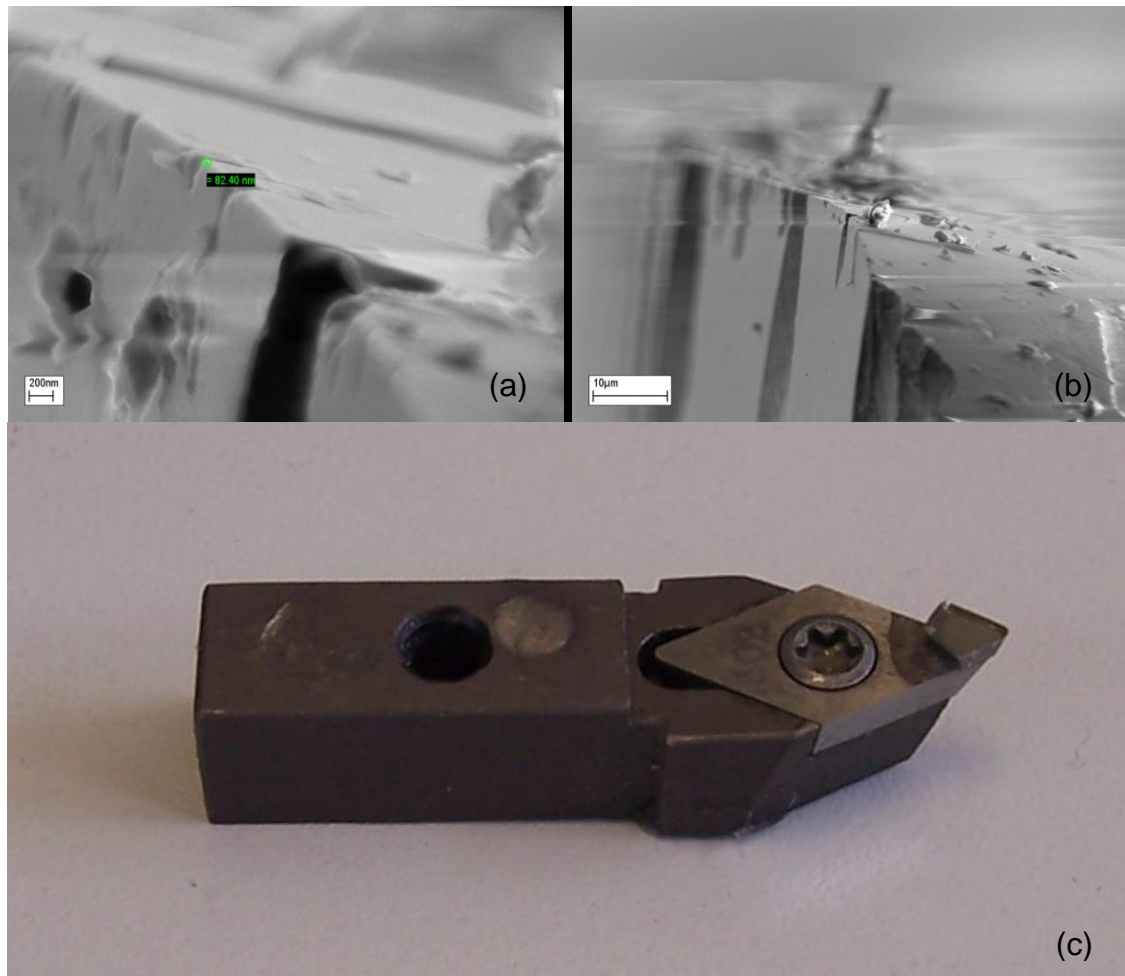
Figure 4.2 The used diamond tool with the tool edge and nose radius of 82.40 nm and 0.302 mm respectively: built up edges, cracks and defects observed: (a) magnification of 80k, (b) magnification of 5k, (c) diamond cutting and tool shank

The experimental investigation was setup and implemented the three cases study of micro-featured slots cutting. The two cases study were square and triangle slots which different dimensions and cutting conditions as illustrated in Figure 4.3, a and b, respectively.

The dimensions and specifications of the first two cases of micro-squared slots have performed by FTS with amplitude (A) 10 μm (pulsed DC input voltages to the FTS) and cycle time (CT) 4 seconds as shown in Figure 4.3 (a). Both of them were machined by conducting CNC programming with different cutting conditions as following described. The first case study (case 1) was performed without depth of cut (0 DOC), feed rate (Fr) 15 mm/min., and rotational speed

600 RPM (10 Hz), respectively. Meanwhile, the second case study (case 2) was performed with DOC 5 µm, Fr 12 mm/min, and rotational speed 600 RPM, respectively. The micro-triangle slot (V-shaped slot) as the third case study (case 3) was performed by FTS with A 10 µm and CT 2 seconds as illustrated in Figure 4.3 (b). The cutting conditions conducted on case three by CNC machining as equal to DOC 3 µm, Fr 12 mm/min, and rotational speed 600 RPM, respectively. The details of experimental planning can be found in section 3.2.1.
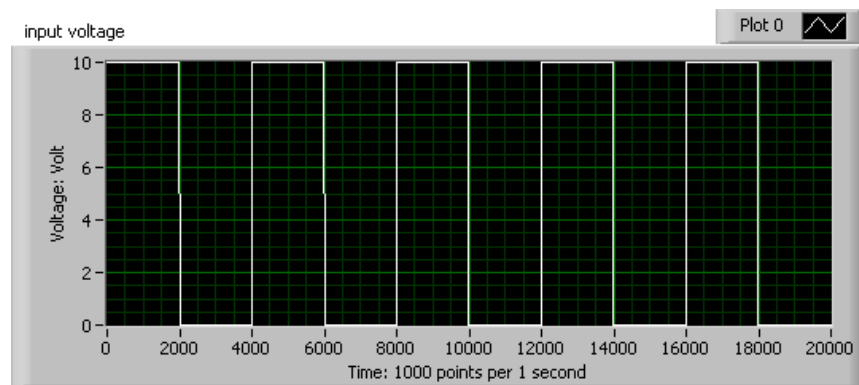
(a)
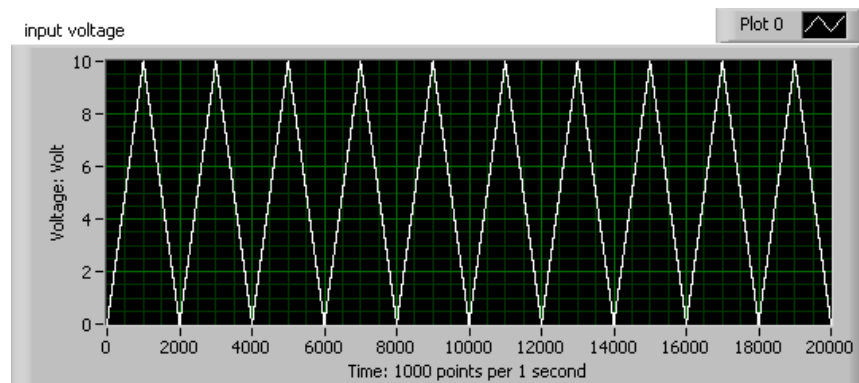
(b)

Figure 4.3 The micro slots: (a) the first two cases study (case 1, 2) of micro-squared slots, and (b) the third case study (case 3) of micro-triangle slot

4.3 Dynamic stiffness in ultra-precision diamond turning

As dynamic stiffness existing in dynamic cutting processes, it can influence the cutting performances, and consequently it should be taken in consideration in ultraprecision and micro machining particularly at an industrial scale. In this research, therefore, dynamic stiffness is verified in implementations of the three cases study of micro-featured slots by the diamond turning. The real time dynamic cutting forces and characteristic movements of dynamic displacements were collected. Consequently, applied a simply and fundamentally theoretical formulation of dynamic stiffness as proposed which is the dynamic cutting forces divided by dynamic displacements of cutting tool movements during cutting process (N/μm). Thus, the calculated dynamic stiffness could then be obtained for the whole period of machining process of each micro-featured slot. Figures 4.4 to 4.6 illustrated the dynamic stiffness of three cases study of micro-featured slots by employed the normal cutting.
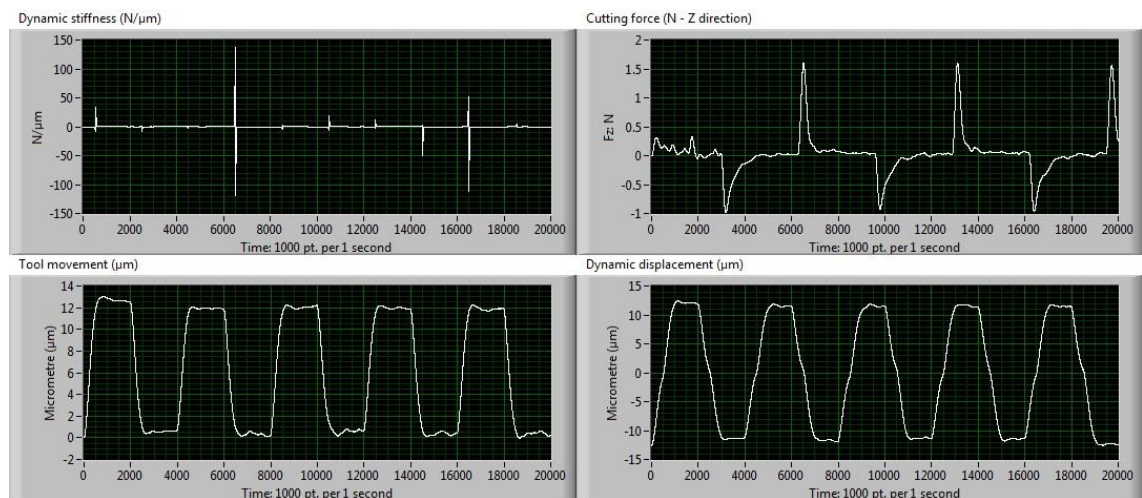
Figure 4.4 The dynamic stiffness (top-left), tool movement (bottom-left), cutting force (top-right) and displacement (bottom-right) of the normal cutting on square slot of the first case study
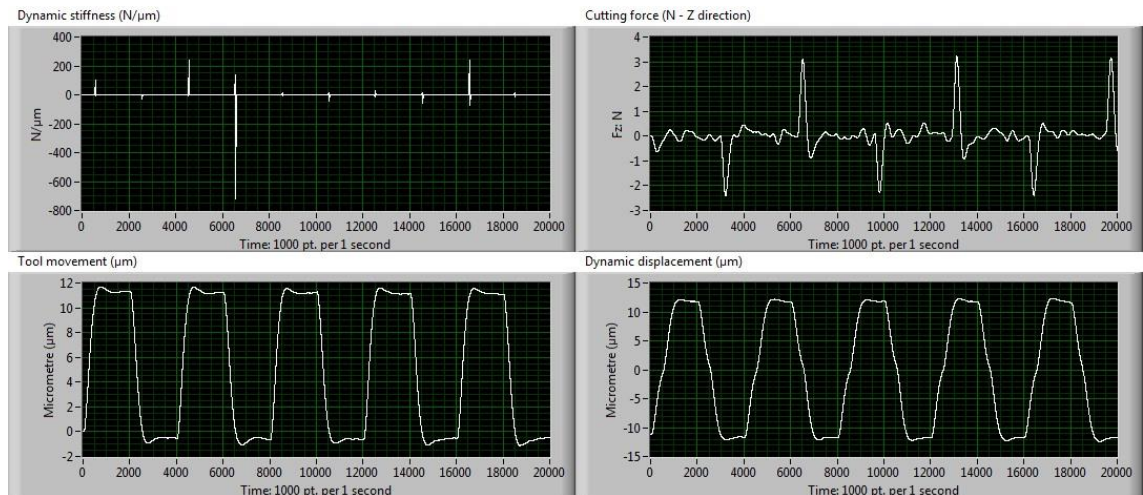
Figure 4.5 The dynamic stiffness (top-left), tool movement (bottom-left), cutting force (top-right) and displacement (bottom-right) of the normal cutting on square slot of the second case study
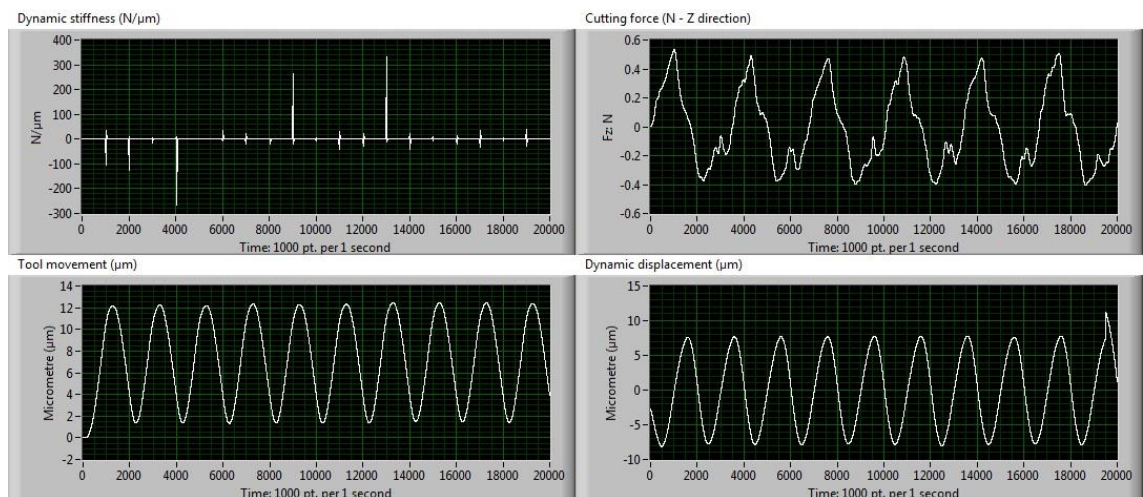
Figure 4.6 The dynamic stiffness (top-left), tool movement (bottom-left), cutting force (top-right) and displacement (bottom-right) of the normal cutting on triangle slot of the third case study

As seen from Figures 4.4 to 4.6, the characteristics and variances of dynamic stiffness for the whole cutting period of micro-featured slots can be observed. Dynamic stiffness is always changing and varying due to cyclic dynamic changes of the cutting force and dynamic displacements, it can be assumed that the dynamic stiffness exists and not totally equal to the static stiffness. This result is agreed well as the research proposed. Thus, based on the experimental outcomes, the definition and formulation of dynamic stiffness could be established according to the divided product of dynamic excitation

67

loads by dynamic displacements for any specific cutting time. This research finding of formulation can be simply modelled as following equation:

$$S_{dyn} = \frac{F_{c_i}}{\delta_i}$$ (4.1)

Where S_{dyn} is dynamic stiffness, ΔF_{c_i} is dynamic cutting force, and $\Delta \delta_i$ is dynamic displacement, respectively for any specific cutting time.

The micro-featured slots of three cases study can be observed from Figures 4.7 to 4.9.
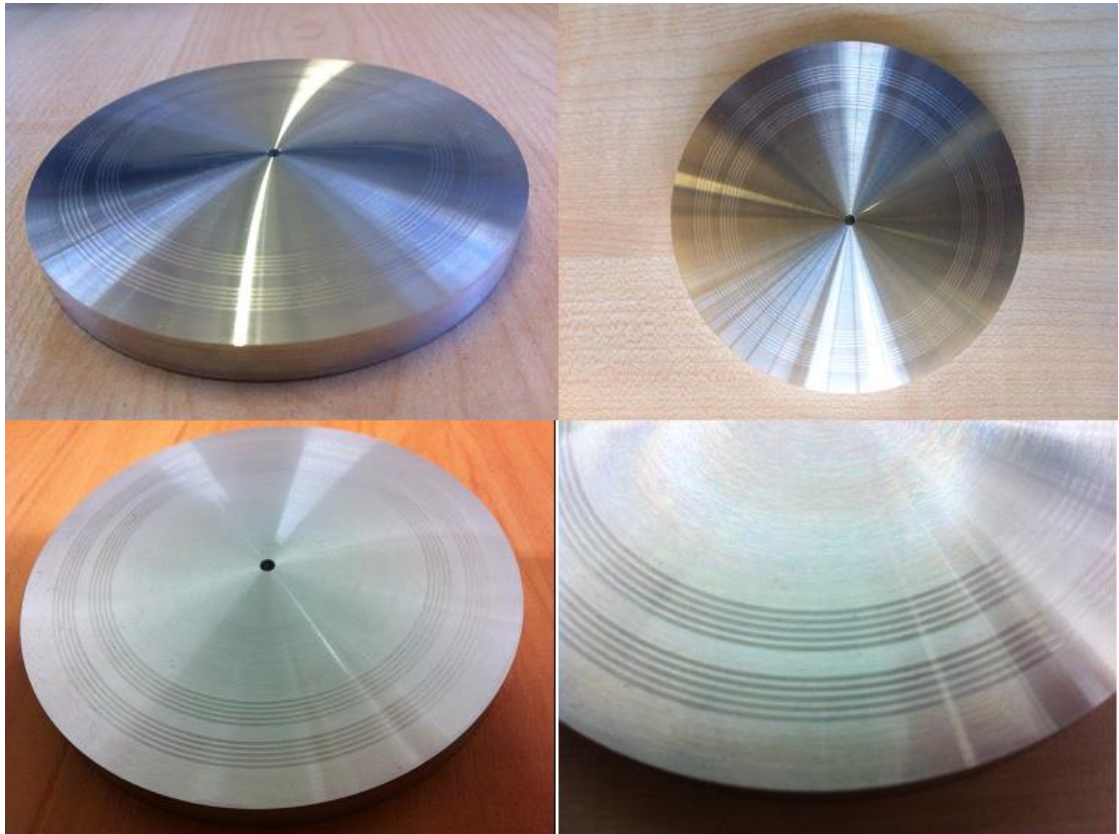
Figure 4.7 The micro-squared slot of cutting experiment in case 1
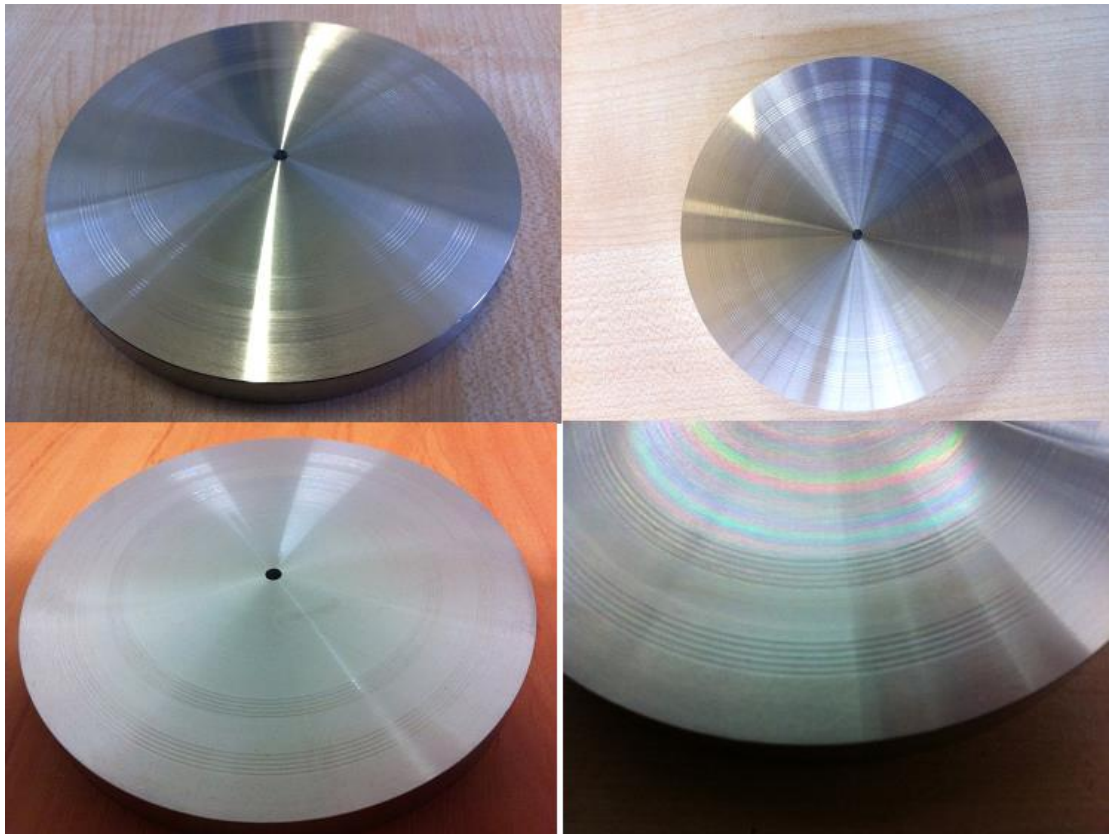
Figure 4.8 The micro-squared slot of cutting experiment in case 2
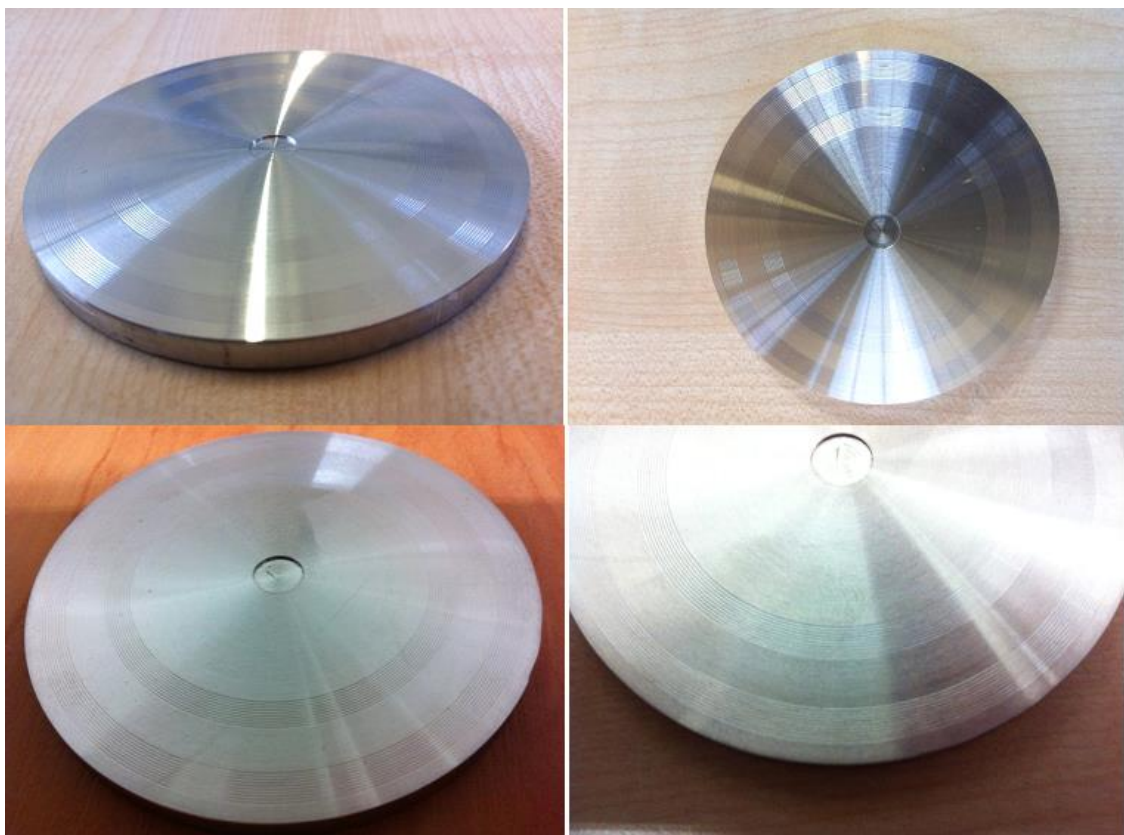
Figure 4.9 The micro-triangle slot of cutting experiment in case 3

4.4 Dynamic stiffness effects and control strategies

It is presented that the dynamic stiffness exists and its characteristics are not similar to the static stiffness. Thus, it should effect the cutting process which accordantly total differ from the static stiffness effects. In this section, the exploration and investigation of dynamic stiffness effects are performed. As observations from previous experimental results, the excessive dynamic stiffness possibly effects on the micro slots accuracy and burrs formation. In other words, an excessive dynamic stiffness can cause the huge micro-squared and triangle slot dimensional errors and burrs formation. However, less stiffness may affect to machine system and easily being destroyed by dynamic excitation loads (Cheng, 2009; Merritt, 1965; Hale, 1999; Ramesh, et al., 2000). Therefore, if the dynamic stiffness can be well-controlled and optimised, it might be able to control and minimise the micro slot dimensional errors and burrs formation. Consequently, the hysteresis compensation module is proposed as the controllable method to control, optimise and minimise the errors of dynamic movements of diamond tool and consequent the dynamic stiffness.

The theoretical background of the hysteresis compensation module is presented in Figure 4.10 (Lin & Chen, 2012 ; Cuttino, et al., 1999; Panusittikorn, 2010). The inherent behaviours of hysteresis of piezoelectric actuator are characterised as always nonlinear and consequently never have the same trends on both charging and discharging of input voltage. Thus, the controllable method is proposed to compensate these hysteresis behaviours based on using the K-compensator (K_{comp}). The theoretical basis of the controllable method is that the K_{actual} describes a nonlinearity imposed by the piezoelectric actuator while the $K_{desired}$ is what characteristics of the actuator are needed for both the charging and discharging input voltages to be the same. Thus, the so called K-compensater (K_{comp}) is applied and modeled as a fixed gain for the linear behaviors of the actuator at any specific time. K_{comp} can then be modeled and formulated for any specific time of charging or discharging as following equation:

$$Kcomp = \frac{Kdesired}{Kactual} \tag{4.2}$$
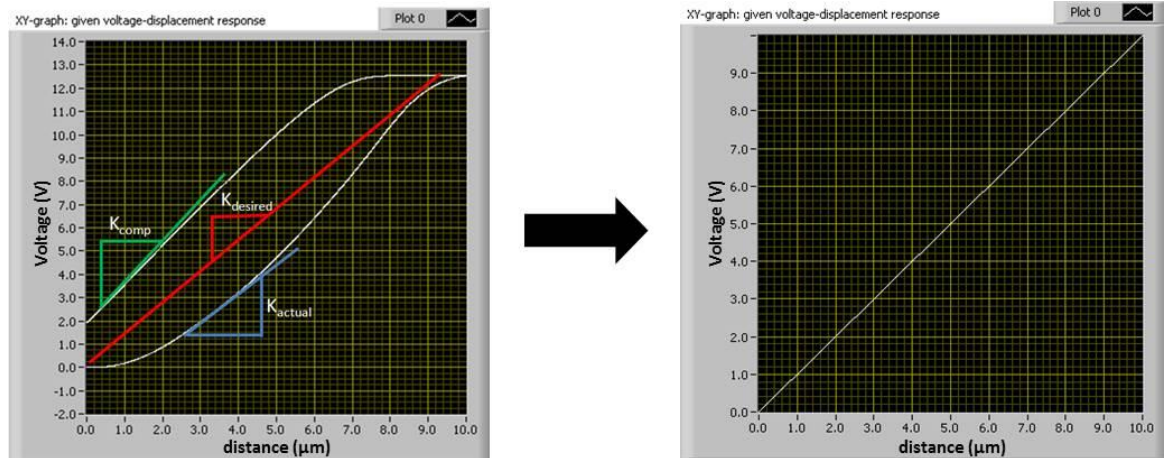
Figure 4.10 The schematic algorithm of hysteresis compensated module and its favourable outcome

In order to improve the characteristic movements of the dynamic cutting tool, minimise cutting forces, optimise dynamic stiffness, and consequently gain benefits of the minimisation of micro slots error and burrs formation, the hysteresis compensated module was employed in single point diamond turning (SPDT) to machine the micro-featured slots. The results indicate that there are obviously different characteristics of dynamic stiffness, cutting forces, tool movements, and displacements when compared with the normal cutting. On the other hand, dynamic cutting forces and excessive dynamic movements of cutting tool, which mainly result in the dynamic changing of cutting tool displacements, are much reduced when employed hysteresis compensation module in cutting process. Thus, the excessive movements and dynamic displacements are much improved (Figures 4.11 to 4.13); subsequently dynamic stiffness could be well-controlled and optimised. Therefore, burrs formation and micro slot dimensional errors are improved and minimised accordingly.

4.5 Dynamic stiffness and its characteristic results by hysteresis compensated cutting

As observed from Figures 4.11 to 4.13, the dynamic cutting forces and their characteristics are decreased when hysteresis compensated cutting is taken

place. The second issue is dynamic movements of cutting tool can be well-controlled during the whole period of cutting process. Therefore, the calculated dynamic stiffness would then be controlled, optimised and consequent huge reduced. Finally, the improvements of micro slot errors and micro burrs can then be distinctly observed when compared to the normal cutting.
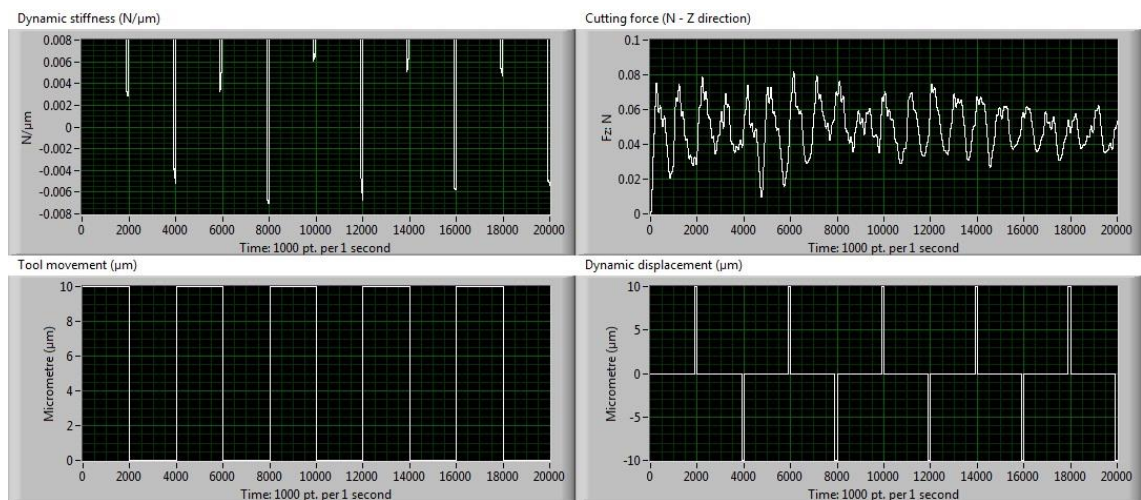
Figure 4.11 The dynamic stiffness (top-left), tool movement (bottom-left), cutting force (top-right) and displacement (bottom-right) of the hysteresis compensated cutting on square slot of the first case study
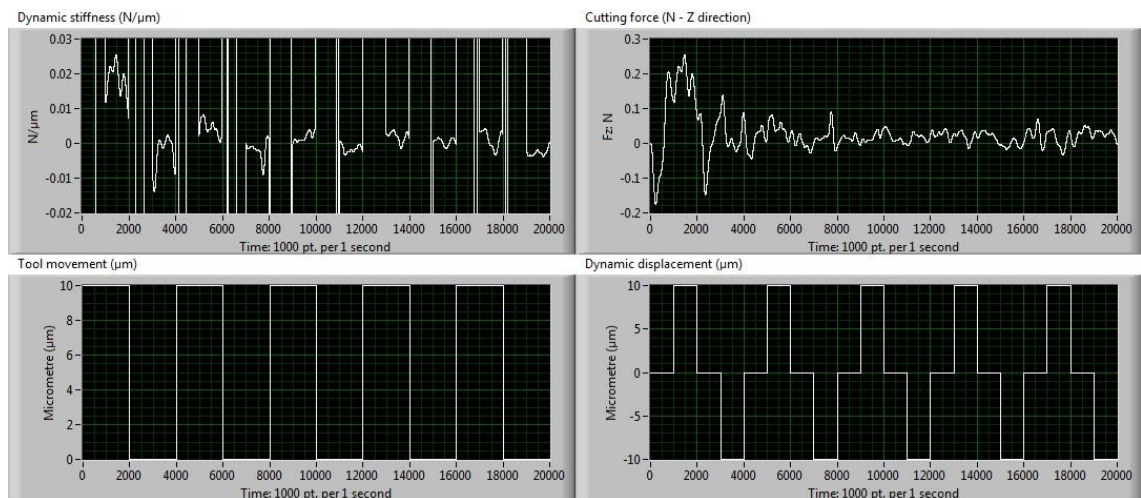
Figure 4.12 The dynamic stiffness (top-left), tool movement (bottom-left), cutting force (top-right) and displacement (bottom-right) of the hysteresis compensated cutting on square slot of the second case study

72
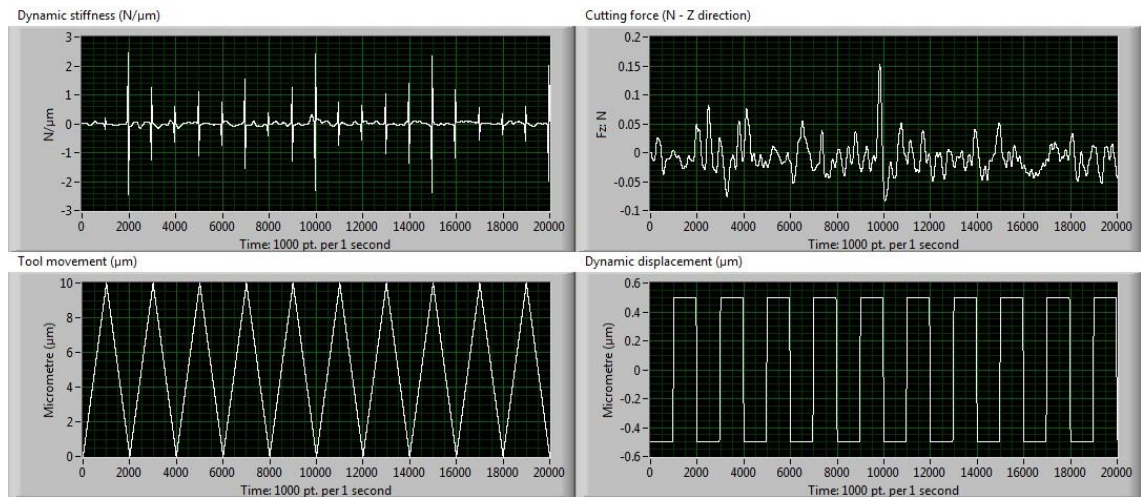
Figure 4.13 The dynamic stiffness (top-left), tool movement (bottom-left), cutting force (top-right) and displacement (bottom-right) of the hysteresis compensated cutting on triangle slot of the third case study

4.6 Comparison results of normal and hysteresis compensated cutting

This section conducts the comparisons of normal and hysteresis compensated cutting of three case studies of micro-featured slots. The results indicate that the improvements of micro slots accuracy and reductions of micro burrs formation when the hysteresis compensated cutting is employed.

4.6.1 Micro slots accuracy

Figures 4.14 and 4.15 compare the slot measurements of both normal and hysteresis compensated cutting of micro-squared slot as the first case study. It is noted that the desired dimensions of micro-squared slot i.e., the amplitude (peak to valley) and slot width are equal to 10 µm and 500 µm, respectively. The amplitude resulted from control of cutting tool movements by input the desired voltage to the FTS. Meanwhile, the slot width of micro-squared slot of the first case study is calculated based on cutting conditions which uses a half cycle time and feed rate as equal to 2 seconds and 15 mm/min, respectively.
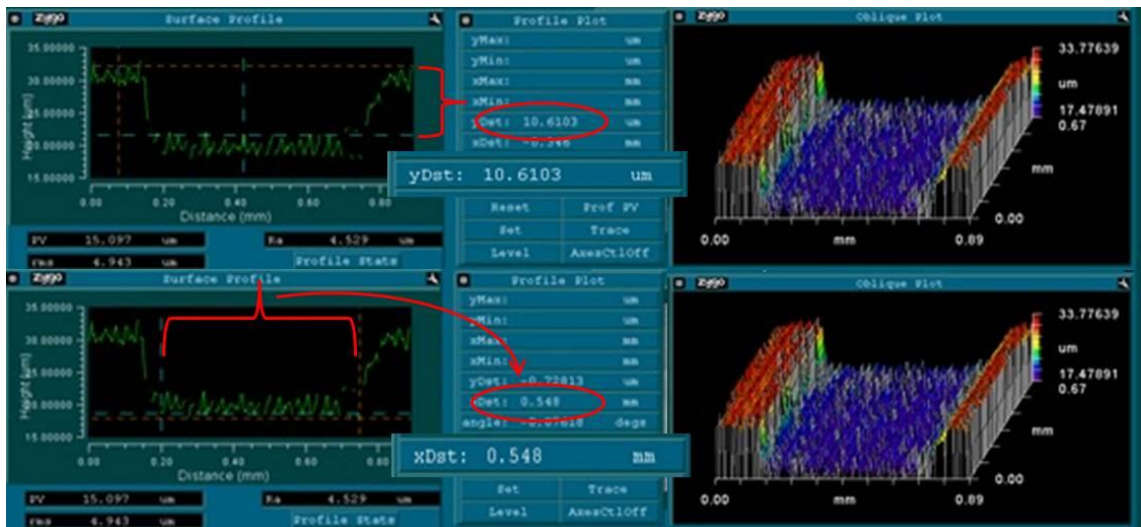
Figure 4.14 Micro-squared slot measurements of the first case study by the normal cutting; top: peak to valley 10.61 μm, bottom: slot width 548 μm.
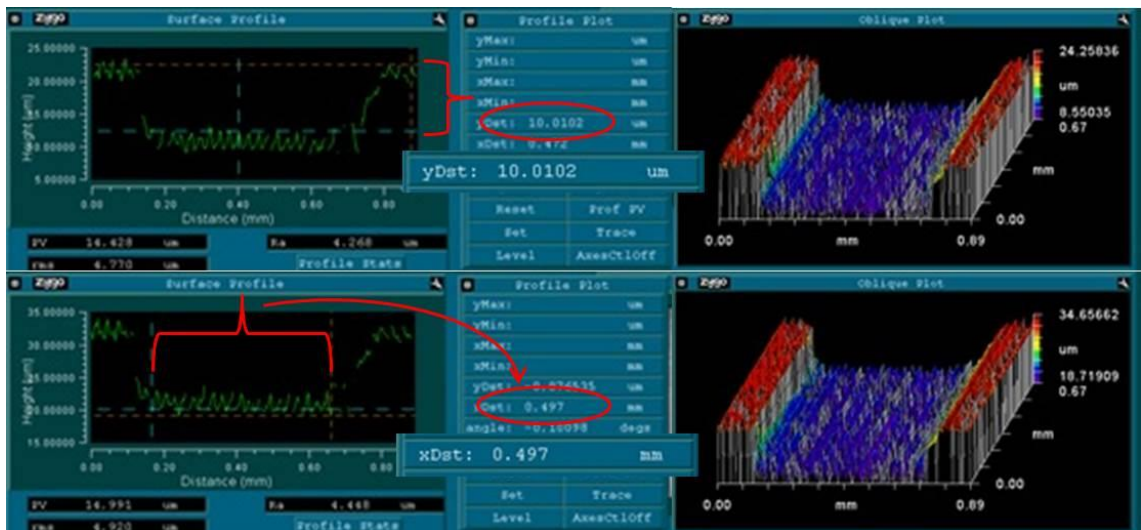
Figure 4.15 Micro-squared slot measurements of the first case study by the hysteresis compensated cutting; top: peak to valley 10.01 μm, bottom: slot width 497 μm.

Figures 4.16 and 4.17 compare the slot measurements of both normal and hysteresis compensated cutting of micro-squared slot as the second case study. The desired dimensions of micro-squared slot i.e., the amplitude (peak to valley) and slot width are equal to 10 μm and 400 μm, respectively. As with previous calculations, the amplitude and slot width of the second case study are

calculated based on the same principle of the first case study, but only different in feed rate as equal to 12 mm/min.
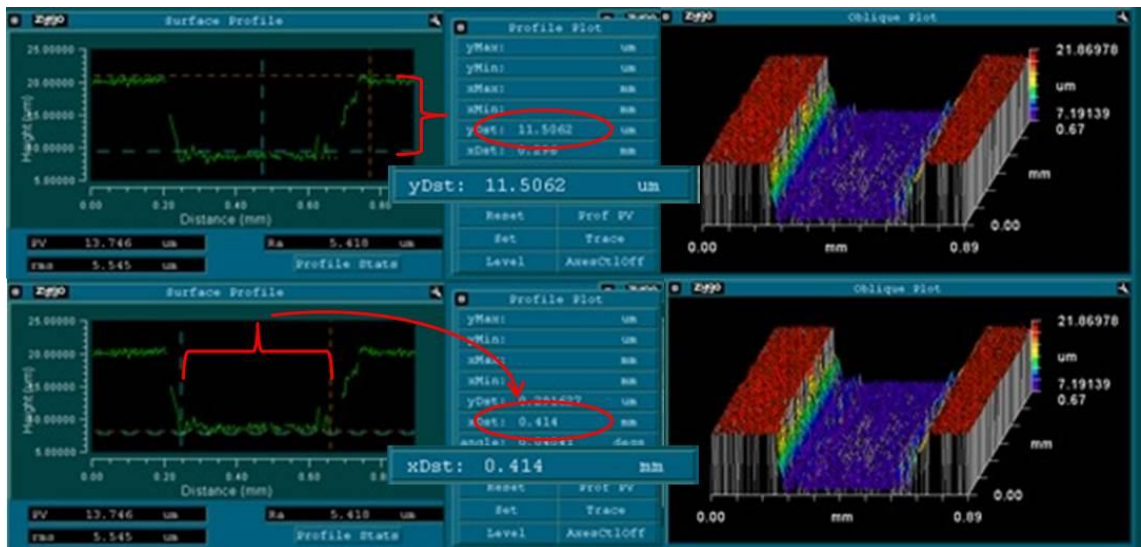
Figure 4.16 Micro-squared slot measurements of the second case study by the normal cutting; top: peak to valley 11.5 μm, bottom: slot width 414 μm.
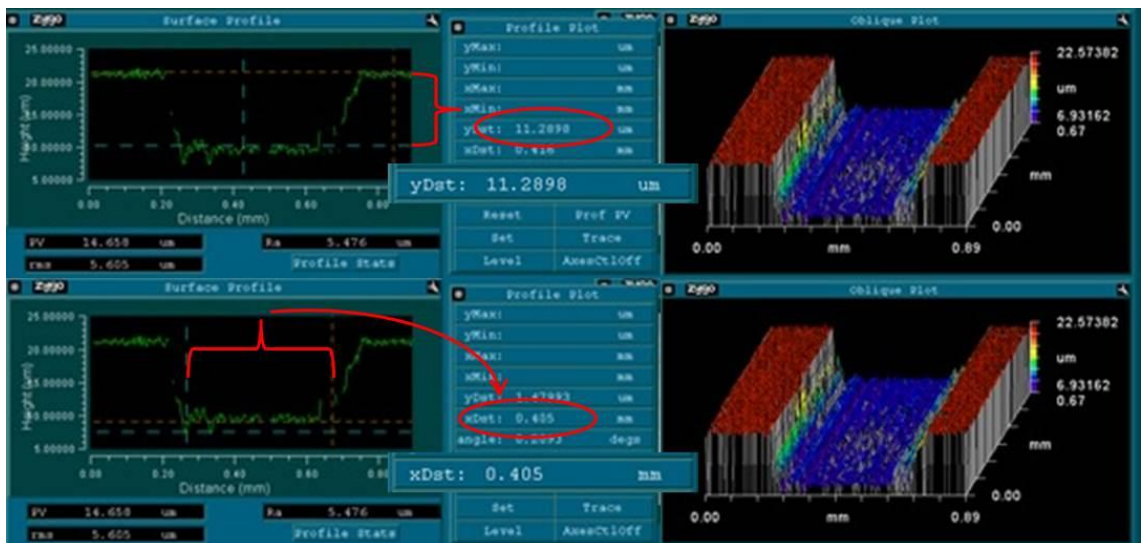
Figure 4.17 Micro-squared slot measurements of the second case study by the hysteresis compensated cutting; top: peak to valley 11.29 μm, bottom: slot width 405 μm.

Figures 4.18 and 4.19 compare the slot measurements of both normal and hysteresis compensated cutting of micro-triangle slot as the third case study. The desired dimensions of micro-triangle slot i.e., the amplitude (peak to valley) and slot width (peak to peak) are equal to 10 μm and 400 μm, respectively. The

amplitude and slot width of micro-triangle slot are calculated based on the same principle of micro-squired slot, but use different cutting conditions using a cycle time and feed rate equal to 2 seconds and 12 mm/min, respectively.
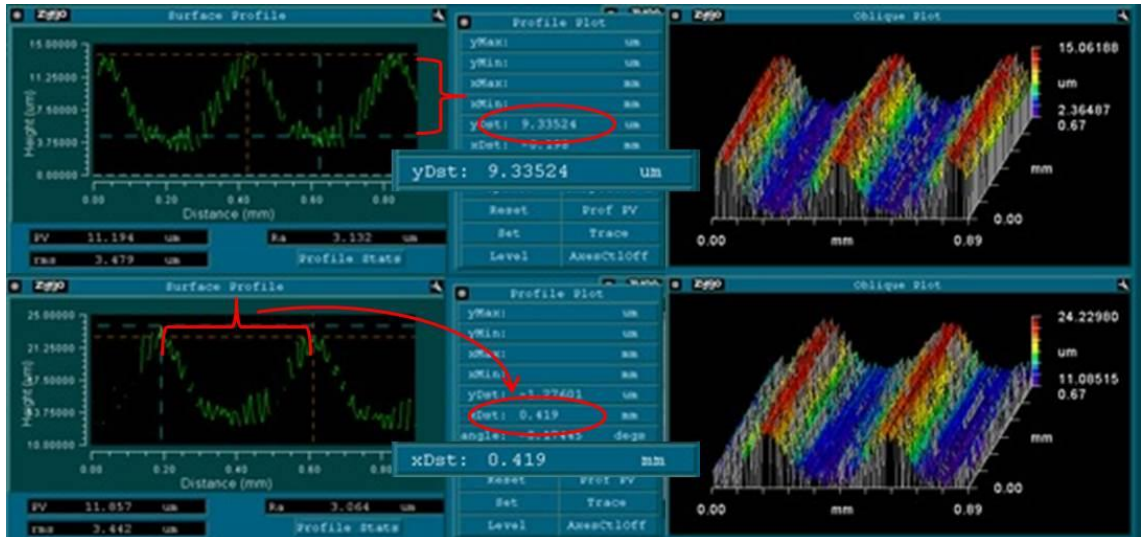
Figure 4.18 Micro-triangle slot measurements of the third case study by the normal cutting; top: peak to valley 9.33 µm, bottom: peak to peak 419 µm.
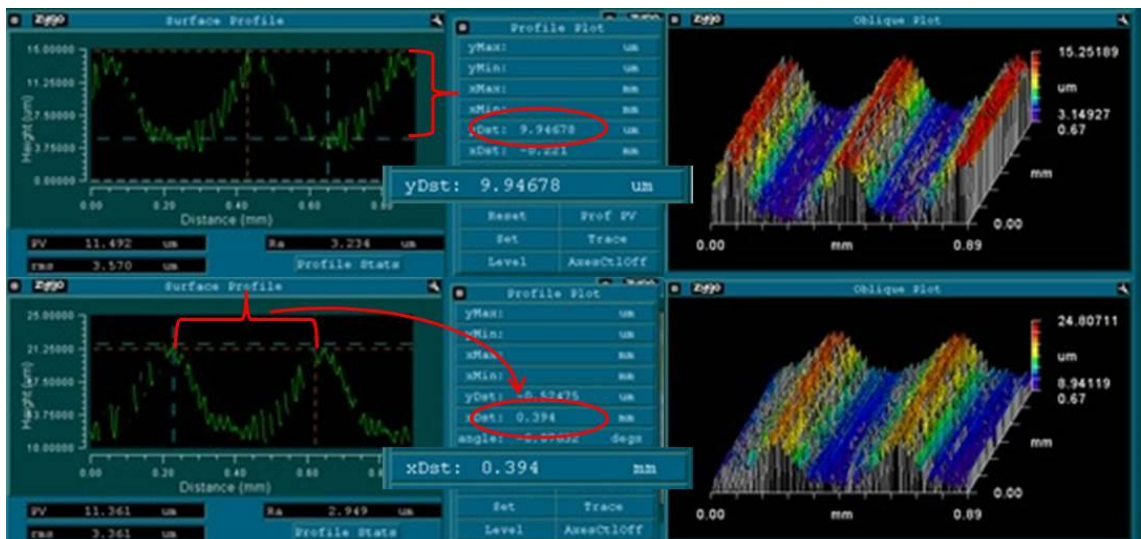
Figure 4.19 Micro-triangle slot measurements of the third case study by the hysteresis compensated cutting; top: peak to valley 9.95 µm, bottom: peak to peak 394 µm.

These results show a significant improvement on accuracies and dimensions of both micro-squared and triangle slots when the hysteresis compensation

module is employed in the cutting process as observed in Figures 4.15, 4.17 and 4.19.

4.6.2 Burrs formation

The burrs formation is another issue which is caused by dynamic stiffness. Although burrs formation is generally dominated by the worn cutting tool which was used in the experiments, it also occurs on the machined surface areas with high dynamic stiffness in particular at peaks and valleys of the micro-squared and triangle slots. The micro burrs of three cases studies of micro square and V-shaped slots in comparison of both normal and hysteresis compensated cutting were observed by the microscope Axio Scope.A1 and measured with the microscope scale. The results show that the burrs are influenced by high dynamic stiffness at peaks or valleys areas in particular, also dominated by the cutting tool at any tool marks. Thus, once the hysteresis compensated module is employed, burrs formation can be controlled and minimised as illustrated in Figures 4.21, 4.23, and 4.25.
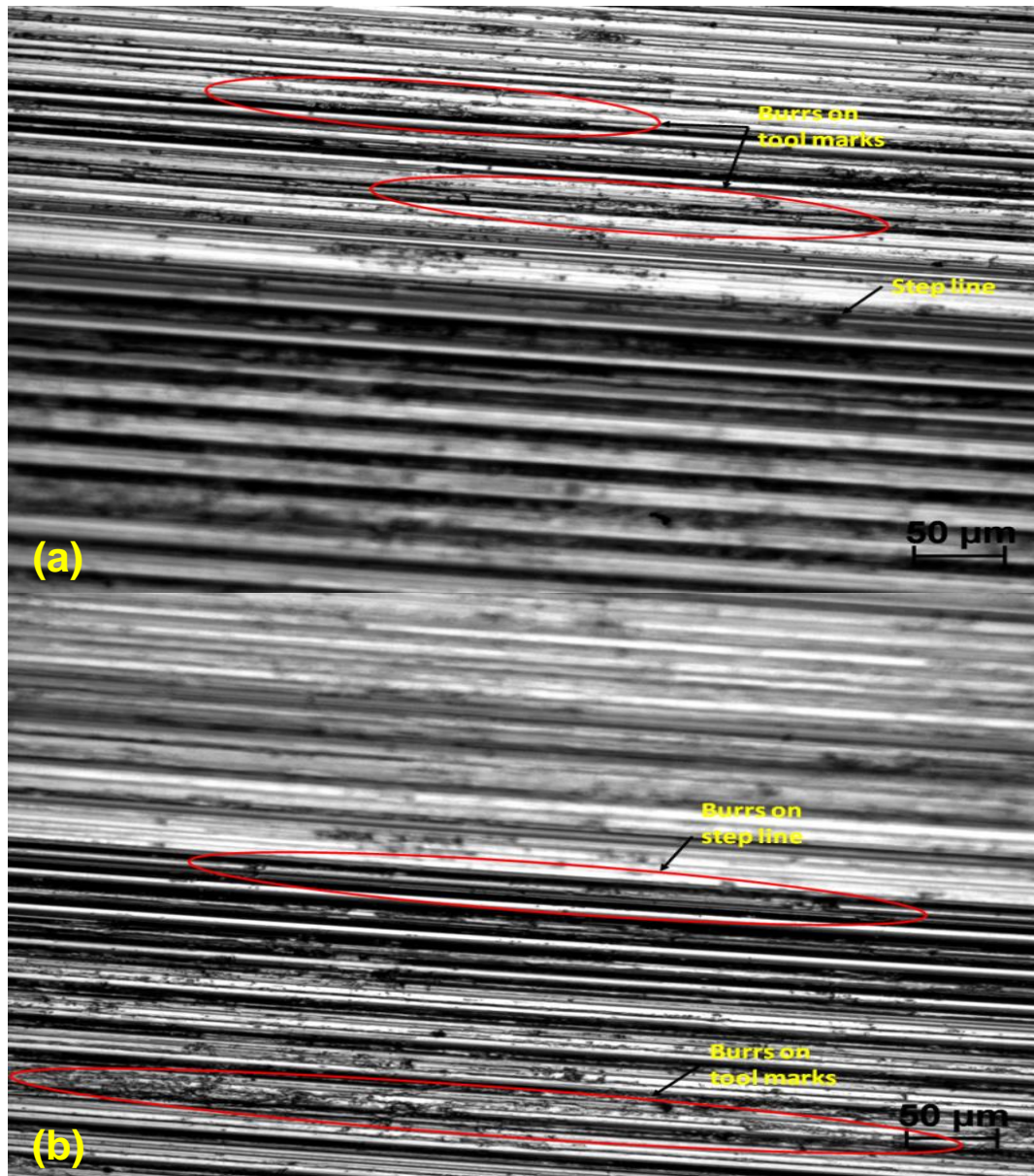
Figure 4.20 The normal cutting of micro-squared slot of the first case study ((a) and (b) showing the different focuses due to the different heights of the machined surface)
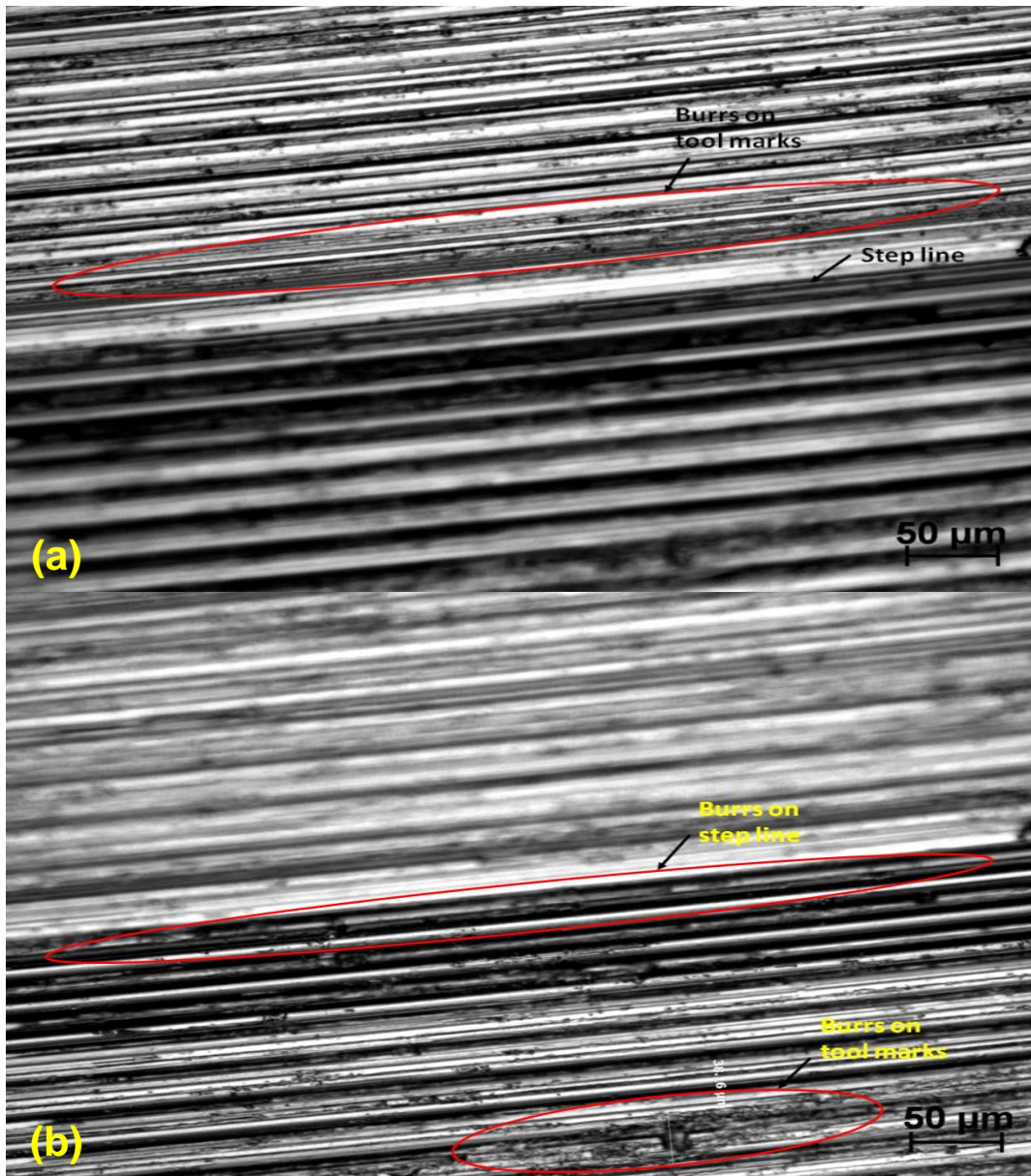
Figure 4.21 The hysteresis compensated cutting of micro-squared slot of the first case study ((a) and (b) showing the different focuses due to the different heights of the machined surface)
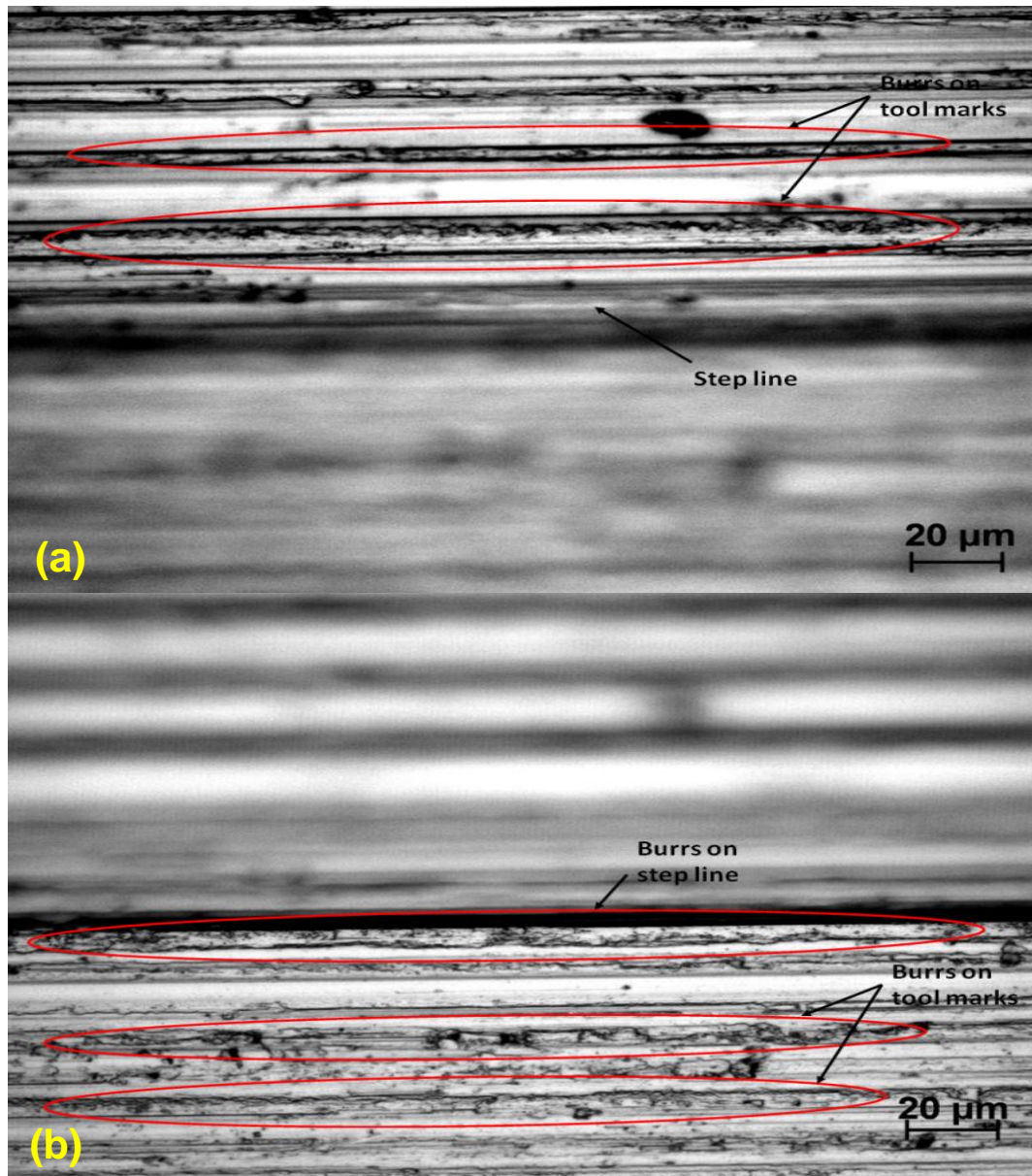
Figure 4.22 The normal cutting of micro-squared slot of the second case study ((a) and (b) showing the different focuses due to the different heights of the machined surface)
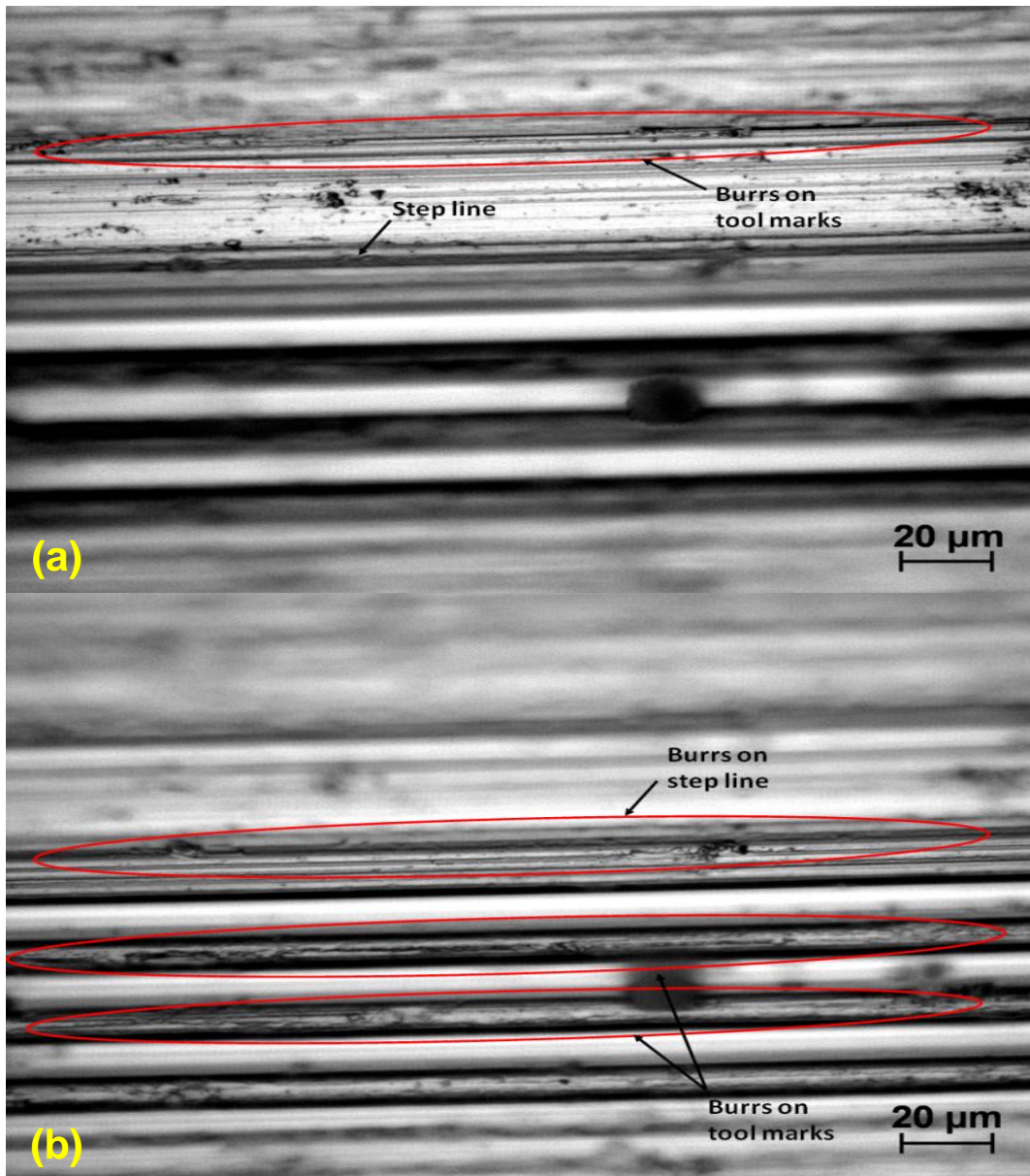
Figure 4.23 The hysteresis compensated cutting of micro-squared slot of the second case study ((a) and (b) showing the different focuses due to the different heights of the machined surface)
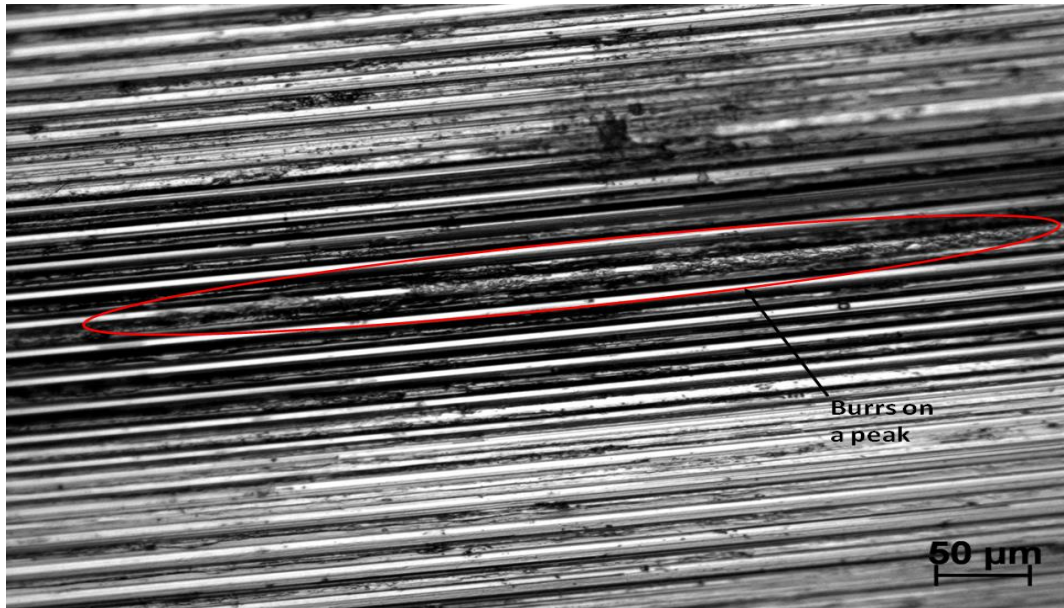
Figure 4.24 The normal cutting of micro-triangle slot (V-shaped slot) of the third case study
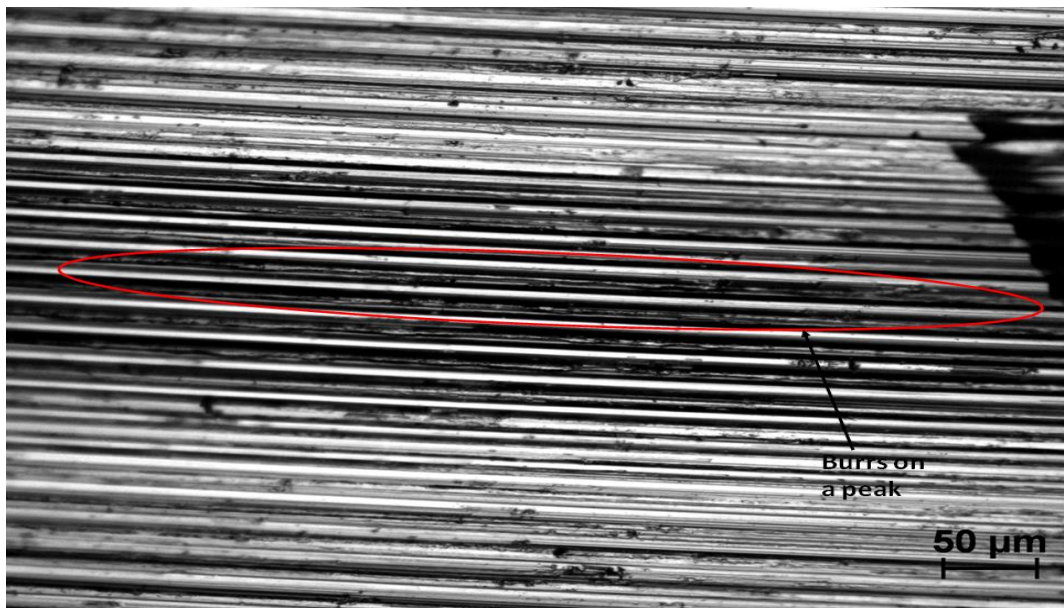
Figure 4.25 The hysteresis compensated cutting of micro-triangle slot (V-shaped slot) of the third case study

4.7 Discussion of experimental results

This chapter describes the sets of experimental cutting on three case studies of micro-featured slots, implemented to define and investigate the dynamic stiffness and its effects in micro cutting. The ultimate outcome is syntax

confirmed and possible counter act each other that the micro-featured slot dimensional errors and burrs formation could be influenced by dynamic stiffness. Consequently, they can be minimised by well-controlled and optimised dynamic stiffness of cutting process. In other words, the smaller the dynamics stiffness, the higher slot accuracies and lesser burrs formation can be achieved. The discussions, conclusions, and further suggestions are given as followed.

4.7.1 Micro slots accuracy

(1) The dimensions of the micro slots conform well with the desired dimensions when the dynamic stiffness is controlled and optimised by the hysteresis compensated cutting as observed from case studies 1 and 3 in Figures 4.15 and 4.19 as illustrated, respectively.

(2) The micro slot errors for the second case study are difficult to control. In other words, the accurate amplitude of micro slots cannot be observed on both normal and even hysteresis compensated cutting as illustrated in Figures 4.16 and 4.17. As the second case study is carried out with the depth of cut of 5 μm by CNC programming, plus superimposed with another 10 μm resulting from control of the cutting tool with the FTS in order to perform the amplitude and contours of micro-squared slot, this may cause the duplicated control of cutting tool movements and consequently the total machining errors for the whole cutting period. Therefore, consequently inaccurate amplitude of micro-featured slots is obtained for second case study.

(3) Although micro-triangle slots of the third case study were machined by the depth of cut of 3 μm, and superimposed with another 10 μm by FTS as similar to the second case study, micro slots dimensions are still accurate and well-controlled. This may be caused by the peak and valley of triangle slots being too small an area which cannot be comparable to the peak and valley areas of square slots. Therefore, the total machining errors would not have too much affect to machining accuracies; consequently the hysteresis compensated cutting could help in improvements of the accuracy of micro-triangle slots as observed in Figure 4.19.

4.7.2 Burrs formation

(1) The burrs can be clearly observed through the lines on top of the peaks and valleys of square and triangle slots. In addition, burrs can be observed on areas of peak and valley of micro-featured slot which resulted from tool marks when machined with the normal cutting. The observations can be made for all cases study in Figures 4.20, 4.22 and 4.24, respectively.

(2) Once hysteresis compensated cutting was employed, burrs were reduced on both the lines on top and areas of peak and valley of square and triangle slots as was observed from cases study 2 and 3 in Figures 4.23 and 4.25.

(3) However, the different burrs formation between normal and hysteresis compensated cutting can be observed when conducted on the first case study as seen in Figures 4.20 and 4.21. This may be caused by the first case study, machined without depth of cut, consequently the surface, particularly at areas of peak and valley of micro-squared slot, were possibly not cut by the diamond tool. Thus, the burrs which were left by previous cuts remain on the machined surface. Subsequently, the hysteresis compensated cutting cannot help to minimise the burrs as observed in Figure 4.21.

4.8 Conclusions

The dynamic stiffness in the dynamic micro cutting process affects the cutting performances, particularly the machining accuracy and burrs formation. The dynamic stiffness is thus formulated and quantitatively analysed. The effects of dynamic stiffness i.e., micro slot errors and burrs formation can be minimised by the employed hysteresis compensated module to manipulate the dynamic movements of cutting tool and consequent control and optimisation of the dynamic stiffness. Finally, the improvements of machining accuracy and burrs formation can be achieved by benefits of study on dynamic stiffness.

The worn cutting tool with built up edges, cracks and defects, which can cause the poor quality of machined surfaces and micro burrs on any tool marks, was used in this experimental investigation. This used cutting tool may result in influence on the quality of machined surface rather than dynamic stiffness

effects. Therefore, it is difficult to investigate how the dynamic stiffness influences the surface roughness by using worn cutting tools. Similarly, there is no clear evidence of the different qualities of machined surface between normal and hysteresis compensated cutting. Thus, in order to thoroughly investigate the machined surface quality of micro-featured slots in correlation to dynamic stiffness, an unworn diamond tool should be employed.

Chapter 5 Cutting force modelling using specific cutting forces and its implementation

5.1 Introduction

Cutting forces have always been used to analyse the cutting process behaviour and cutting performances including the cutting mechanics, chip formation, surface generation and the machined surface roughness, size effects and tool wear, since it can represent the complex cutting process behaviour collectively even with more than a dozen of process variables. Direct measurement using a dynamometer through real cutting trials is useful in evaluation and validation of the cutting forces modelling, robust cutting force models are essential in the cutting process optimization and control. The cutting forces in diamond turning play an important role in characterising the cutting mechanics and physics including chip formation, surface generation, and tool wear, which are similar to those aspects in conventional cutting namely but quite different in scale, i.e. normally 1000 times smaller but at the 0.1-1 N scale (Lee & Cheung, 2003), and the consequent micro cutting mechanics and physics.

In recent years, a number of researchers have been working on cutting force modelling for diamond turning in particular. Table 5.1 lists the proposed cutting force models and their respective characteristics. However, these models highlighted in Table 5.1 are formulated through approaches aiming at the absolute value of cutting forces and the associated quantitative analysis, which is same as the modelling approach employed in conventional metal cutting. This obviously causes the problem of low accuracy and difficultly measuring the cutting forces encountered in ultraprecision and micro cutting processes.

The micro cutting force model, due to the ploughing forces in micro cutting processes cannot be fully represented in the macro cutting model. In addition, the dynamic component effects on the cutting process have not been

thoroughly investigated yet (Chae, et al., 2006). The specific cutting force has been used by a few studies in investigating the micro cutting phenomena, for instance, Kim et al (Kim & Kim, 1995) analysed the effect of negative rake angle of the rounded edge of the tool, and the friction due to the elastic recovery of the workpiece at the clearance face. Their analysis compared the cutting force per unit width (N/mm) of two orthogonal micro cutting models. However, it has not been used for investigating the micro cutting mechanisms generically.

Currently, ultraprecision and micro cutting using diamond tools is becoming increasingly one of determinant micro manufacturing technologies at an industrial scale, e.g. applied in machining i-Phone frames, vary focus glasses, and silicon-based infrared devices, etc. The accurate and robust cutting force modelling is needed for predicting, analysing and better understanding of ultraprecision and micro cutting processes. A novel approach to cutting forces modelling is essential for coping with the new industrial requirements on productivity, industrial volume and quality. The modelling approach should have the underlying significance for the process optimization and optimal design of cutting tools against the tool wear and tool life, and for future ultraprecision and micro cutting processes.

In this research, an innovative cutting force modelling approach is proposed for ultraprecision and micro cutting based on the specific cutting force at the unit length or area and the cutting force analysis against a short dynamic interval of cutting time. The specific cutting forces at the unit length or area is called the amplitude aspect of the model formulation, while the forces analysis against a short cutting time interval is called the spatial aspect of the formulation. The micro cutting mechanics and physics especially chip formation and size-effects were analysed and interpreted by the modelling amplitude aspect. The spatial aspect analysis on tool wear monitoring in single point diamond turning (SPDT) was carried out using wavelet transform technique associated with standard deviation analysis. The proposed cutting force modelling approach can likely be used for investigating the future micro cutting mechanics and physics at 0.1-1N scale of micro cutting forces and beyond.

Table 5.1 Summary of the cutting force models for diamond turning and micro cutting as developed in recent years

Methodology	Author	Cutting force modelling	Benefits	Correlation analysis with tool wear	Methodology analysis	remarks
Experimental based	Lee (Lee, et al., 2002)	microplasticity model	predicted the pattern of cyclic variation of cutting forces in diamond face turning	Not included	Power spectrum analysis	
	Moriwaki (Moriwaki, 1989)	cutting force model	Determined relationship between the principle force and thrust force varied with very small depth of cuts	Not included	Experimental measurements data discussions	
	Drescher (Drescher & Dow, 1990)	A quantitative model relationship between tool edge sharpness and tool forces.	predicted the diamond tool edge condition from tool forces during a turning operation		Experimental measurements the absolute forces	
	Scheffer (Scheffer & Heyns, 2001)	time-series model coefficients (based on data collection of 3 directions signals: X-feed force, Y- thrust force, and Z-Acceleration signal)	tool condition monitoring (TCM)		Correlation coefficient approach (based WPD analysis) & The self-organising map (SOM)	
	Fang (Fang, et al., 2012)	Correlation of tool-edge wear with the cutting forces and vibrations model	detected the tool-edge wear		wavelet packet transform	high-speed turning (diamond turning not included)
	Dornfeld (Dornfeld, 1990)	multilayered perceptron type neural network model (based on raw signals from the **AE,** force, and the current sensors)	on-line tool wear monitoring system		multichannel autoregressive **(AR)** & artificial neural network	
Numerical based (FEA)	Lo-A-Foe (Lo-A-Foe, et al., 1988)	the forces relationship numerical model	estimated the surface roughness of SPDT	Not included	Cutting experiments to evaluate the model	
	John (III & Strenkowski, 1988)	FE-based cutting process model	determined the detailed stress and strain fields, chip geometry and tool forces	Not included	Lagrangian model & Eulerian model (based FEA)	
	Ravindra (Ravindra, et al., 1993)	mathematical models: wear-time and wear-force relationships	Estimated progressive tool wear-force relationships		Multiple regression analysis & cutting experiments validation	diamond tool not included
Mechanics based	Kim et al (Kim & Kim, 1995)	two orthogonal micro-cutting models comparison (based on cutting force, thrust force)	Determined 2 factors (elastic recovery & tool edge radius) which effect on micro-cutting with under 1 µm (or less) depth of cut	Not included	Comparison between simulation results: cutting/thrust force per unit width (N/mm) & specific cutting/thrust force (N/mm^2) and the experimental results of the others	

5.2 An innovative cutting force modelling approach

The micro cutting forces are usually quite small down to 0.1-1N scale and have different cutting mechanisms when compared with those in conventional cutting. Consequently, there is the difficulty and low accuracy in representing the micro cutting mechanics, such as the chip formation, size effect and tool wear mechanism, etc, by using conventional cutting force models. Therefore, the innovative cutting force modelling is proposed instead of using the absolute micro cutting forces, which can provide an insightful quantitative analysis on the micro cutting mechanics especially in SPDT operations. This modelling approach is represented using two aspects of modelling formulation as follows:

$$F_{Novel} = \begin{cases} \frac{F}{\Delta l}, \frac{F}{\Delta A} & \text{amplitude aspect} \\ \int_{\Delta t_0}^{\Delta t_1} F dt & \text{spatial aspect} \end{cases} \quad (5.1)$$

The amplitude aspect of the formulation is the specific cutting force at the cutting edge, i.e., cutting force against the unit length or area where the cutting tool and the workpiece engaged each other; while the spatial aspect of the formulation represents the dynamic analysis of the cutting force against the varied instant cutting time interval but in a cyclic frequency domain. The two aspects are taken into account simultaneously but assessed respectively against axiomatic principles of mechanics and dynamics.

5.2.1 Amplitude aspect of the modelling formulation

The amplitude aspect of the formulation presents the specific cutting force defined as the cutting force at the unit cutting area or length. In order to obtain tool-chip contact length, the theoretical cross section of chip in conventional diamond fly cutting is adopted as illustrated in Figure 5.1. Moriwaki (Moriwaki, 1989) expressed the length of the cutting edge contact with the workpiece in diamond turning as:

$$L = R(\cos^{-1}\frac{(R-t)}{R} + \sin^{-1}\frac{f}{2R}) \quad (5.2)$$

Where R is the tool noise radius (mm), t is nominal depth of cut (μm), and f is feed rate (mm/rev) respectively. The specific cutting area (A) can be obtained as $L \times f$ (mm^2). Therefore, the specific cutting force at the unit cutting area or cutting contact length can be formulated as:

$$F_{sfA} = \frac{F}{\Delta A}, \; F_{sfL} = \frac{F}{\Delta L} \hspace{4cm} (5.3)$$

Where F_{sfA} is specific cutting force at the unit cutting area (N/mm^2), F_{sfL} is specific cutting force at the unit cutting contact length (N/mm), and F is cutting force (N) respectively. The analysis on amplitude aspect of the cutting force modelling approach can provide a better insight to the micro cutting mechanics especially linked to the chip formation and size effect.
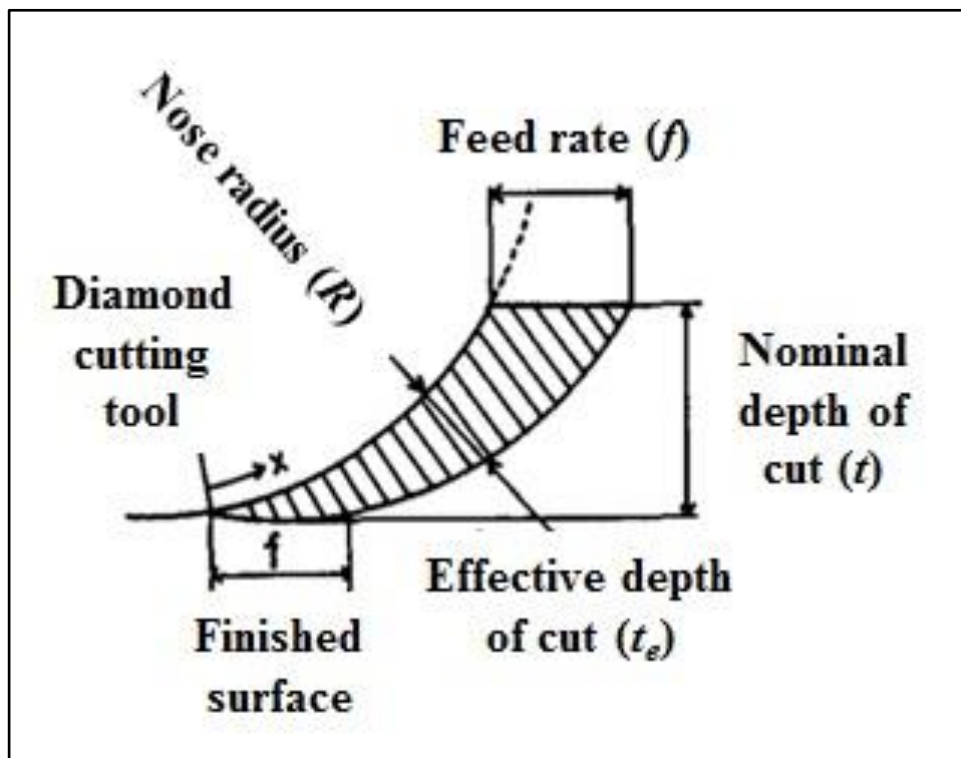
Figure 5.1 Illustration of theoretical cross section of the chip

5.2.2 Spatial aspect of the modelling formulation

The variation of the cutting force against a short cutting time interval in a dynamic cyclic frequency domain is considered as a spatial aspect of the modelling formulation. It may imply significant information about the dynamic cutting process and its dynamic effects on tool-workpiece interface. For instance, although the cyclic dynamic changes of the cutting force are minimal using the amplitude scale, their changing frequencies and orientations can be studied against the instant cutting time intervals, i.e. in a dynamic cyclic manner. This can cause dynamic cyclic stress at the tool-workpiece interface and consequent fatigue, which leads to the tool wear even in diamond cutting tools through the tool-workpiece interface. Therefore, the spatial aspect of the formulation can be used for correlation analysis with the tool wear particularly in ultraprecision and micro cutting processes where the dynamic micro cutting force plays a critical role in causing the diamond tool wear. By monitoring and understanding the spatial aspect of the cutting force modelling formulation will provide the industrially-feasible means to measure and monitor the tool wear in process, which is increasingly important in ultraprecision and micro machining at an industrial scale.

5.3 Experimental and cutting trials setup

The cutting experiments were conducted using the diamond turning test rig as shown in Figure 5.2. The cutting was setup to be six face turning operations repeated on each material including single-crystal silicon, titanium Ti-6Al-4V, and aluminium AA 6082-T6 with diameter and thickness equal to 60 and 10 mm. respectively. The first cuts on each material was performed by a sharp cutting tool with the same cutting conditions as depth of cut (a_p) 10 µm, constant surface speed (V_c) 100 m/min., and feed rate (f) 5 mm/min. respectively. The feed and cutting forces were recorded by Labview data acquisition through the NI DAQ 9234 card. The sampling frequency was set as 4,000 Hz to observe the frequency range of 0 to 2,000 Hz. The details of experimental planning can be found in section 3.2.2.
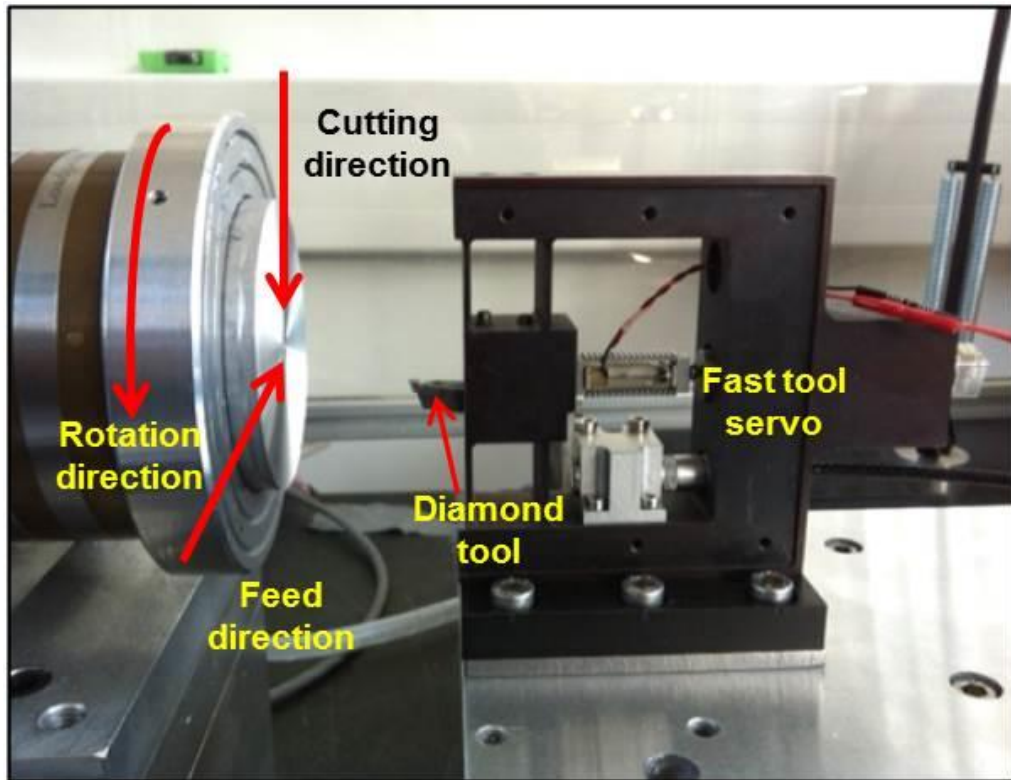
Figure 5.2 Schematic of diamond turning test rig equipped with the fast tool servo (FTS)

5.4 Amplitude aspect applied to micro cutting mechanics

5.4.1 Interpretation of chip formation mechanism

Since the absolute cutting force is very small, reported as 0.1-1 N at micro cutting scales, it cannot be reasonably interpreted, how these very small forces can be used to split the workpiece material in a chip formation mechanism. Thus, amplitude aspect of the formulation using the specific cutting force at the unit cutting area is then proposed for better interpretations of the micro cutting mechanics phenomena e.g. chip formation instead of using absolute forces. In order to determine specific cutting force as proposed in eq. 3, the tool-chip contact length and cutting area is required to calculate by determining important parameters as described below.

Feed force of cutting single crystal silicon
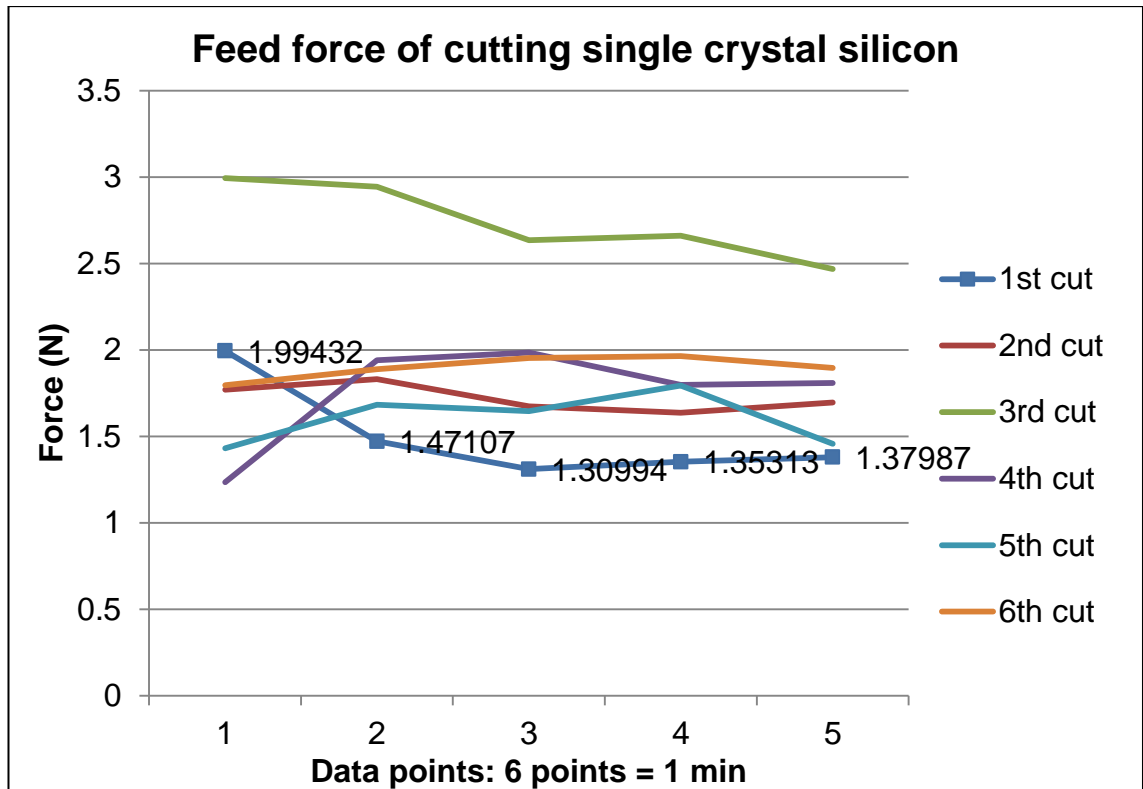
Figure 5.3 Trends of feed forces in cutting single crystal silicon from the first to sixth cut

The tool noise radius was measured by the Tesa-Scope profile projectors which equal to 0.385 mm. The depth of cut, constant surface speed, and feed rate in the real experiment were equal to 10 µm, 100 m/min, and 5 mm/min respectively. The silicon workpiece diameter is 60 mm. Thus, the feed per revolution can be approximated as equal to 0.01 mm/rev. Accordingly, contact length and cutting area can then be calculated as about 93 µm and 930 µm^2, respectively.

Due to the cutting process at very small cutting scales, the sufficiently specific force is needed until the chip can be formed and separated away from the workpiece. Thus, a material property is needed in order to be used as an identified criterion in comparison to this calculated specific cutting force. Consequently, In order to know how much specific force would be for separating chips, the ultimate strength property is selected in comparing to specific cutting force at the unit area (F_{sfA}).

The cutting process was mainly dominated by the feed force rather than cutting force in this experimental investigation. Thus, feed force is selected for using in calculation of specific cutting force as expressed in Equation 5.3. Moreover, In case of the lowest specific cutting force, it might occur in anywhere during cutting processes. Subsequently, in order to verify this lowest specific cutting force can overcome the ultimate strength of the selected material, the lowest of cutting force should be selected in specific cutting force calculation. Therefore, the lowest feed force at 35 seconds of the first cut on silicon is 1.30994 N (as shown in Figure 5.3) which is selected and used in this calculation to compare with the identified criteria. The specific cutting force at the unit area can then be calculated as:

$$F_{sfA} = \frac{F}{A} = \frac{1.30994}{930 \times 10^{-6}} = 1408.5 \text{ N/mm}^2 \text{ or MPa}$$

The ultimate strength of silicon wafers tested by previous report (Rupnowski & Sopori, 2009) is 125 MPa. Consequently, It can be seen that the F_{sfA} is much larger than the ultimate strength of single crystal silicon. In the other words, this specific cutting force at the unit area easily overcomes the material Young's modulus, and then chip can be easily formed.

5.4.2 Interpretation of size-effect phenomenon

Figure 5.4 illustrates the FE-based simulation being developed to validate the cutting experiments especially in interpreting the size effect by considering the cutting force against the cutting contact length which is equal to chamfer length. All the cutting conditions were set as similar to the experimental setup. In other words, the 2D FE model and simulation setups of depth of cut (a_p) equal to 10 µm, and cutting speed 1667 mm/sec in the cutting direction (Figure 5.4) which comparative to constant surface speed (V_c) 100 m/min of experimental setup. The chamfered tool was used in the FE model and simulation due to the simplest model being required, and also the complicated simulation procedure and consequent inaccurate model and simulation result is essentially avoided. The chamfer lengths at the tool tip varies with rake angles (α) were carried out in order to simulate and depict trends of cutting force and specific cutting force

at every steps time interval of 5.0 x 10^{-6} sec. for total simulation time of 10^{-4} sec. the details of physical properties of diamond tool and workpiece and constitutive material modelling of workpiece are given in table 5.2-3. The FE simulation details and procedures can be found in section 6.2.

Table 5.2 Physical properties of AA6082-T6 and diamond tool

	E(Gpa)	v	c(J/kg^{o}C)	ρ(kg/m^3)	K(W/m^{o}C)
AA6082-T6	70	0.33	896	2,700	180
Diamond tool	1,050	0.1	420	3,520	1,000

Table 5.3 Johnson-cook constitutive material model parameters for AA6082-T6

A	B	C	n	m	$\dot{\overline{\varepsilon}}_0$	T_{melt}
403.57	306.56	0.00185	0.7769	1.73	0.00419	855

The simulation outcomes are presented a significant analysis of micro cutting phenomena particularly in the size effect interpretation as illustrated in Figures 5.5 and 5.6.
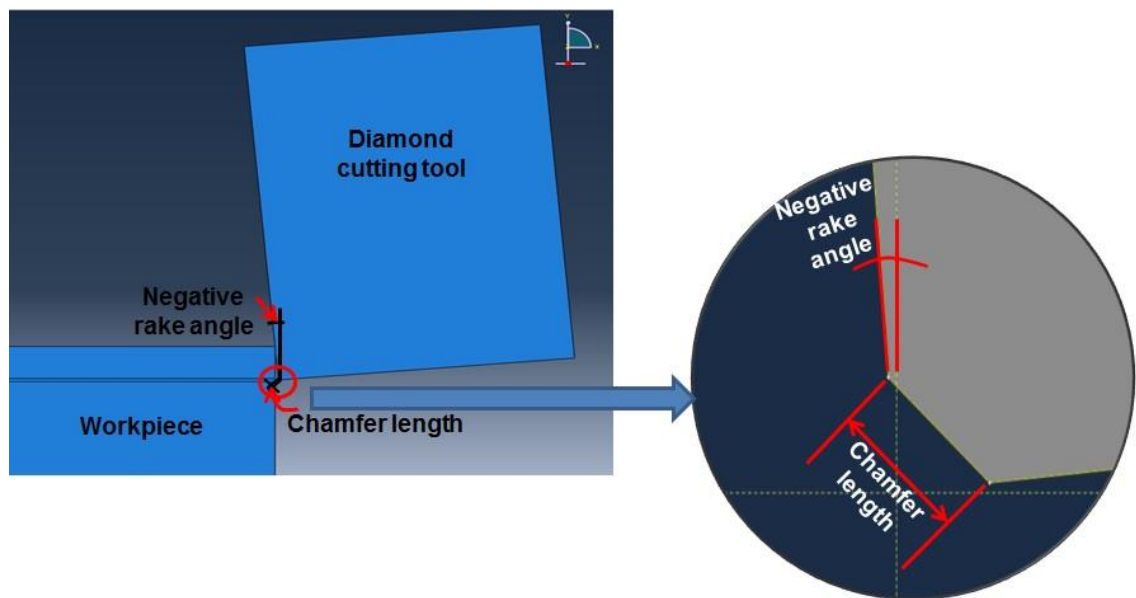
Figure 5.4 Illustration of chamfer length against to rake angle variation on cutting aluminium AA6082-T6 by FE-based simulation
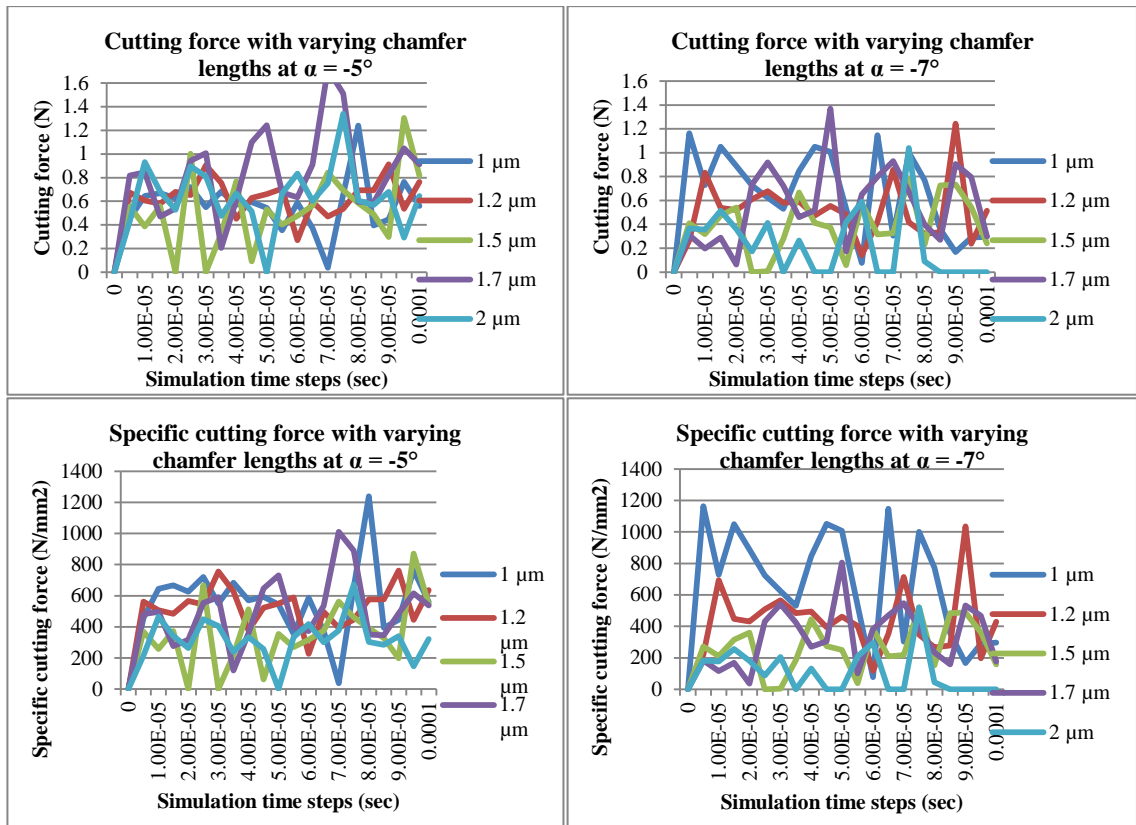
Figure 5.5 Simulation results on cutting aluminium AA6082-T6 show variation of cutting and specific cutting forces at different chamfer lengths of the tool tip with rake angle -5° and -7° for 10^{-4} seconds of simulation time interval

As shown in Figure 5.5, the trends of cutting forces on both α = -5° and -7° seem similar to each other when conducting simulation by varying chamfer lengths from 1 to 2 μm. However, the increasing trends of specific cutting force were observed while reducing the chamfer lengths specially when applied α = -7° (as seen in Figure 5.5: bottom-right). In order to more clearly depict these trends, the average cutting and specific cutting forces were performed as depicted in Figure 5.6. It is clearly seen that the cutting force at α = -7° trends to be decreasing when chamfer length is increasing while the cutting force at α = -5° is stable along all chamfer lengths. Meanwhile, the specific cutting force on both rake angles dramatically increase especially for α = -7° when the reducing of chamfer length is applied. In other words, the cutting pressure and cutting force are increasing while the contact length is decreasing especially when more negative rake angle is employed. This is a corresponding correlation to the size effect in micro cutting.
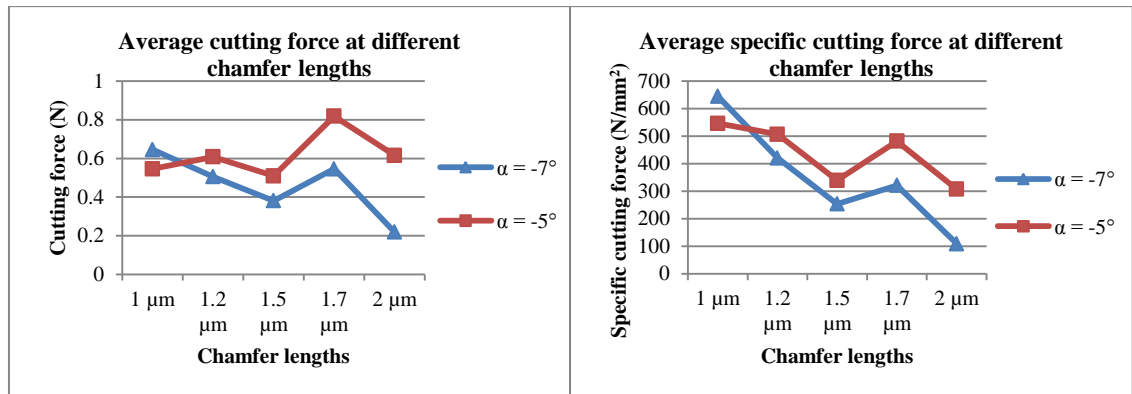
Figure 5.6 The average cutting and specific cutting forces at different chamfer lengths compared between rake angles -5° and -7°

The scientific investigations on size effect were proposed by numerous studies (Liu, 2005; Cheng & Huo, 2013; Ikawa, et al., 1991; Dornfeld, et al., 2006; Ng, et al., 2006). They stated that when the tool edge radius is comparable to the undeformed chip thickness in micro cutting, the specific cutting energy (or specific cutting force) will be increasing nonlinearly as the undeformed chip thickness is decreased. Furthermore, the negative rake angle has significant effects on the size effect in specific cutting energy. In this study, if chamfer length is comparable to the undeformed chip thickness, the reducing chamfer length consequently leads to higher specific cutting force as theoretically aforementioned. The negative rake angle in this simulation outcome also has influences on size effect that; the more negative rake angle applied, the higher specific cutting force and energy dominate the cutting process as illustrated in Figure 5.6. This may be claimed that the amplitude aspect of the model formulation using specific cutting force at the unit contact length can interpret size effect in micro cutting better than using only absolute cutting force. Finally, the comparison of experimental cutting and FE-based simulation validation has also been performed to show that the simulation is in agreement with the cutting trials as illustrated in Figure 5.7.
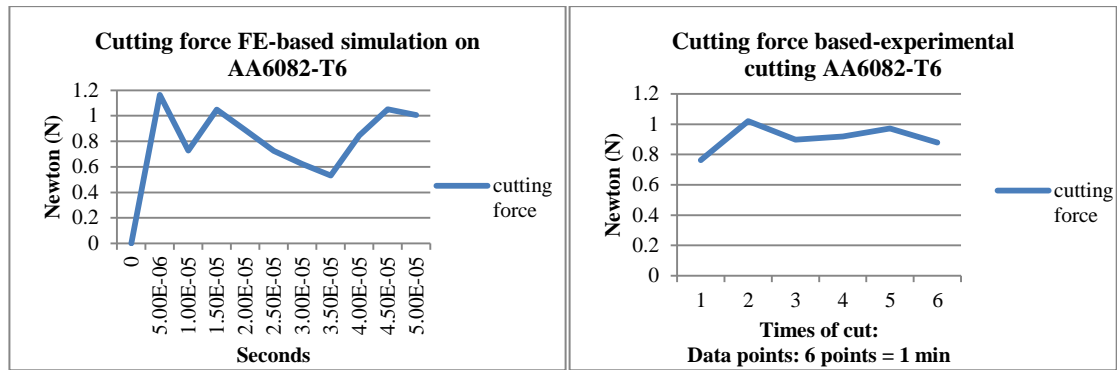
Figure 5.7 The experimental cutting and FE-based simulation validation of diamond cutting on aluminium AA6082-T6

5.5 Spatial aspect applied to correlation analysis with tool wear

The application case study in correlation to tool wear monitoring and analysis can be conducted according to the spatial aspect using the dynamic analysis of the cutting force against the varied instant cutting time interval. This analysis was implemented by the wavelet transform techniques in correlation to standard deviation analysis which can possibly detect the status and feature of tool wear. Firstly, the Daubechies wavelets (dbN) are basically suitable for detecting abruptly changing frequency in a signal. The higher order N of the wavelet, the more complicated signal processing is required (Wang, et al., 1998). Thus, the db3 was selected and used for analysing the wavelet coefficients and consequently theirs standard deviation of feed and cutting force signals of cutting single crystal silicon. The standard deviation of raw signal (S) and the different wavelet coefficients included its low frequency component or approximation (A1), and high frequency components or details at level 1 (D1) to level 4 (D4) were implemented. These approximation coefficients at level 1 (A1) and detail coefficients at level 1 (D1) to level 4 (D4) were extracted through Labview programming. Figure 5.8 shows the standard deviation of raw signal and its different wavelet coefficients at level 1-4 of feed and cutting forces, respectively.
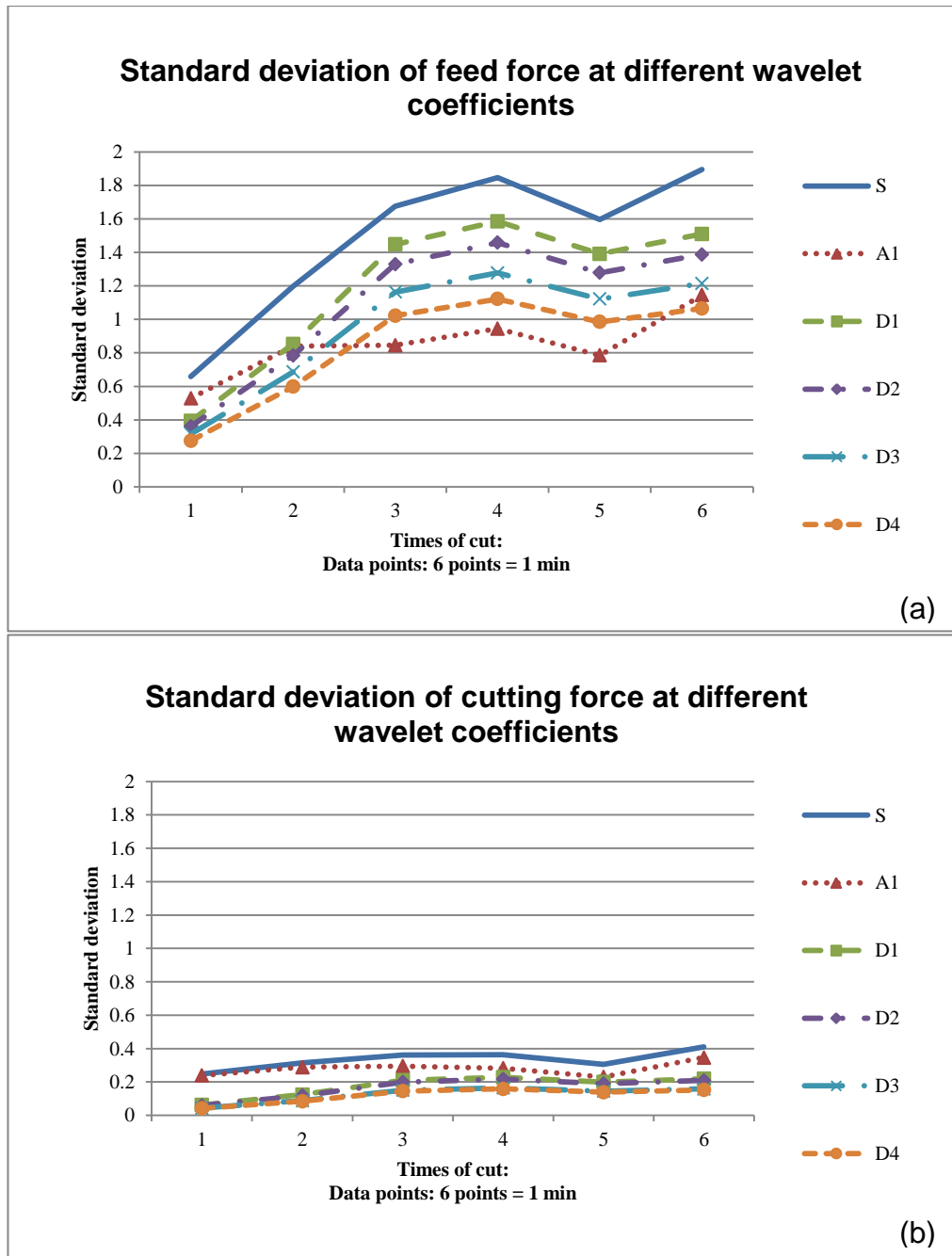
Figure 5.8 Standard deviation of raw signals of feed (a: top) and cutting (b: bottom) forces, and theirs decomposition at different wavelet coefficients

As shown in Figure 5.8, the shapes of D1 (Figure 5.8.a) and A1 (Figure 5.8.b) are the most similar trends to their raw signals (S) namely feed force (Figure 5.8.a) and cutting force (Figure 5.8.b), respectively. Thus, the D1 of feed force and A1 of cutting force are selected to further investigate how these components significantly affect the cutting process outcomes and the corresponding tool wear. Accordingly, the force signals acquisited are analysed by decomposing the approximation coefficient (A1) of cutting force and detail

coefficient (D1) of feed force for the first cut to last cut (sixth cut) on silicon wafer with new tool as illustrated in Figure 5.9.

As shown in Figure 5.9, the amplitude of wavelet coefficients at D1 of feed force is dramatically increased until the third cut (about 1.8 to 7) which caused by higher frequency bands at higher levels (Wang, et al., 1998), then slightly increased from the third to the last cut (about 7 to 9). Meanwhile, the amplitude of wavelet coefficients at A1 of cutting force is slightly increased from the first to last cut, or even quite similar level at some cuts. Therefore, it can be assumed that the feed force mainly dominates the cutting process outcomes and subsequent cutting tool wear rather than the cutting force. Consequently, tool wear can be caused by feed force since the first cut is taken. SEM micrographs are also taken after the last cut in order to validate tool wear observations. In agreement with the results, the micro-fracture and the flank wear in the feed direction are observed while there is no crater wear in cutting force direction as shown in Figure 5.10. Thus, it may be claimed that the diamond tool wear is mainly caused by feed force in feed direction when cutting on single crystal silicon with the cutting conditions as aforementioned setup.
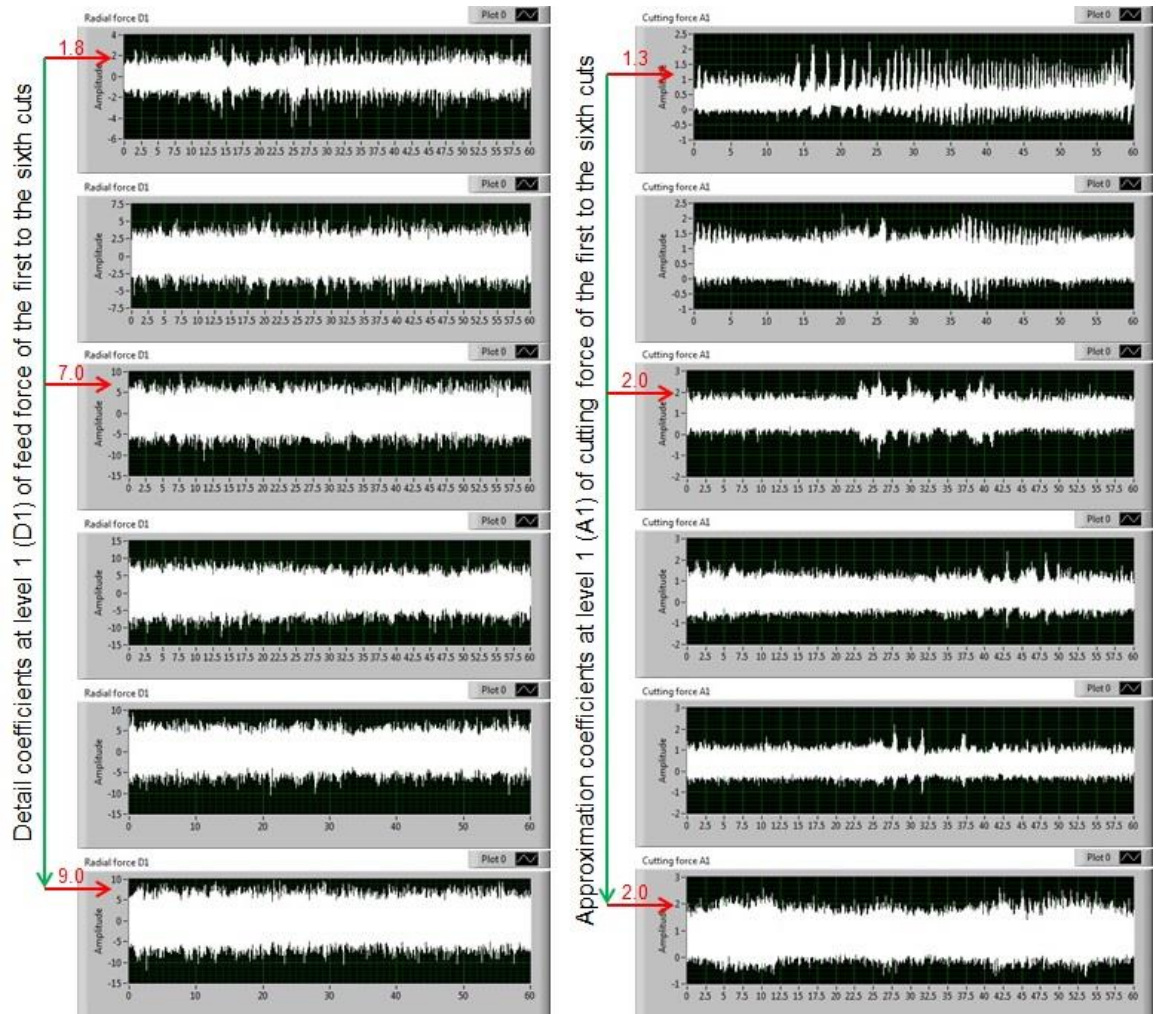
Figure 5.9 Computation of wavelet coefficients at D1 of feed force, and A1 of cutting force respectively from 1st to 6th cut (top to bottom) of diamond turning on single crystal silicon within 1 min (60 data points)

Further investigations on micro cutting of titanium Ti-6Al-4V and aluminium AA6082-T6 have been conducted to compare with cutting silicon, this investigates how the forces react relative to tool wear. Thus, the feature extraction and analysis of the high frequency component or the detail coefficients of both feed and cutting forces of titanium and aluminum cutting were conducted. Clarifying the cutting force signal with the increasing wavelet levels, is easier for detecting tool failure from signal analysis (Kwak, 2006). Therefore, the selection of detail coefficients at level 4 (D4) was performed in this investigation due to its highest wavelet level in this case study. Thus, the standard deviation of feed and cutting force signals decomposition through the

detail coefficients at level 4 (D4) of cutting Ti and Al with a new tool were carried out.
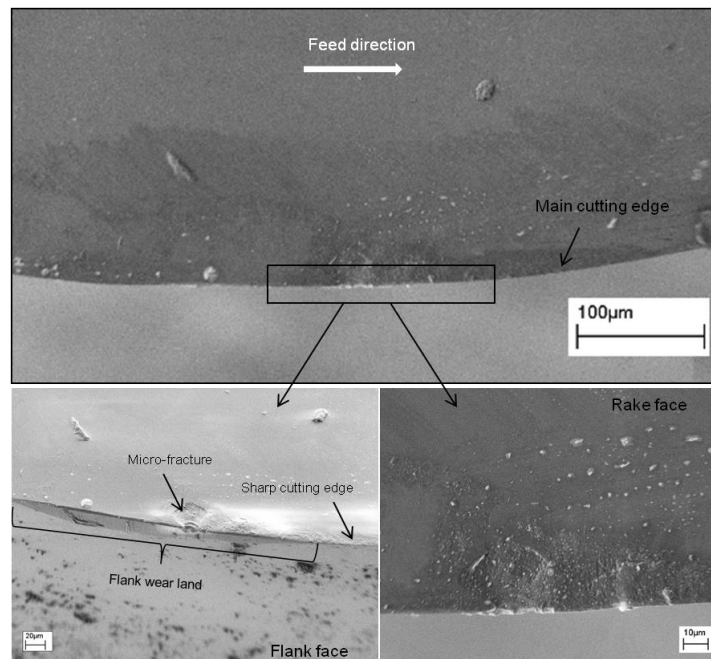
Figure 5.10 SEM photographs of the cutting edge taken after the sixth cut

It is observed that there are small changing trends of standard deviation on both feed and cutting forces of Ti and Al. It is slightly increased by 0.01 on both of them for all cuts as illustrated in Figure 5.11. Thus, it may imply that there is no significant effects on the tool wear. Correspondingly, no wear was observed after the sixth cut on both Ti and Al confirmed by SEM observation. Furthermore, the standard deviation of cutting force on Al is higher than radial force for all cuts. This may cause crater wear rather than flank wear if longer cutting distances (or cutting time) are sufficiently taken for tool wear to occur. Meanwhile, standard deviations on both feed and cutting forces have almost the same trends when cutting of Ti. Thus, it might be assumed that the flank and crater wear have equal possibility to occur when approaching the minimum number of cuts which are required for tool wear. In addition, It might be noted that the possibility of reaching a tool wear state when cutting titanium is faster than aluminium due to Ti cutting having higher standard deviation than Al cutting on both feed and cutting forces.
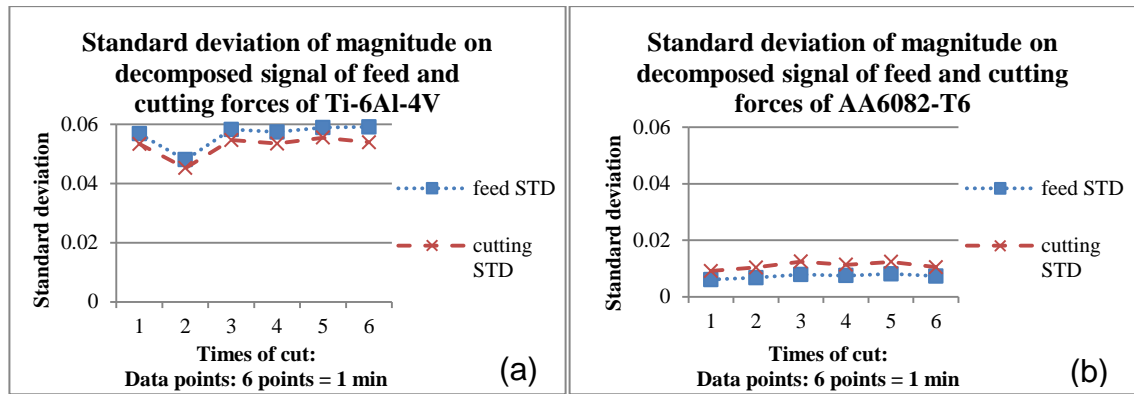
Figure 5.11 Standard deviation of magnitude on decomposed signals of feed and cutting forces of Ti-6Al-4V (a) and AA6082-T6 (b) cutting

5.6 Conclusions

An innovative cutting force modelling approach is proposed based on the amplitude and spatial aspects of cutting forces formulation, so as to better interpret the micro cutting mechanics and physics including chip formation, size effect, surface generation and tool wear in single point diamond turning. The amplitude aspect of the modelling formulation is defined as the cutting force at the unit area or contact length. The micro cutting phenomena especially on chip formation and size effect can be better interpreted by using the amplitude aspect. The spatial aspect is analysed as the cutting force at a short cutting time interval, which can provide a better insight into the dynamic variation of cutting forces and its correlation to tool wear. The application of spatial aspect on the tool wear detection is carried out by using WT techniques correlated with standard deviation analysis. The analysis on standard deviation of feed and cutting force signals decomposition is capable for detecting tool wear in process and being useful in classifying the tool wear. The cutting force modelling approach as a whole can be used as a powerful means to investigate future ultraprecision and micro cutting processes in the industrial scale.

Chapter 6 Partitioned distribution of cutting heat/temperature in micro cutting

6.1 Introduction

Cutting temperature in micro cutting can play a significant role in the machining performance particularly on tool wear, surface generation and integrity, and machining accuracy (Kim, et al., 2012). Even when only small amounts of heat in micro cutting can occur, it should not be neglected because the temperature is comparably high in the small cutting zone, area or volume. Many works have attempted to study the effects of the cutting temperature on the micro cutting processes including the tool wear, quality of machined surfaces, and machining accuracy. For instance, Ikawa et al (Ikawa, et al., 1991) stated that even a small increment of cutting temperature can cause an expansion of the tool shank and in turn, deterioration of the machining accuracy. Furthermore, it governs the wear rate of a diamond tool which is fatal to the machined surface roughness. Kim et al (Kim, et al., 2012) proposed that the quality of micro cutting features can be maintained by reducing the tool wear and generation of cutting heat in the micro cutting process under various cutting lubrication conditions. Moriwaki et al (Moriwaki, et al., 1990) stated that the machining error by the cutting heat is not negligible even in micro diamond cutting based on their experimental and theoretical analyses of the thermal deformation of the cutting tool and workpiece as a result of the cutting heat. Chen et al (Chen, et al., 2013) studied a set of micro cutting experiments by measuring the cutting temperature in the micro cutting process with a fast-response high accuracy thermocouple supported with FE modelling and simulation validation. They also claimed that the effect of heat generation needs to be addressed especially when high machining accuracy is required. Therefore, it is essential to obtain a scientific understanding of the effects of micro cutting temperature on a quantitative analysis basis. Especially because micro cutting heat partition distribution on diamond tool-workpiece-chip interface is currently not well-understood. This

study may interpret how the generated heat affects each component, e.g., tool, workpiece and chip respectively, in micro cutting and its consequent deterioration on these components.

In this chapter, a quantitative investigation on cutting temperature and heat partitioned distribution in micro cutting particularly in proportion of the generated heat on the cutting tool, workpiece and chip is presented. The cutting temperature is measured by using a thermal imaging camera. The experimental investigations are conducted using three kinds of materials in comparison supported with the FE-based model and simulation. The chapter also extensively discusses the effects of cutting temperature on the tool wear, surface generation and machining accuracy.

6.2 FE-based simulation on micro cutting temperature

In recent years, modelling and simulation of micro cutting has been studied by many researchers. However, very few investigations have been carried out on the micro cutting temperature and heat generation which has different effects from those of conventional cutting. Moreover, the simulation study of micro cutting temperature is quite challenging because the meshing elements are badly distorted even when adaptive meshing is used during the simulation. The consequent errors with model definition always exists when solving the heat transfer equation. However, FE-based modelling and simulation is needed due to the difficulty and complexity of the real micro machining in some cases. Consequently, accurate modelling needs to improve until inherent micro cutting mechanisms have been accurately modeled and simulated. Generation of micro cutting temperature in diamond turning is caused by very low temperature and generated heat, and, subsequently, thermal effects. Thus, there is a need to carefully study the modeling of micro cutting temperature in oder to accurately simulate the cutting temperature.

6.2.1 Material Constitutive modelling

In order to model and characterise the cutting temperature in micro cutting, accurate material modelling is very important and represents the actual changes of physical propertires during machining. Thus, the Johnson-cook model is employed (Duan, et al., 2009; Liu & Melkote, 2007; Zong, et al., 2007). It is expressed as the flow stress which is a function of strain, strain rate and temperature in terms of the functional equation below.

$$\bar{\sigma} = [A + B(\bar{\varepsilon})^n]\left[1 + C\mathrm{Ln}\left(\frac{\dot{\bar{\varepsilon}}}{\dot{\bar{\varepsilon}}_0}\right)\right]\left[1 - \left(\frac{T-T_0}{T_{\mathrm{melt}}-T_0}\right)^m\right] \tag{6.1}$$

Where $\bar{\sigma}$ is the equivalent stress, $\bar{\varepsilon}$ is the equivalent plastic strain, $\dot{\bar{\varepsilon}}$ is the plastic strain rate, $\dot{\bar{\varepsilon}}_0$ is the reference strain rate (1.0 s^{-1}), T_0 is room temperature, T_{melt} is the melting temperature, *A* is the initial yield stress (MPa), *B* is the hardening modulus, *n* is the work-hardening exponent, *C* is the strain rate dependency coefficient (MPa), and *m* is the thermal softening coefficient. Physical properties and material constants of Johnson-cook model for diamond tool (Zong, et al., 2007) and aluminium AA6082-T6 are presented in Table 6.1 and 6.2. (Özel & Karpat, 2007)

Table 6.1 Physical properties of AA6082-T6 and diamond tool

	E(Gpa)	*v*	*c*(J/kg°C)	ρ(kg/m^3)	*K*(W/m°C)
AA6082-T6	70	0.33	896	2,700	180
Diamond tool	1,050	0.1	420	3,520	1,000

Where *E* is Young's modulus, v is Poisson's ratio, *c* is specific heat, ρ is material density*,* and *K* is thermal conductivity respectively.

Table 6.2 Johnson-cook constitutive material model parameters for AA6082-T6

A	*B*	*C*	*n*	*m*	$\dot{\bar{\varepsilon}}_0$	T_{melt}
403.57	306.56	0.00185	0.7769	1.73	0.00419	855

6.2.2 Modelling of the chip separation criteria

In order to simulate the seperation of chip i.e., chip formation phenomenon, a dynamics failure model is also employed for the Johnson-cook model. The Johnson-cook damage parameter is based on the value of the equivalent plastic strain at element integration points. The failure is assumed to occur when the damage parameter *D* exceeds 1:

$$D = \Sigma \left(\frac{\Delta \bar{\varepsilon}^{pl}}{\bar{\varepsilon}_f^{pl}} \right) \tag{6.2}$$

Where $\Delta \bar{\varepsilon}^{pl}$ is the increment of equivalent plastic strain, $\bar{\varepsilon}_f^{pl}$ is the strain at failure which is assumed equal to

$$\bar{\varepsilon}_f^{pl} = \left[d_1 + d_2 exp \left(d_3 \frac{p}{q} \right) \right] \left[1 + d_4 Ln \left(\frac{\dot{\bar{\varepsilon}}^{pl}}{\dot{\varepsilon}_0} \right) \right] \left(1 + d_5 \frac{T - T_0}{T_{melt} - T_0} \right) \tag{6.3}$$

Where d_1-d_5 are failure parameters namely including Initial failure strain, Exponential factor, Triaxiality factor, Strain rate factor, and Temperature factor respectively. The damage parameters for Johnson-cook model are presented in table 6.3 (Zhou, et al., 2013).

Table 6.3 Johnson-cook failure model parameters for AA6082-T6

d_1	d_2	d_3	d_4	d_5
0.0164	2.245	-2.798	0.007	3.658

6.2.3 Conditional equation on heat and temperature distribution

The temperature and heat distribution during the cutting process is modelled and simulated. The main sources of generated heat are the plastic work and the friction at the tool-chip interface which are converted into heat. A three-dimensional thermal conduction analysis (Fang & Zeng, 2005; Mamalis, et al., 2001; Marusich & Ortiz, 1995) is then developed and coupled into the cutting

model. Thus, the governing differential equation for thermal conduction is given by

$$k\left[\frac{\partial^2 T}{\partial x^2} + \frac{\partial^2 T}{\partial y^2} + \frac{\partial^2 T}{\partial z^2}\right] - \rho c\left[u\frac{\partial T}{\partial x} + v\frac{\partial T}{\partial y} + w\frac{\partial T}{\partial z}\right] + \dot{Q}_g = 0 \qquad (6.4)$$

Where *k* is the thermal conductivity, *ρ* is the density, *c* is the specific heat, and $\dot{Q}_g$ *is* the volumetric generation rate. During the cutting process, the heat generated from both plastic work and friction can be calculated by

$$\dot{Q}_g = \frac{1}{V}\int_V \sigma\dot{\vec{\epsilon}}_p\,dV + \frac{1}{V}\int_V \tau\dot{s}\,dV \qquad (6.5)$$

Where $\dot{\vec{\epsilon}}_p$ is the effective plastic strain rate, τ is the friction stress, $\dot{s}$ is the tangential velocity component at the chip–tool interface, and *V* is the element volume.

The same cutting conditions as the experimental setups as shown in the next section (section 6.3) are used. Thus, a comparison of FE-based simulation associated with cutting experimetal results and discussions are given in sections 6.2.4 and 6.6 respectively.

6.2.4 Simulation results

The micro cutting temperature can be modeled with the Johnson-cook constitutive Material modeling as previously mentioned. In order to correct the cutting temperature results and avoid the distortion of mesh elements which causes errors whilst solving heat transfer equations in the simulation procedure, optimising the three main parameters that directly influence the cutting temperature is needed. The optimisation of three influencing parameters can be conducted by trial and error method. They particularly include friction coefficient *(µ)* between diamond tool and workpiece's surfaces as being used under condition of the constant friction model (Tan, 2002) which was applied in this FE model and simulation, damage evolution *(D)* of material, and mesh sizes of tool *(M_t)* and workpiece *(M_w)*. In the simulation process, the workpiece is divided as

108

a small strip at the interaction areas with the cutting tool tip so that chips can be formed. Thus, damage evolution will be D for the strip and the rest of the workpiece's elements, i.e, D_s and D_w respectively. Finally, the optimum parameters for validation of the cutting experimental results can be illustrated in Figure 6.1., and the simulation and experimental validation and comparison can also be found in section 6.6.
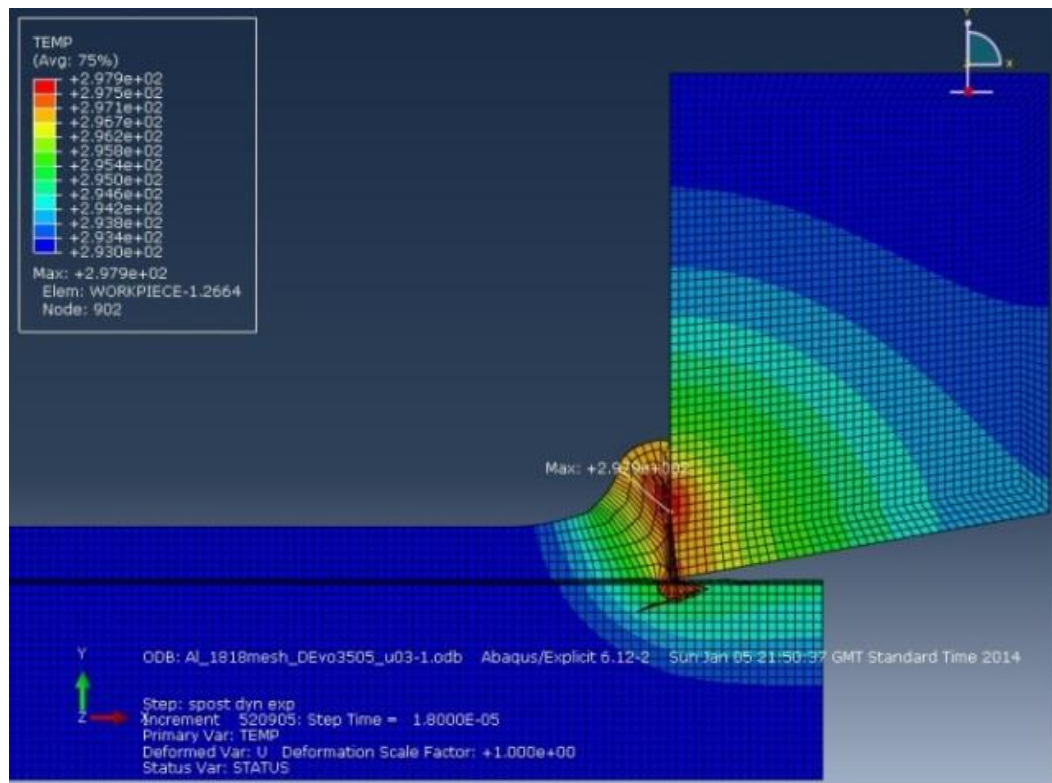
Figure 6.1 The simulation results of micro cutting temperautre and generated heat illustatation by Abaqus/explicit (µ = 0.3)

6.3 Experimental and measurement setup on cutting temperature and heat partitioned distribution

The experiment setup shown in Figure 6.2 is used to cut three materials: titanium Ti-6Al-4V, aluminium AA6082-T6 and single crystal silicon. The same cutting conditions are applied, i.e. depth of cut 10 µm, constant surface speed 100 m/min., and feed rate 5 mm/min. with the same diamond tool to make comparisons for all materials. Each material was repeatedly and continuously cut three times until completion of the third cut. The Optris PI160 thermal imaging camera was used to conduct real-time measurement of cutting

temperature at the cutting zone. Four areas at diamond tool, workpiece, chips and tool tip, are measured for titanium while only three areas namely diamond tool, workpiece and tool tip are measured for aluminium and silicon. This is because chips generated by the cutting of aluminium and silicon are too small to be captured because of the limited capability of the thermal imaging camera. The technical specifications of the thermal imaging camera can be found in appendix 5, the cutting experiments and micro cutting temperature results are further illustrated in Figure 6.3.
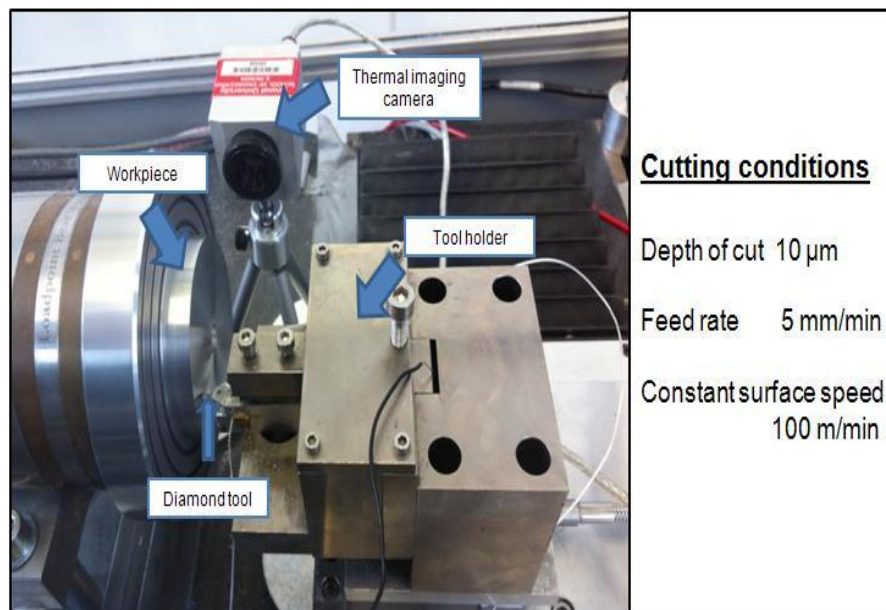
Figure 6.2 Schematic of the experimental and measured setups on cutting aluminium AA6082-T6, single crystal silicon and titanium Ti-6Al-4V with same cutting conditions

Figure 6.3 Cutting temperature and the associated heat partitioned distribution in micro cutting process

6.4 Experimental results and discussions

Each material is repeated three times, cutting with the same cutting conditions (Figure 6.2). The cutting temperature is recorded from the first to the third cutting. The different time intervals are caused by the different diameters of materials. In order to get the maximums, minimums, and ranges between maximum and minimum values of cutting temperature for each cutting area particularly including diamond tool, workpiece, and tool tip, if the selected method for determine these value by just conducting the lowest points of cutting temperature subtracted from the highest points of the selected cutting area. This kind of method is not sufficiently reliable. Thus, in order to reduce or avoid the variances caused by errors in measuring and collecting data, the best fitting curve has been applied. The reliable and optimal ranges of cutting temperature on each cut can then be calculated. Cutting temperature results, including their maximums, minimums and ranges for micro cutting of these three materials, are further discussed below with observations.

6.4.1 Micro cutting of aluminium AA6082-T6

As shown in Figure 6.4, an increase in tool temperature level was much quicker than in workpiece by a few seconds of cutting time. This is possibly caused by

much higher thermal conductivity of diamond tool than aluminuim. Meanwhile, an increase in temperature in workpiece took a longer time but it kept rising until specific cutting time has reached about 3 minutes so that the workpiece temperature reaches tool temperature level. This may be caused by the positive value of temperature coefficient of aluminium (0.0039 ^{o}K^{-1}, ^{o}C^{-1}) which results in increasing thermal conductivity when temperature of cutting process is increasing (Moran & Shapiro, 2006). Thus, workpiece temperature will then increase according to an increase in the thermal conductivity.

The best fitting curves of micro cutting temperature on aluminuim (and also the others) are conducted using polynomial equation at polynomial order 7 (Figure 6.5). The comparision curves and its maximum, minimum and range values between raw signal graphs and curve fitting graphs are listed in Table 6.4.

6.4.2 Micro cutting of single crystal silicon

As shown in Figure 6.7, cutting tool temperature is always higher than that of workpiece for the whole cutting period which is different from aluminium cutting behaviour. This is because the silicon has negative temperature coefficient (−0.075 ^{o}K^{-1}, ^{o}C^{-1}) which causes lower thermal conductivity while cutting temperature increases in the process (Michael J. Moran, 2006). Thus, the workpiece temperature slightly increased and almost reaches room temperature at starting point of cutting. The second observation can be presumed that more interrupted cuts may cause thermal effects corresponding to cutting tool wear. Trends of temperature partitioned distribution lines between the first cut and the following cuts; i.e., more numbers of cuts, higher and more numbers of spikes on the tool temperature curves can be observed (Figure 6.7). Also more chatter marks on the workpiece can be found for the whole cutting areas as shown in Figure 6.8. Therefore, it is supposed that the tool can be gradually dulled relatively few continuous cuts.
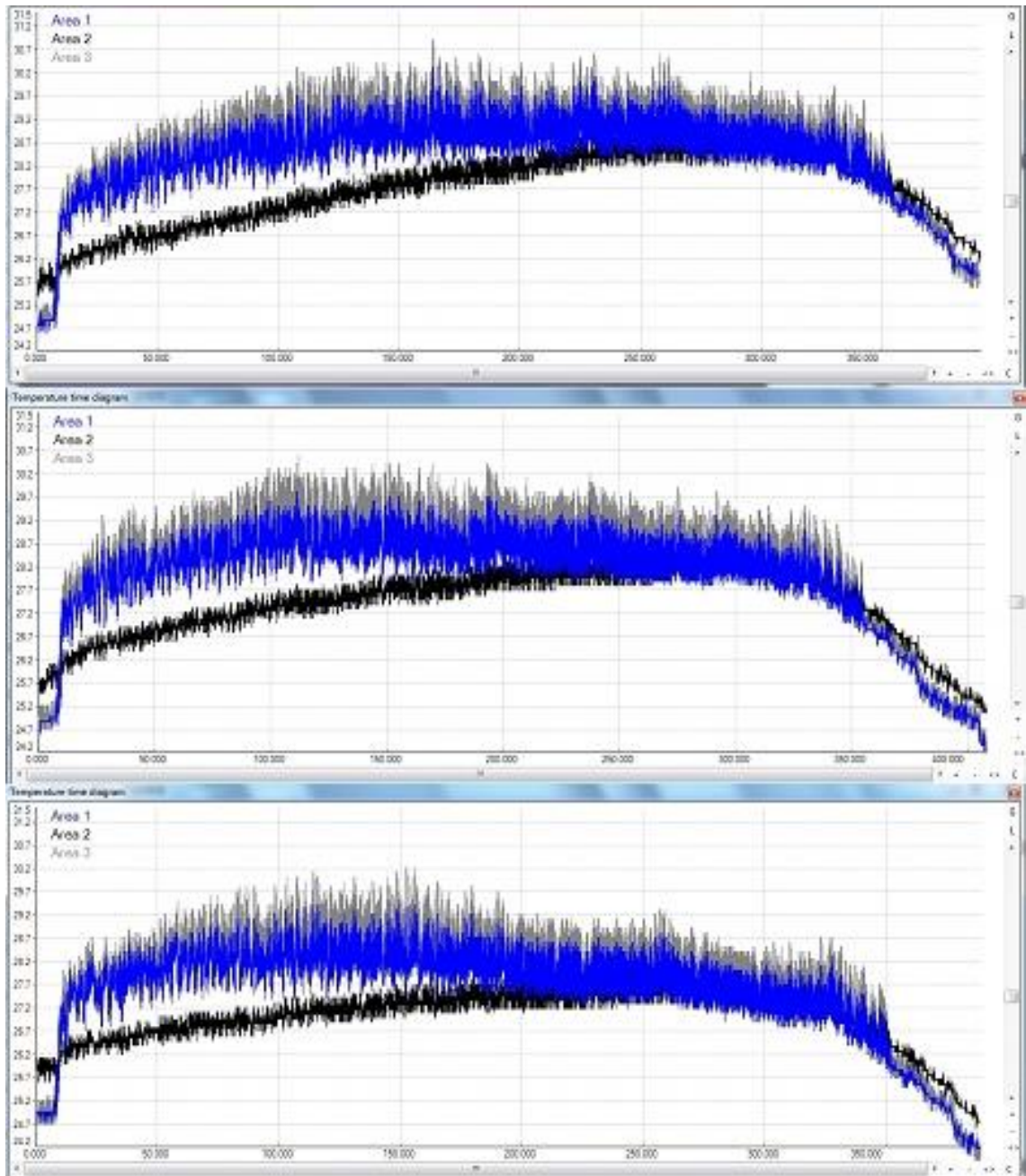
Figure 6.4 Micro cutting temperature against time interval of AA6082-T6; area 1: diamond tool, area 2: workpiece, and area 3: tool tip (first to last cuts: in the top-down order)

Figure 6.5 The best fitting curves of temperature partitioned distribution of cutting AA6082-T6 on diamond tool (blue dash line), workpiece (red dash line), and tool tip (green dash line) for whole cutting time interval (°C - min)

Table 6.4 Comparison of curves and its maximums, minimums and ranges between raw signal and curve fitting graphs of cutting aluminium AA6082-T6

Cutting temperature - Aluminium AA6082-T6							
	Cutting areas	Raw signal curves (°C)			Polynomial fitting curves (°C)		
		Maxumum	Minimum	Ranges	Maxumum	Minimum	Ranges
1st cut	diamond tool	30.1	24.7	5.4	29.0	24.5	4.5
	workpiece	28.8	25.5	3.3	28.5	25.6	2.9
	tool tip	30.7	24.7	6	29.3	24.6	4.7
2nd cut	diamond tool	29.6	24.2	5.4	28.7	24.5	4.2
	workpiece	28.5	25	3.5	28.2	25.0	3.2
	tool tip	30.4	24.3	6.1	29.2	24.6	4.5
3rd cut	diamond tool	29.3	24	5.3	28.3	24.1	4.2
	workpiece	27.8	24.6	3.2	27.5	24.6	2.9
	tool tip	30	23.9	6.1	28.7	24.0	4.7

The corresponding feed and cutting forces in respect to micro cutting temperature of aluminium AA6082-T6 are also illustrated as in Figure 6.6. It can be observed that the feed force has more influence than the cutting force.
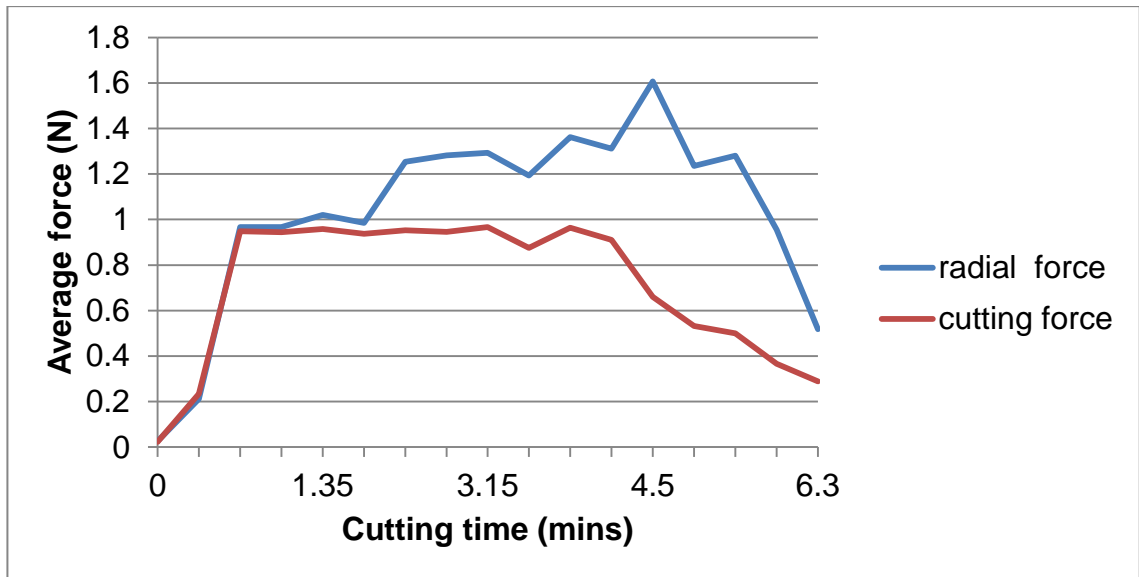
Figure 6.6 The average of correlated forces of cutting AA6082-T6 with respect to cutting temperature

It is surprising that when only three repeated cuts were taken, an increase in spikes distributing along cutting tool temperature curves of the following cuts are much higher than that of the curve of the first cut. As a result, it should be noted that the severe tool wear can be result of a few cuts on silicon even when cutting temperature is low. Therefore, it should be taken into consideration that a quick and unpredictable increase in heat and temperature can occur during continuous machining on silicon in micro cutting. Therefore, the effective and reliable a tool condition monitoring (TCM) system should be applied if silicon machining is required.
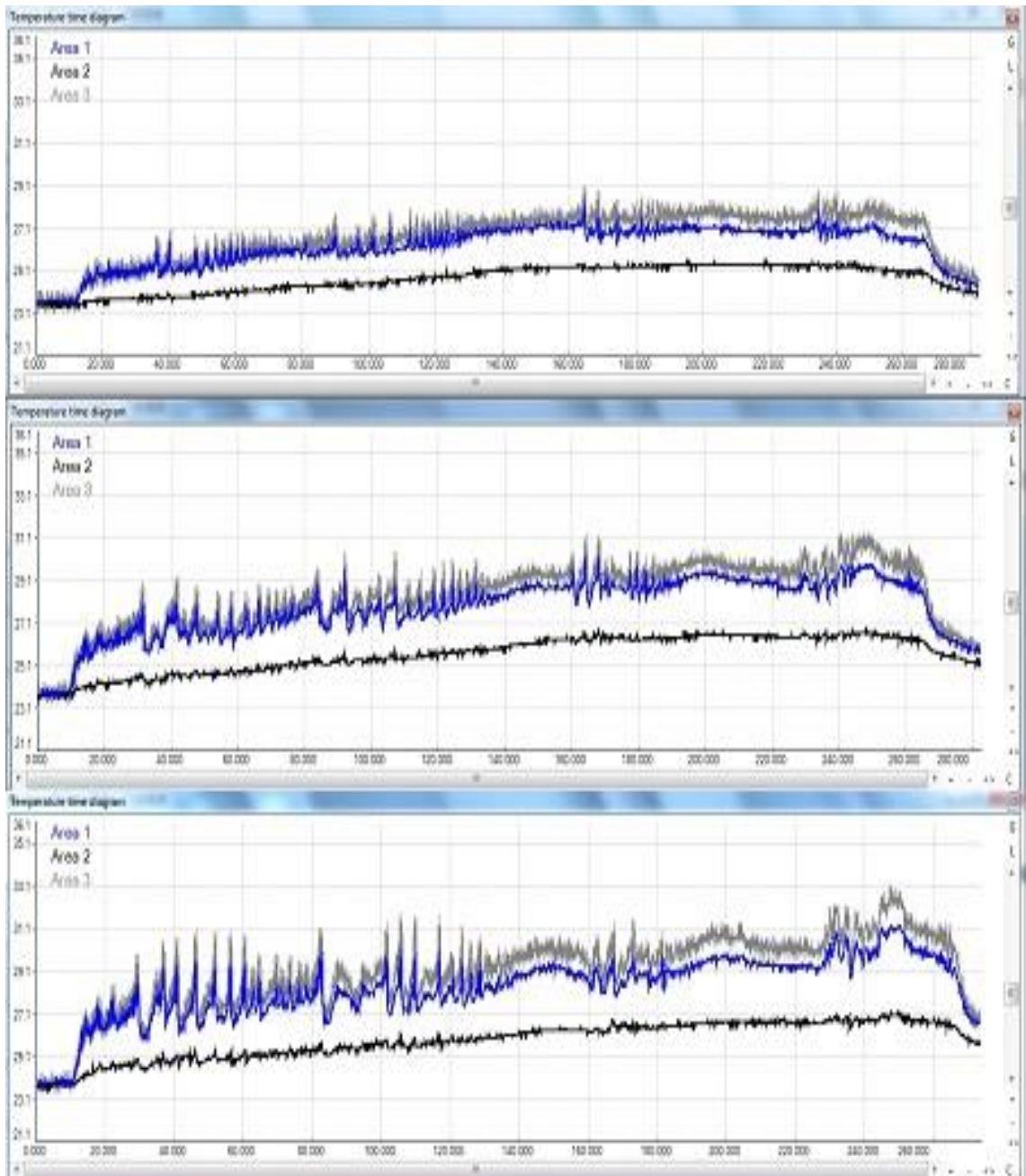
Figure 6.7 Micro cutting temperature against time interval of silicon wafer; area 1: diamond tool, area 2: workpiece, area 3: tool tip (first to last cuts: in the top-down order)

Figure 6.8 The chatter marks on the silicon workpiece taken after third cuts
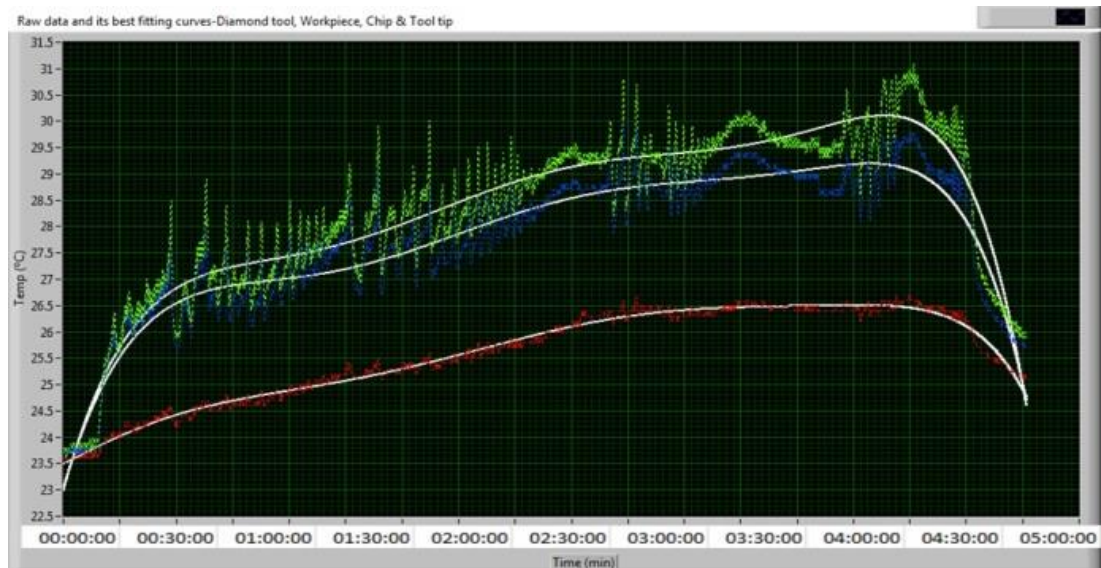
Figure 6.9 The best fitting curves of temperature partitioned distribution of cutting single crystal silicon on diamond tool (blue dash line), workpiece (red dash line), and tool tip (green dash line) for whole cutting time interval (°C - min)

Table 6.5 Comparison of curves and its maximums, minimums and ranges between raw signal and curve fitting graphs of cutting single crystal silicon

	Cutting areas	Raw signals (ºC)			Polynomial fitting curves (ºC)		
		Maxumum	Minimum	Ranges	Maxumum	Minimum	Ranges
1st cut	diamond tool	28	23.5	4.5	27.1	23.2	3.9
	workpiece	25.4	23.4	2	25.3	23.4	1.9
	tool tip	28.6	23.4	5.2	27.8	23.3	4.5
2nd cut	diamond tool	30	23.7	6.3	29.2	23.0	6.2
	workpiece	26.7	23.5	3.2	26.5	23.5	3.0
	tool tip	31.1	23.6	7.5	30.1	23.0	7.1
3rd cut	diamond tool	31.2	23.7	7.5	30.4	23.0	7.3
	workpiece	27.1	23.6	3.5	26.9	23.5	3.4
	tool tip	32.7	23.6	9.1	31.5	23.1	8.4

The corresponding feed and cutting forces in respect to micro cutting temperature of single crystal silicon are also illustrated as in Figure 6.10. It can be observed that the feed force quite higher influence than the cutting force for the whole cutting period.
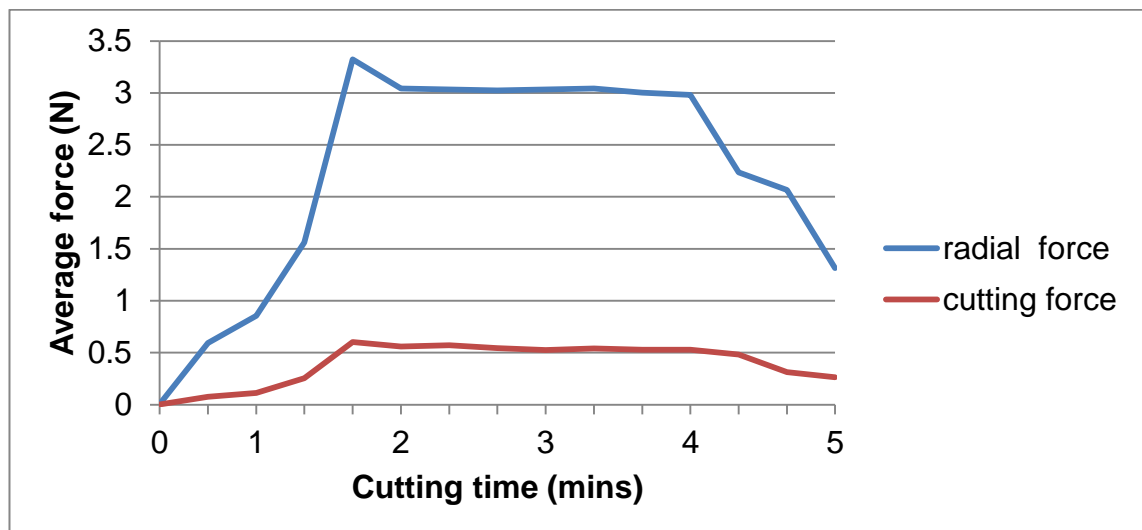
Figure 6.10 The average of correlated forces of cutting silicon with respect to cutting temperature

6.4.3 Micro cutting of titanium Ti-6Al-4V
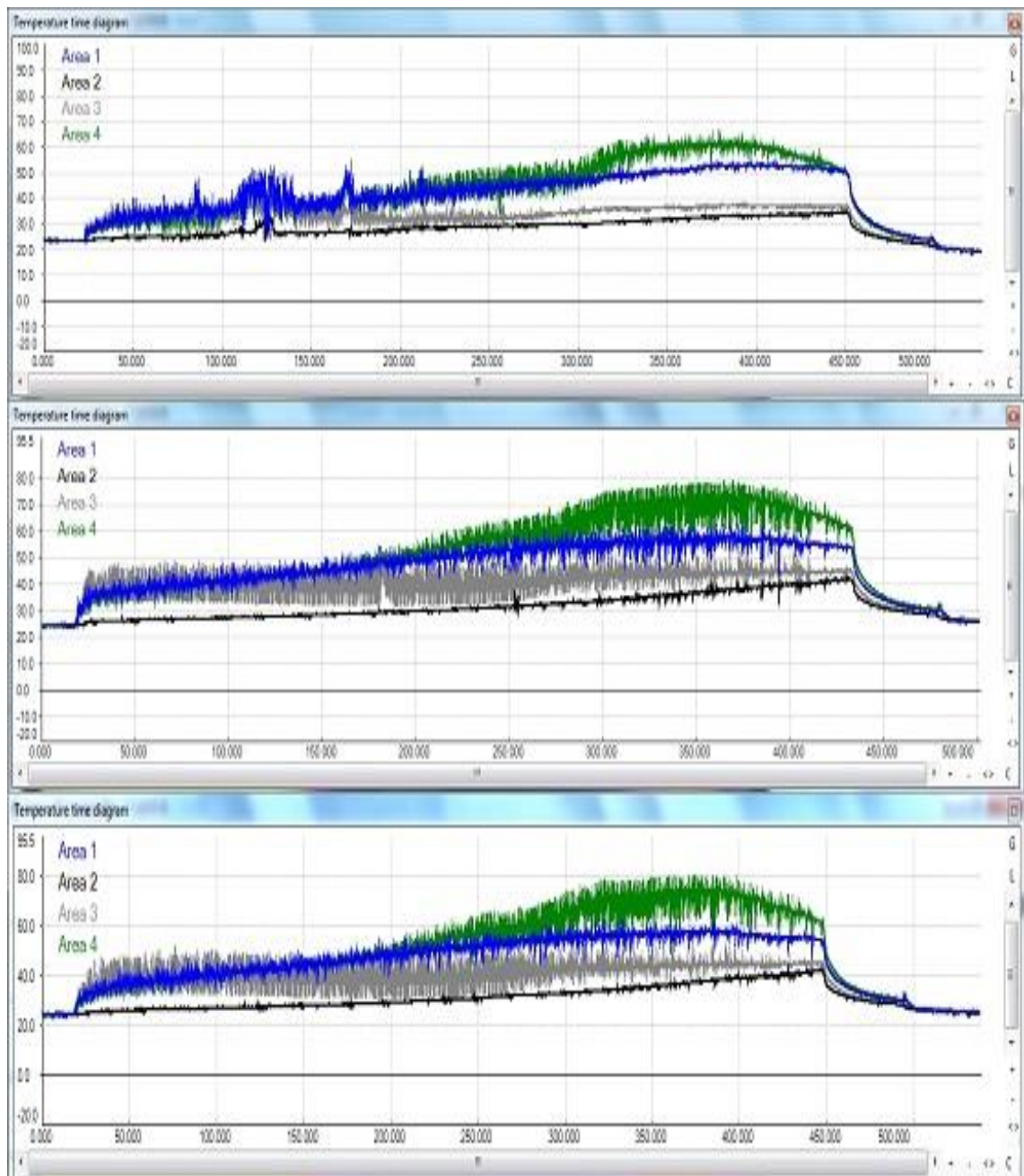
Figure 6.11 Micro cutting temperature against time interval of titanium Ti-6Al-4V; area 1: diamond tool, area 2: workpiece, area 3: chip, area 4: tool tip (first to last cuts: in the top-down order)

Titanium cutting was the only one which has continuous chips of sufficient size to capture and measure chip temperature. Even though there were less spikes distributed on the tool temperature curve lines than silicon cutting, cutting temperature (table 6.6) was much higher especially on cutting tool and tool tip.

In addition, the trends were unstable (Figure 6.11) when more cuts were performed similar to the silicon cuts. Thus, the highest micro cutting temperature occur when conducted cutting titanium. Accordingly, it may easily destroy the cutting tool tip with thermal effects if very small machining scales (undeformed chip thinckness and cutting depth) agaist cutting area/volume are employed.
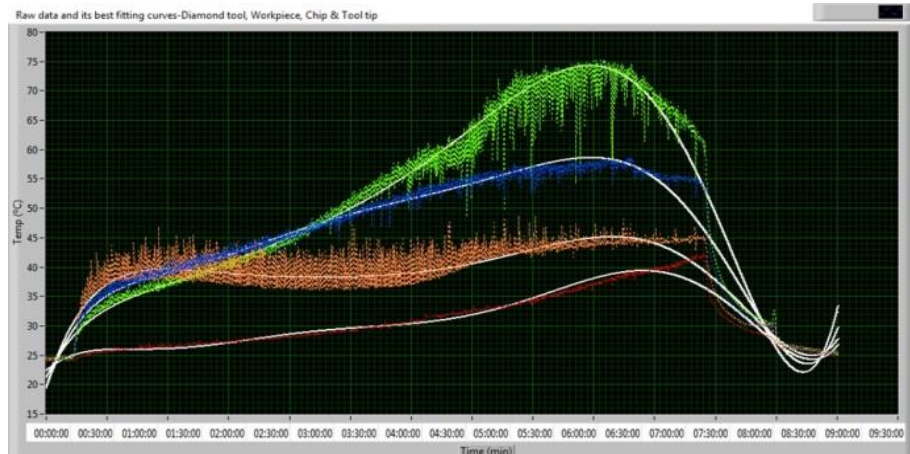
Figure 6.12 The best fitting curves of temperature partitioned distribution of cutting Ti-6Al-4V on diamond tool (blue dash line), workpiece (red dash line), chip (brown dash line), and tool tip (green dash line) for whole cutting time interval (°C - min)

The corresponding feed and cutting forces in respect to micro cutting temperature of titanium Ti-6Al-4V are also illustrated as in Figure 6.13. Again, It can be observed that the feed force has a larger influence than the cutting force for the whole cutting period.

Table 6.6 Comparison of curves and its maximums, minimums and ranges between raw signal and curve fitting graphs of cutting titanium Ti-6Al-4V

	Cutting areas	Raw signals (°C)			Polynomial fitting curves (°C)		
		Maxumum	Minimum	Ranges	Maxumum	Minimum	Ranges
1st cut	diamond tool	53.5	19.1	34.4	54.2	18.6	35.6
	workpiece	34.9	19.1	15.8	33.9	18.9	14.9
	chip	41.2	19.3	21.9	38.1	19.2	18.8
	tool tip	62.8	19	43.8	62.3	18.1	44.3
2nd cut	diamond tool	58.8	24.1	34.7	58.7	17.9	40.8
	workpiece	42.1	24	18.1	39.6	21.9	17.7
	chip	52.2	24.3	27.9	45.3	18.5	26.8
	tool tip	75	24.1	50.9	74.1	18.7	55.4
3rd cut	diamond tool	58.7	24.2	34.5	58.6	19.3	39.3
	workpiece	42.1	24	18.1	39.4	22.3	17.0
	chip	48.8	24.4	24.4	45.1	19.4	25.7
	tool tip	75.4	24.2	51.2	74.3	21.1	53.1

Cutting temperature - Titanium Ti-6Al-4V
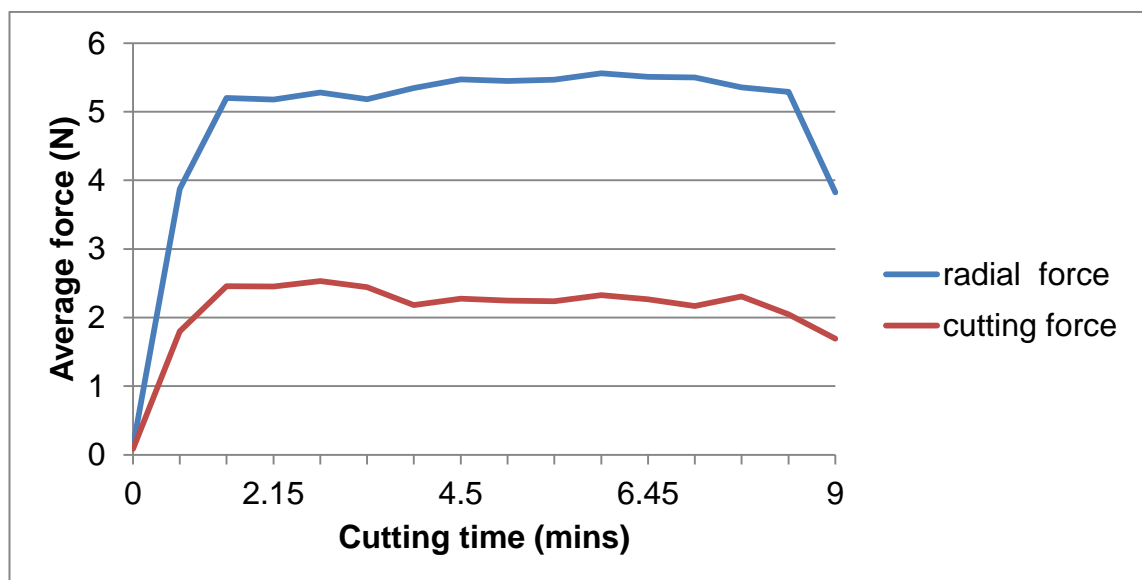
Figure 6.13 The average of correlated forces of cutting Ti-6Al-4V with respect to cutting temperature

6.5 Analysis on heat partitioned distribution in micro cutting

Heat transfer is a critical issue when cutting temperature is considered. The excessive heat generated in a cutting process can deteriorate the tool or surface integrity, e.g., thermal effects can cause tool wear and breakage, poor quality of machined surfaces, and reduced machining accuracy. Thus, the tool-workpiece-chip heat partitioned distribution is investigated in order to scientifically understand the heat and thermal effects on each part of the cutting process composition, i.e., tool, workpiece and chip. The severe effects on each of components of micro cutting can then be avoided or minimised. Therefore, the heat transfer by conduction i.e., the transferring heat energy by microscopic diffusion and collisions of particles between solid bodies in contact due to a temperature gradient (Michael J. Moran, 2006) is selected. This conductive heat transfer is applied for analysing and determining heat partitioned distribution on elements of micro cutting namely tool, workpiece, and chip respectively. It can be expressed based on Fourier's Law as the following equation:

$$q = -kA \left[\frac{T_2 - T_1}{s} \right] \tag{6.6}$$

Where q is the rate of heat transfer in considering direction (W, J/s), A is heat transfer area (m^2), k is thermal conductivity of the material (W/m.K or W/m ^{o}C), dT (or T_2-T_1) is temperature difference across the material (K or ^{o}C), s is material thickness (m) respectively. The minus sign is a consequence of energy transfer in the direction of decreasing temperature.

If $q_D, q_W, q_C, q_T, k_D, k_W, k_C, k_T, dT_D, dT_W, dT_C, dT_T$ stand for conductive heat transfer, thermal conductivity (Zong, et al., 2006; Maycock, 1967; Ezugwu, et al., 2005; Fratini & Buffa, 2005), and differences or ranges of temperature across material, i.e., the deferent temperature between maximum and minimum values at the considerd area, in diamond tool (the generated heat on the whole area of diamond), workpiece, chip, and tool tip (the generated heat at the tool tip only), respectively, the heat partitioned distribution at the diamond tool-workpiece-chip interface can be presented as the heat transfer across cutting process for instant time as following equation:

122

$$q_D{:}\,q_W{:}\,q_C{:}\,q_T = \frac{k_D \times A \times dT_D}{s} : \frac{k_W \times A \times dT_W}{s} : \frac{k_C \times A \times dT_C}{s} : \frac{k_T \times A \times dT_T}{s} \qquad (6.7)$$

The assumption of cutting area *(A)* and thickness *(s)* of the cutting zone are all equal due to single point diamond turning (SPDT) process. Thus, all *A* and *s* in above equation can be subtracted, therefore the equation will then be:

$$q_D{:}\,q_W{:}\,q_C{:}\,q_T = k_D \times dT_D{:}\,k_W \times dT_W{:}\,k_C \times dT_C{:}\,k_T \times dT_T \qquad (6.8)$$

6.5.1 Aluminium AA6082-T6

From Table 6.4, the avearage of cutting temperature on diamond tool, workpiece and tool tip is determined and presented in Table 6.7.

Table 6.7 Ranges of polynomial curves fitting of micro cutting temperature for aluminium

Aluminium AA6082-T6 cutting temperature				
Cutting areas	ranges of cutting temperature (°C)			Average
	1st cut	2nd cut	3rd cut	
diamond tool	4.5	4.2	4.2	4.3
workpiece	2.9	3.2	2.9	3
tool tip	4.7	4.5	4.7	4.6

Thus, conductive heat transfer for aluminium cutting can be calculated as:

$$k_D \times dT_D : k_{W(Al)} \times dT_{W(Al)} : k_T \times dT_T = 1000 \text{ x } (4.3) : 180 \text{ x } (3) : 1000 \text{ x } (4.6) =$$
4,300 : 540 : 4,600

$$= 8 : 1 : 8.5$$

It can be summarised that conductive heat transfer has occurred in the diamond tool and tool tip against aluminium workpiece about 8 and 8.5 times,

respecively. The micro cutting temperature on the whole cutting areas is similar to that of each other for all cuts. Therefore, it should be noted that the continuing cuts on aluminium are more stable and predictable than others. The thermal effects would not affect the cutting process of aluminium machining.

6.5.2 Single crystal silicon

From Table 6.5, the average cutting temperature on diamond tool, workpiece and tool tip is determined and presented in Table 6.8.

Table 6.8 Ranges of polynomial curves fitting of micro cutting temperature for silicon cutting

Silicon wafer cutting temperature				
Cutting areas	ranges of cutting temperature (°C)			Average
	1st cut	2nd cut	3rd cut	
diamond tool	3.9	6.2	7.3	5.8
workpiece	1.9	3	3.4	2.8
tool tip	4.5	7.1	8.4	6.7

Thus, conductive heat transfer for silicon cutting:

$$k_D \times dT_D : k_{W(Si)} \times dT_{W(Si)} : k_T \times dT_T = 1000 \times (5.8) : 150 \times (2.8) : 1000 \times (6.7)$$

$$= 5,800 : 420 : 6,700$$

$$= 13.8 : 1 : 16$$

As a result, it can be summarised that conductive heat transfer have occurred in diamond tool and tool tip against silicon workpiece about 14 and 16 times, respectively. It must be noted that this partition is approximated for this case study due to a difference in trends of distributed temperature between first cut and following cuts. On the other hand, micro cutting temperature on silicon tends to nonlinearly increase on tool, workpiece, and tool tip from the first to following cuts continuously. Therefore, the heat generated on the tool/tool tip

tends to increase nonlinearly for any following cuts. Subsequently, the average range of cutting temperature of silicon cutting and consequent cutting heat partioned distribution may change in differences of experimental setup and case study.

6.5.3 Titanium Ti-6Al-4V

From Table 6.6, the average cutting temperature on diamond tool, workpiece, chip and tool tip is evaluated and presented in Table 6.9.

Table 6.9 Ranges of polynomial curves fitting of micro cutting temperature for titanium Ti-6Al-4V

Titanium Ti-6Al-4V cutting temperature				
Cutting areas	ranges of cutting temperature (^{o}C)			Average
	1st cut	2nd cut	3rd cut	
diamond tool	35.6	40.8	39.3	38.6
workpiece	14.9	17.7	17	16.5
chip	18.8	26.8	25.7	23.8
tool tip	44.3	55.4	53.1	50.9

Thus, conductive heat transfer for titanium cutting can be calculated as:

$k_D \times dT_D : k_{W(Ti)} \times dT_{W(Ti)} : k_C \times dT_C$ = 1000 x (38.6) : 6.7 x (16.5) : 6.7 x (23.8) : 1000 x (50.9) = 38,600 : 110.55 : 159.46 : 50,900

$$= 349.2 : 1 : 1.4 : 460.4$$

The excessively generated heat can occurr for titanium cutting at diamond tool and tool tip against titanium workpiece about 350 and 460 times, respectively. However, it has occurred at chip just about 1.4 times of titanium workpiece. In addition, the sparking fire which occurred during cutting titanium by the used

tool was observed. Therefore, cutting titanium should not be recommended for diamond machining.

6.6 Simulation and experimental validation

In order to compare the simulation to experimental results, the tool tip element, the nearest element to tool tip on workpice and chip are selected (Figure 6.14) to illustrate the cutting temperature on tool tip, workpiece, and chip, respectively. The predefined temperature of tool and workpiece are equal to 298 K (25 $^{\circ}$C) which are similar to the experimental value, and simulation time interval 3 x 10^{-5} seconds. Thus, the comparison of results between experiments and FE-based simulation are implemented in table 6.10
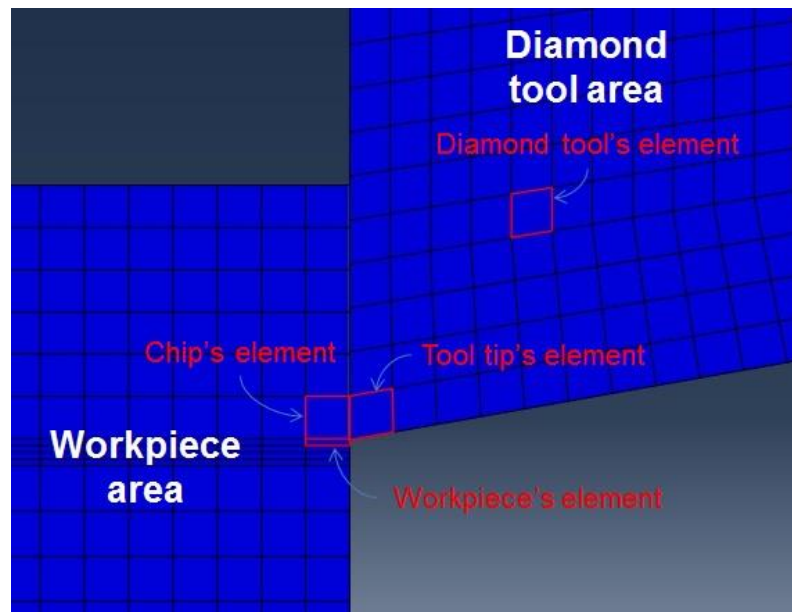
Figure 6.14 The selected elements of diamond tool, workpiece, chip, and tool tip on FE-based simulation of micro cutting temperature
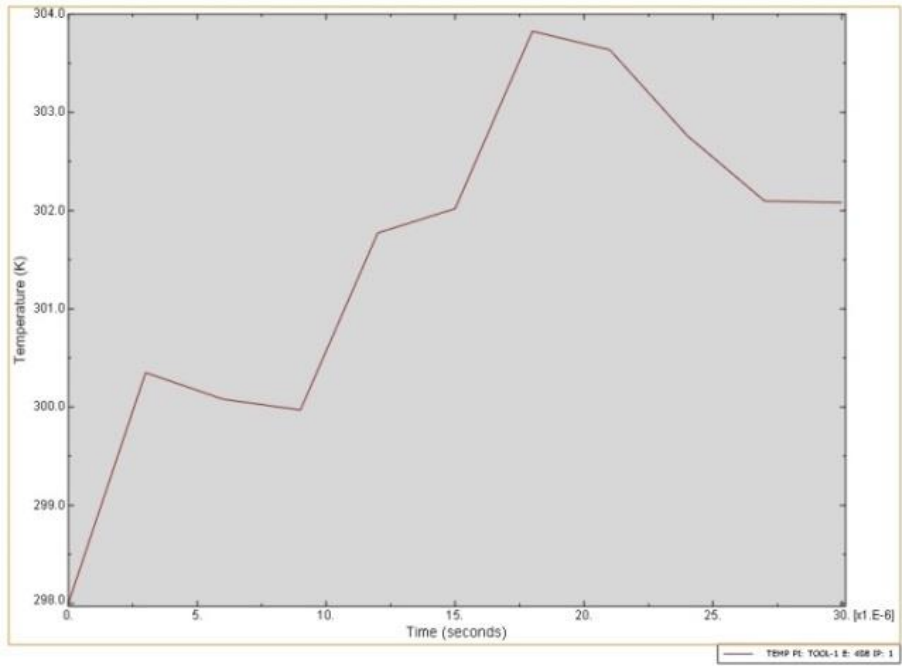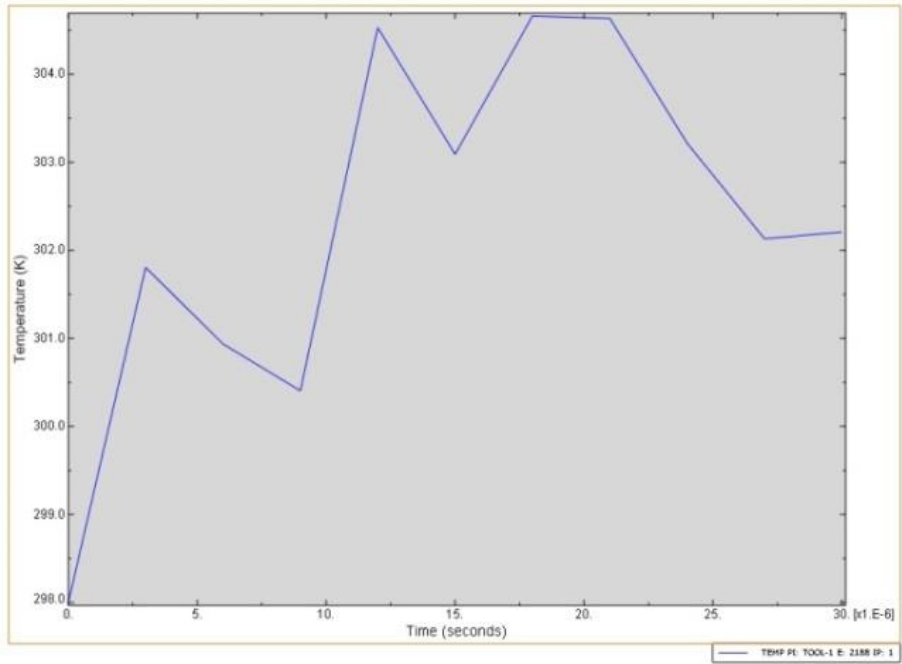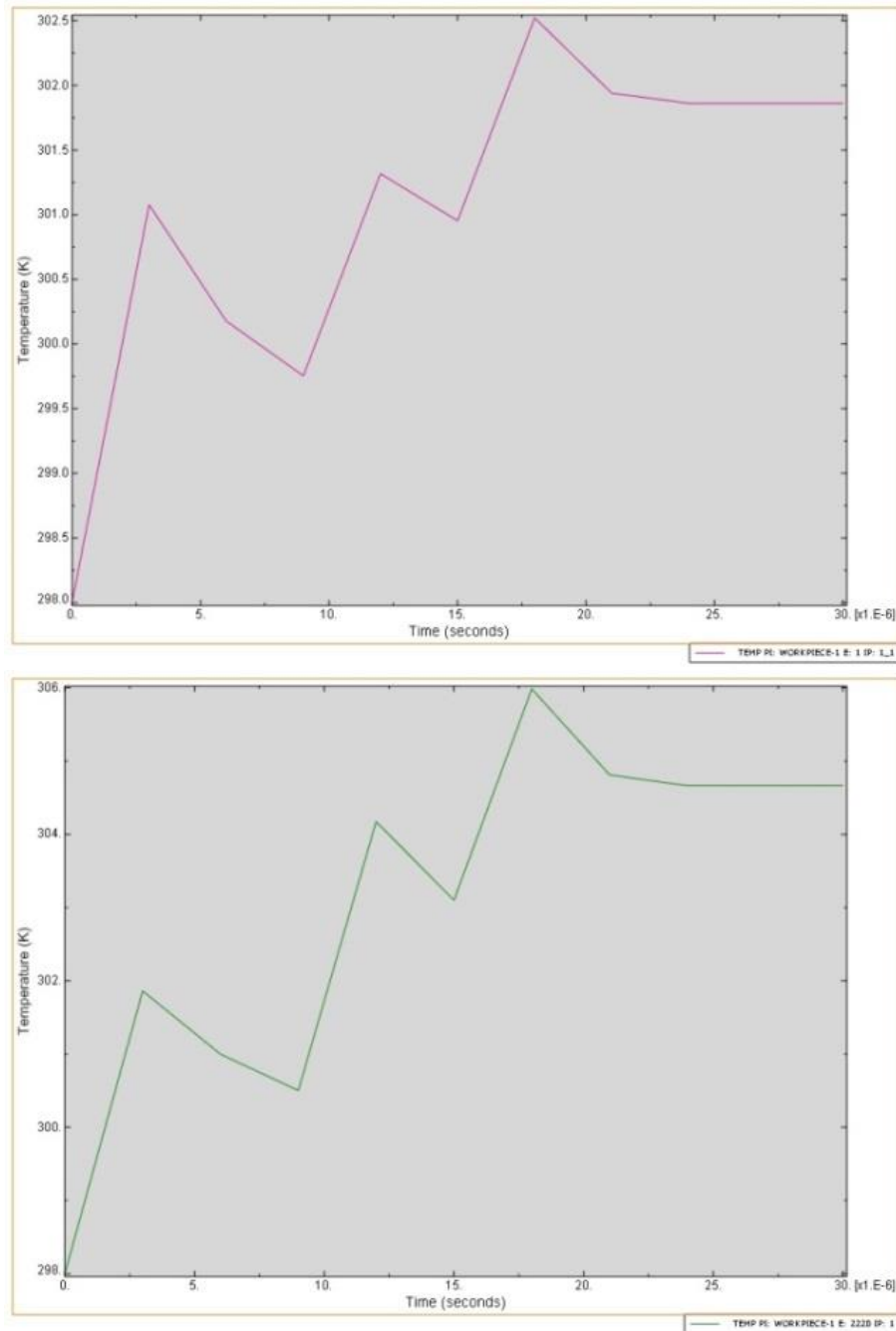
Figure 6.15 The graphical trends of micro cutting temperature in micro cutting compositions within 3×10^{-5} s simulation time interval: tool tip's element (blue line), diamond tool's element (brown line), workpiece's element (pink line), and chip's element (green line), respectively (first to last cuts: in the top-down order)

As shown in table 6.10, it can be clearly observed that the cutting temperature on diamond tool, tool tip and workpiece is very promising in agreement with the experimental ones. Chip temperature cannot be directly measured via real experiments caused by chip, which is too small to capture and measure

128

temperature data due to limitation of thermal imaging camera. However, the chip temperature taking place in the experimental cutting can be assumed that it would be similar to the simulation results. Since both simulation and experimental results are in agreement with each other, the increasing chip temperature can then be predicted as about 8.0 ºC.

Table 6.10 The comparison and validation of micro cutting temperature between simulation and experimental results

Cutting temperature - Aluminium AA6082-T6						
	Cutting areas	Experimental results (ºC)			Simulation results (ºC)		
		Maxumum	Minimum	Ranges	Maxumum	Minimum	Ranges
1st cut	diamond tool	30.1	24.7	5.4	30.8 (303.826 K)	25 (298 K)	5.8
	workpiece	28.8	25.5	3.3	29.5 (302.522 K)	25 (298 K)	4.5
	tool tip	30.7	24.7	6	31.7 (304.661 K)	25 (298 K)	6.7
	chip	N/A	N/A	N/A	33.0 (305.986 K)	25 (298 K)	8.0
2nd cut	diamond tool	29.6	24.2	5.4			
	workpiece	28.5	25	3.5			
	tool tip	30.4	24.3	6.1			
3rd cut	diamond tool	29.3	24	5.3			
	workpiece	27.8	24.6	3.2			
	tool tip	30	23.9	6.1			

The above results are simulated based on the Johnson-cook constitutive materials modeling and damage parameters which are suitable for materials deformed in the ductile regime as the so-called plasticity deformation. Thus, the brittle material such single crystal silicon cannot be employed in this kind of model. The silicon, therefore, needs the different specifications of material model, chip separation criterion, and accordingly cutting temperature model. The study of FE-based model and simulation of micro cutting silicon remains challenging and needs further investigations.

6.7 Conclusions

In this chapter, the micro cutting temperature is investigated by the cutting of three materials including aluminium AA6082-T6, single crystal silicon and titanium Ti-6al-4V. The analysis on conductive heat transfer in micro cutting is conducted to verify the cutting heat partitioned distribution in SPDT processes particularly including diamond tool, workpiece, and chip. It can be indicated that generated heat at diamond tool/tool tip about 8/8.5 times against workpiece for aluminium cutting, 14/16 times for silicon cutting, and 350/460 times for titanium cutting, respectively. It should be noted that silicon is one of the materials, which can possibly be machined by diamond machining like aluminium or other soft materials. Since proportion of cutting heat transferring into diamond tool/tool tip is not too high and almost the same as that in machining aluminium, it should be taken into consideration that a rapid and unpredictable increase in heat and temperature can occur during continuous machining on silicon. Meanwhile, machining titanium with diamond tool should be avoided because high heat generated onto tool tip can cause thermal effects, leading to severe tool wear if specific cutting areas or volumes are very small.

Comparisons of results from the FE-based simulation on cutting heat and temperature in micro cutting are also in agreement with the experimental study as previously mentioned. Thus, the increase in chip temperature can be approximately assumed by 8.0 ºC for aluminium cutting.

Chapter 7 A case study on micro cutting of single crystal silicon based devices

7.1 Introduction

The single-crystal silicon is an interesting material due to it is popularly and wide use in the microelectronics industry in the manufacturing of integrated circuits, infrared optics, micro electro-mechanical systems (MEMS), opto-electronic, etc. (Yan, et al., 2001; Leung, et al., 1998). Since, the single-crystal silicon has been popular and has various uses, the technological methodology of machining silicon becomes essential to concern due to it being hard, brittle and difficult to cut. Although the excellent conditions of ultra-precision machine tools, associated with the sharp cutting edge of diamond tool are needed for substantial quality of machined surface, these are always limited by cost effects especially for small businesses and research laboratories. Thus, it requires proper methods or procedures for improving machine performances, and consequent quality of micro products and components.

This chapter, the application of micro cutting on single-crystal silicon is carried out in order to get better understandings of characteristics of cutting hard and brittle material such single-crystal silicon. Thus, the improvements of cutting performance, machined surface quality, tool life rate as well as productivity could be achieved.

7.2 Inherent properties and characteristics of single crystal silicon

Single-crystal silicon is a brittle material, which means its fracture strength is lower than its yield strength. When silicon is deformed at room temperature by tension or bending, it fractures before any permanent measurable plastic deformation occurs. This causes the difficulty of moving dislocations in silicon at room temperature (Leung, et al., 1998). This makes silicon difficult to be cut at low temperature which always occurs in micro machining. Thus, the diamond

tool wears out rapidly and consequently the machined surface quality whilst cutting silicon can be poor. Accordingly, this becomes challenging in order to obtain the high quality of machined surface such as a mirror surface finish by diamond turning without subsequent polishing process. Some main properties of single-crystal silicon are listed in Table. 7.1.

Generally, machining of brittle materials such silicon with conventional machining may not be employed, this caused by the materials crack on the surface and subsurface due to marks left by the motion of the tool. However, it has been discovered that the surface and subsurface damage can be reduced as the undeformed chip thickness is decreased (Venkatachalam, et al., 2009; Blackley & Scattergood, 1991; Bifano, et al., 1991). It has also been observed that there exists a critical value of undeformed chip thickness which no subsurface damage is observed. This critical value is known as the transition undeformed chip thickness. And the process of machining brittle materials in such a fashion is called ductile-regime machining which is categorised as the precision or ultra-precision machining. In other words, the brittle material cracks and forms discontinuous chips are occurred when undeformed chip thickness is large, but continuous chips are formed leaving a crack-free surface on the material when the undeformed chip thickness is below the threshold value (Patten, et al., 2005). Hence ultra-precision machining process is needed for ductile-regime machining. Otherwise, the high performance of controlling scales of machining (undeformed chip thickness) on the order of a few microns or below and extremely rigid of machine tool are required.

Furthermore, the tool wear caused by cutting brittle materials is another critical issue especially in respect to the high cutting temperature of micro cutting silicon. Yan et al (Yan, et al., 2003) reported that the high cutting temperature may occur at the flank land due to rubbing force between the tool and the workpiece when the cutting edge recedes and the flank wear land becomes predominant. Consequently, the wear rate increases abruptly when the temperature at the trailing edge of the flank wear land reaches the thermal deterioration point of diamond (Ikawa & Shimada, 1985).

Table 7.1 The main properties of silicon (Leung, et al., 1998).

Crystal structure	Diamond cubic
Primary slip system	{111} .110•
Number of slip systems	6
Number of independent slip systems	2
Young's modulus E (GPa)	168
Vickers's hardness H_v (Gpa)	10.0
Poisson's ratio v	0.27
Density ρ (g cm^{-3})	2.34
Toughness K_c (MN m$^{-3/2}$)	0.6

In regard to modelling and simulation, fundamental studies of the damage associated with microhardness indentations and scratches in silicon have been used to simulate the possible mechanisms of surface deformation and material removal which result from cutting, polishing, and dicing of single-crystal silicon boules and wafers (Zhao & Bhushan, 1998). However, this may not be the best solution to simulate silicon diamond turning by using relevant constitutive models and material parameters based on indentation and scratch studies. Thus, the proper material constitutive model of single-crystal silicon, damage initiation criterion, contact properties, initial cutting conditions, etc., for diamond turning of silicon are critically required. However, it is currently limited due to the constitutive material modelling and relevant parameters of brittle materials such single-crystal silicon are still challenging.

7.3 Micro cutting of single crystal silicon based devices and its limitations

Since silicon is normally a hard and brittle material, machined surface finished by lapping and chemo-mechanical polishing (CMP) can be achieved. Moreover, some attempts have been carried out and currently achieved in ultra-precision machining of silicon. This approach can machine brittle materials such silicon in a ductile mode without the need for subsequent polishing (Yan, et al., 2003). Thus, the plastic deformation of silicon, yielding ductile chips and smooth surfaces are achieved by diamond machining (Nakasuji, et al., 1990; Blake, et al., 1990; Shibata, et al., 1996; Leung, et al., 1998; Yan, et al., 2001). However, this requires the use of an extremely rigid, environmentally controlled ultra-precision machine tool associated with a sharp cutting edge of single-crystal diamond cutting tool with a negative rake angle (Fang & Zhang, 2003). In

addition, the scale of machining (undeformed chip thickness) must be controlled to be extremely small which mimic conditions for ductile mode cutting. This cutting regime scales down to the range of sub-micron to a few tens of nanometres level. Otherwise, ultra-precision machining can cause a crack-damaged layer when cutting brittle material if the depth of cut is too large (Fang & Zhang, 2003).

In practical, the good quality of machined surface of silicon machining by diamond turning without subsequent polishing requires ductile regime machining (Shibata, et al., 1996; Fang & Zhang, 2003). However, this is often limited by many reasons, for instances, rapid wear of diamond tools, machining scales are too large, unstable machine tool, etc. Moreover, the contribution to knowledge of micro cutting heat and temperature on single-crystal silicon can be drawn from chapter 6 indicate that the rapid and unpredictable increase of cutting temperature can occurred when cutting silicon. Consequently, the thermal effect may directly influences the quality of machined surface and tool wear since cutting heat and temperature is significantly influenced by micro cutting. This is according to a previous report (Yan, et al., 2003) that diamond tool can be used to cut nonferrous metals such as aluminium and copper for a distance up to a few hundreds of kilometres, but an initially sharp tool will become worn out rapidly when cutting silicon.

Thus, the integration of smart methods or models is needed for improving these main barriers preventing the ductile regime machining and consequent better surface finish.

Figure 7.1 Poor quality of the machined surface from diamond cutting silicon wafer caused by rapidly worn tool, cutting heat and thermal effect

7.4 Modelling approach for micro cutting of the devices

As seen from Figure 7.1, poor surface finish could occur if several aforementioned effects cannot be solved properly. In addition, in order to support the requirements of fabrications of the miniature and micro product, the substantial improvements on cutting performances are urgently needed including quality of machined surface, protection of tool wear, and productivity, respectively. Thus, the proper methods or models are critical needed to eliminate these effects as much as possible. The modelling approach, the so-called the modelling of micro cutting application (MMCA) is then proposed and employed in micro cutting of single-crystal silicon.

Due to the study on the individual components of micro cutting mechanics and physics, benefits are gained for improving micro cutting performances, the MMCA is based on combination of advantages and benefits of individual components. In other words, the benefits of study on individual components, i.e., dynamic stiffness, micro cutting force modelling, and micro cutting heat/temperature are integrated together to establish the modelling approach

(MMCA) of crystal silicon cutting as to the application case study. The description of MMCA and its sub-modelling are illustrated in Figure 7.2.
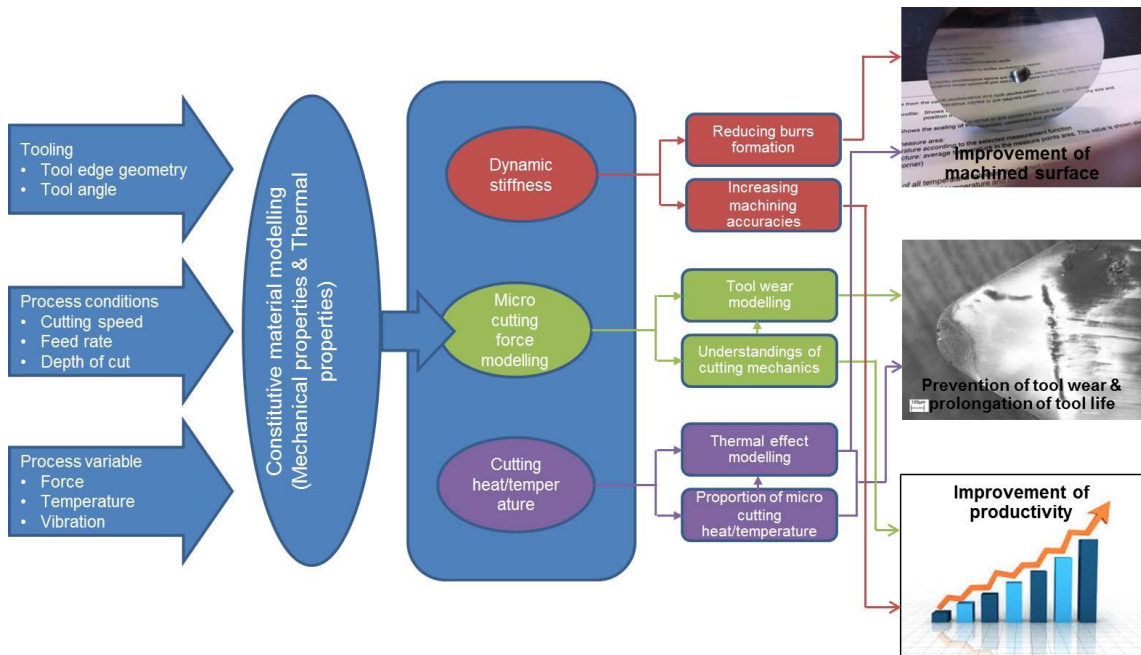
Figure 7.2 The modelling of micro cutting application (MMCA) applied to the cutting performance improvement

The MMCA is a model approach to integrate the benefits of research studies in three main components of micro cutting mechanics and physics as previously presented. The model approach initially depends on parameters including the tooling geometries and process variables, throughout the proper cutting conditions. These parameters are added to the model; consequently constitutive material modelling parameters are then identified. The cutting results include cutting force, cutting temperature, machined surface etc., are generally obtained after the cutting process. Additionally, the three main components of research studies are further integrated to the model in order to improve the micro cutting performances. Consequently, the improvements of cutting results will be achieved as illustrated in Figure 7.2. Thus, three key benefits of cutting performances include quality of machined surface, prolongation of tool life, and improvement of productivity can be improved with the MMCA. In addition, each component of study results in the differently machining improvements which separately explain as following these three sub-topics.

7.4.1 Dynamic stiffness

Based on Chapter 4, the dimensioned errors of micro machining and burrs formation can possibly be reduced by optimised and controlled dynamic stiffness. It can then be summarised that the two main benefits to study in dynamic stiffness are based on decreased burrs formation, and increase machining accuracies, respectively.

Consequently, it can be employed in application of single-crystal silicon cutting as proposed. Thus, the dynamic stiffness in the modelling of micro cutting application (MMCA) can help in decreasing burrs formation and increasing machining accuracy. Accordingly, the quality of machined surface would then be improved corresponding to the reducing of burrs formation. Moreover, the increasing of machining accuracy causes of the improvements of productivity. Thus, the machined surface modelling based on dynamic stiffness control and optimisation is possibly further developed.
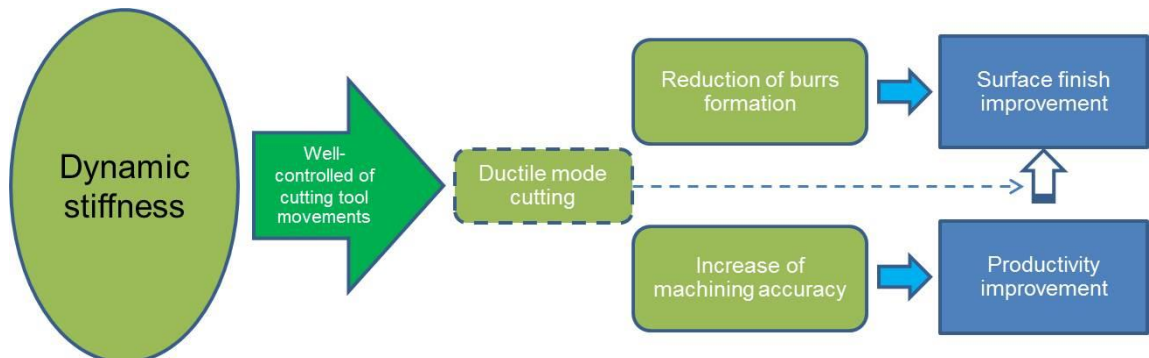
Figure 7.3 Sub-modelling illustrates the benefits of dynamic stiffness study

Further analysis, due to the dynamic movements of cutting tool are always controlled by hysteresis compensated module during the cutting process, consequent and scaling of machining (undeformed chip thickness) as extremely small and constant. This possibly causes the condition for ductile regime machining during cutting process of silicon. Thus, the better surface finish can be achieved. This may also claim that the use of dynamic stiffness control may have improved the ductile mode cutting on brittle material such silicon.

7.4.2 Cutting force modelling

In Chapter 5, the model approach of micro cutting force can be established by dividing the two aspects namely amplitude and spatial aspects. The benefits of the amplitude aspect is based on the better understandings and interpretations of micro cutting mechanics and physics while the real-time tool wear detection can be achieved by spatial aspect. Both benefits can be further integrated to the MMCA in order for improving micro cutting of crystal silicon.

The real-time tool wear detection based on spatial aspect can be further developed as a tool wear modelling method. Accordingly, this tool wear modelling can be further integrated as the detecting tool in the MMCA. This tool modelling associated with the understandings of micro cutting mechanisms based on micro cutting force modelling (amplitude aspect) could be contributed to protection of the cutting tool deteriorations and breakages in diamond cutting of single-crystal silicon. Thus, prevention of tool wear and consequent prolongation of tool life can be achieved.

Also, the better understandings of characteristics of micro cutting are essential for the improvement of productivity. Thus, the two possible improvements when added benefits of micro cutting force modelling to the MMCA that prolongation of tool life and productivity improvement can be attained (Figure 7.4).
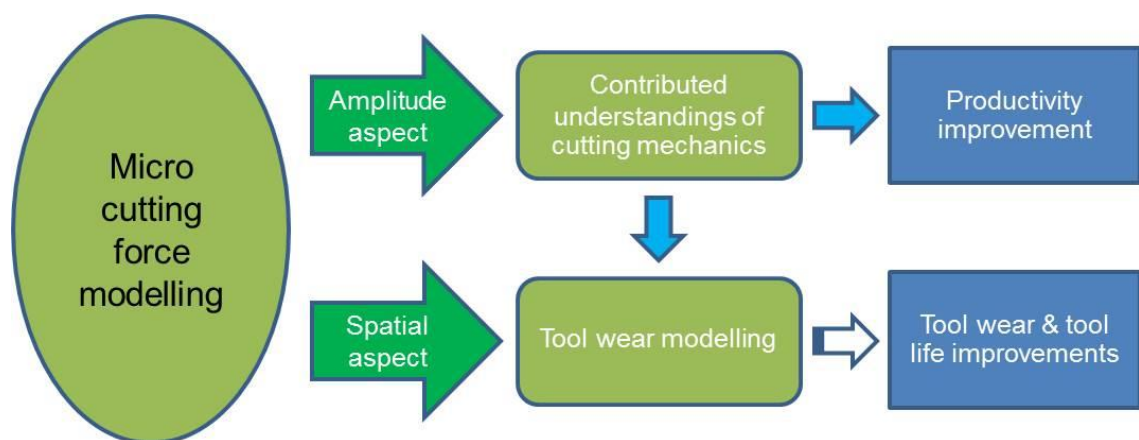
Figure 7.4 Sub-modelling illustrates the benefits of micro cutting force modelling study

7.4.3 Cutting heat and temperature

The contribution to knowledge of micro cutting heat and temperature can be drawn from chapter 6. The contribution of partitioned distribution of cutting heat and temperature in micro cutting particularly included diamond tool, workpiece and chip, respectively, are investigated and analysed. Based on this proportional analysis, the contribution to knowledge that the diamond tool/tool tip is the highest proportion of cutting heat can be acknowledged. Thus, avoidance of cutting heat at tool tip and correspondingly avoiding the thermal effects on cutting tool wear.
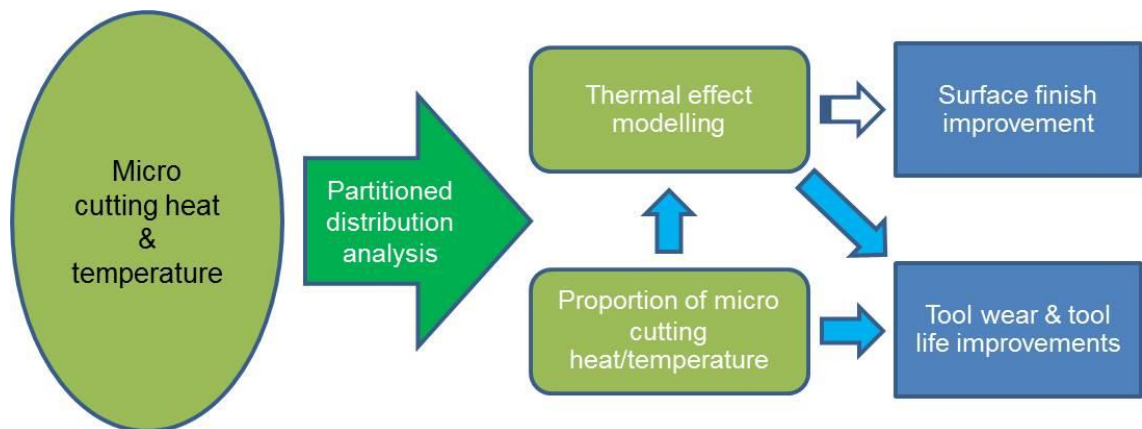
Figure 7.5 Sub-modelling illustrates the benefits of micro cutting heat and temperature study

The further development of thermal effect modelling can be carried out based on this partitioned distribution analysis. Accordingly, the scientific understanding of the remarkably undesirable marks left on machined surface due to thermal effect and consequent tool wear when cutting silicon could be obtained. Thus, the undesirable marks would be eliminated when employing this modelling to the MMCA. Consequently, the tool wear rates and machined surface quality can be improved.
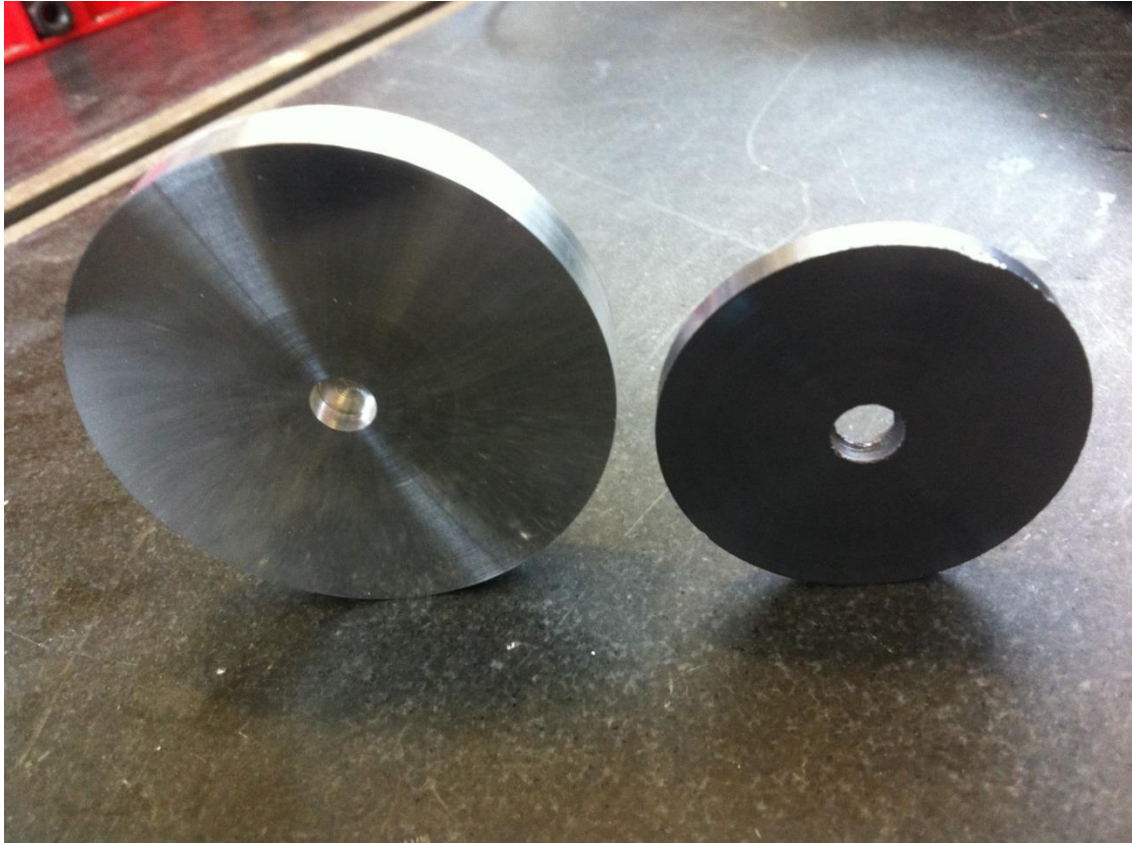
Figure 7.6 The better qualities of surface finish can be achieved when MMCA is employed, A: aluminium alloy (left), B: single-crystal silicon (right)

7.5 Conclusions

The MMCA is the modelling approach for application of silicon cutting with combining all benefits from three main studies on components of micro cutting mechanics and physics as previously investigated in the beginning chapters. This modelling helps in improvement of three main cutting performances especially included quality of machined surface finish, prolongation of tool life, and improvement of productivity, respectively. Figure 7.6 illustrates the better surface finish which can be improved by employed the MMCA.

The control of dynamic stiffness not only helps in increasing the machining accuracy and decreasing the burrs formation, but also it may help in improving the quality of machined surface and productivity improvement. Furthermore, the dynamic stiffness in correlation with the hysteresis compensated module may

possibly help to reach the ductile mode cutting if dynamic movements of cutting tool and consequent very small cutting scales are well-controlled.

The better understandings of micro cutting mechanisms based on micro cutting force modelling associated with the tool wear modelling can draw two main benefits to the MMCA of cutting silicon. The first benefit helps in protecting the tool from wear and prolonging the tool life. The second is improving the productivity of micro machining process.

The scientific understanding of cutting heat and temperature in micro cutting not only obtain contribution to knowledge of the heat partitioned distribution in micro cutting, but also the thermal effect modelling can be further developed which helps in improving machined surface quality. Also, both contributions namely partitioned distribution analysis and thermal effect modelling can finally improve the tool life.

Chapter 8 Conclusions and recommendations for future work

8.1 Conclusions

In order to accomplish the aim and objectives of the research approach, the experimental and simulation results are implemented, analysed, compared, and discussed in previous chapters. The distinctive conclusions can be summarised in this chapter

(1) The dynamic stiffness is identified and explored along with its effects in micro cutting of ultraprecision machining. Thus, the dynamic stiffness is defined and formulated. The micro slots accuracy and burrs formation can be influenced by dynamic stiffness.

(2) The micro slots accuracy and burrs formation can be minimised and reduced by implementing control of the characteristics of cutting tool movements, and consequent control and optimisation of dynamic stiffness. Thus, the minimisation and reduction of burrs formation and dimensional errors of micro slots are substantiated through sets of the experimental cutting associated with control of the dynamics stiffness by using the hysteresis compensation module.

(3) An innovative cutting force modelling approach is proposed for ultraprecision and micro cutting based on the specific cutting force at the unit cutting length and area as the so-called amplitude aspect, and the cutting forces are analysed against the dynamically varied cutting time interval as the so-called spatial aspect.

(4) Amplitude aspect can provide the insight into the micro cutting phenomena particularly in relation with the chip formation and size-effects. Spatial aspect using wavelet transform (WT) technique and standard deviation analysis can render their dynamic components to particularly represent dynamic effects of the cutting process and their correlation with tool wear.

(5) The scientific understanding of cutting temperature and heat partitioned distribution in micro cutting are analysed based on experimental investigation on cutting of titanium (Ti-6al-4V), aluminum (AA6082-T6) and single crystal silicon. The further supported by FE-based modelling and simulation on cutting temperature are conducted.

(6) The analyses on conductive heat transfer to examine the heat partitioned distribution in micro cutting particularly including diamond tool, workpiece, and chip are implemented based on single point diamond turning (SPDT).

8.2 Contributions to knowledge

(1) Dynamic stiffness is examined and formulated, which is verified particularly its dynamic effect on the micro cutting process. The 2 main effects particular include the micro slots accuracy and burrs formation can be minimised by control, optimise, and minimise the dynamic stiffness.

(2) An innovative cutting force modelling approach is proposed by employing the specific cutting force and corresponding quantitative analysis on the dynamic cutting process in diamond turning at the 0.1-1 N cutting force scale in particular (Lee & Cheung, 2003), so as to accurately represent the dynamic cutting behaviour including both amplitude and spatial aspects simultaneously.

(3) The size effect interpretation based on amplitude aspect by FB-based simulation conducted with chamfer lengths varies against rake angles of diamond cutting tool are agreed well with previous literature reviews and the experimental case studies.

(4) The monitoring and understanding the spatial aspect of the modelling formulation has possibility to measure and monitor the tool wear in process, which provide the industrial-feasible means to be used in ultraprecision and micro machining at an industrial scale.

(5) Feed forces are more influencing to the micro cutting process, for instance cutting temperature and tool wear direction, etc., rather than cutting forces in micro cutting.

(6) Scientific understanding of micro cutting heat, temperature and consequent proportions of cutting heat at the tool-workpiece-chip interface of aluminium AA6082-T6, single crystal silicon and titanium Ti-6al-4V, respectively.

(7) The highest cutting heat and temperature is occurred on tool tip, followed by the diamond tool, chip (for titanium cutting only) and workpiece, respectively for all materials which differs from that of conventional cutting.

(8) Such low cutting temperature when cutting of silicon cannot ensure that tool would not be dulled quickly like in aluminium cutting due to rapid and unpredictable increase in heat and temperature occurring during continuous machining on silicon.

8.3 Recommendations for future work

This research, the micro cutting mechanics and physics have been investigated in three previously unexplored areas including: dynamic stiffness, micro cutting force modelling, and micro cutting heat and temperature, respectively. However, due to the limitations of time and available facilities, more thorough investigations are not yet implemented. Thus, the suggestions for future work are recommended as the following areas:

(1) The material constitutive model for brittle materials such single crystal silicon remains challenging and requires an accurate model supported with experimental validations.

(2) The FE-based modelling & simulation on dynamic stiffness to simulate its effects in micro cutting is needed in validation and comparison to the experimental results.

(3) The experiment-based investigations on dynamic stiffness and its effects on brittle material such single crystal silicon is required.

(4) More specific issues of micro cutting mechanics and physics, for instance surface generation, ductile mode cutting, undeformed chip thickness, etc., interpretations using the novel cutting force modelling should be implemented for brittle materials in particular.

144

(5) An application of a smart cutting tool embedded with the model approach of cutting force algorithms can be further investigated in relevant to cutting tool wear detection in real time micro machining with smart cutting tool system.

References

Alting, L., Kimura, F., Hansen, H. & Bissacco, G., 2003. Micro Engineering. *CIRP Annals - Manufacturing Technology,* 52(2), p. 635–657.

Anon., 2005. *LabVIEW Advanced Signal Processing Toolkit: Wavelet Analysis Tools User Manual,* s.l.: National Instruments Corporation.

Aramcharoen, A. & Mativenga, P., 2009. Size effect and tool geometry in micromilling of tool steel. *Precision Engineering,* 33(4), p. 402–407.

Archenti, A., Thesis 2008. *Model-Based Investigation of Machining Systems Characteristics: Static and Dynamic Stability Analysis.* Stockholm: KTH Production Engineering Royal Institute of Technology .

Arefin, S., Li, X. P., Rahman, M. & Liu, K., 2007. The upper bound of tool edge radius for nanoscale ductile mode cutting of silicon wafer. *The International Journal of Advanced Manufacturing Technology ,* 31 (7-8), pp. 655-662 .

Bifano, T. G., Dow, T. A. & Scattergood, R. O., 1991. Ductile-Regime Grinding: A New Technology for Machining Brittle Materials. *Journal of Manufacturing Science and Engineering,* 113(2), pp. 184-189.

Blackley, W. & Scattergood, R., 1991. Ductile-regime machining model for diamond turning of brittle materials. *Precision Engineering ,* 13 (2), pp. 95-103.

Blake, N., P., Scattergood & O, R., 1990. Ductile-Regime Machining of Germanium and Silicon. *Journal of the American Ceramic Society,* 73(4), pp. 949-957.

Born, D. K. & Goodman, W., 2001. An empirical survey on the influence of machining parameters on tool wear in diamond turning of large single-crystal silicon optics. *Precision Engineering,* 25(4), p. 247–257.

Brinksmeier, E., Gläbe, R. & Osmer, J., 2006. Ultra-Precision Diamond Cutting of Steel Molds. *CIRP Annals - Manufacturing Technology,* 55(1), p. 551–554.

Chae, J., Park, S. & Freiheit, T., 2006. Investigation of micro-cutting operations. *International Journal of Machine Tools & Manufacture,* 46(3-4), p. 313–332.

Chapman, G., 2004 . *Ultra-precision Machining Systems; an Enabling Technology for Perfect Surfaces,* s.l.: Moore Nanotechnology Systems LLC.

Cheng, K., 2009. *Machining dynamics : fundamentals, applications and practices.* s.l.:Springer Series in Advanced Manufacturing .

Cheng, K. & Huo, D., 2013. *Micro-Cutting: Fundamentals and Applications.* s.l.:Wiley.

Chen, G. et al., 2013. Measurement and finite element simulation of micro-cutting temperatures of tool tip and workpiece. *International Journal of Machine Tools & Manufacture,* Volume 75, pp. 16-26.

Cuttino, J. F., Arthur C. Miller, J. & Schinstock, D. E., 1999. Performance optimization of a fast tool servo for single-point diamond turning machines. *IEEE/ASME Transactions on Mechatronics,* 4 (2), pp. 169-179.

Dan, L. & Mathew, J., 1990. Tool wear and failure monitoring techniques for turning—A review. *International Journal of Machine Tools and Manufacture,* 30(4), p. 579–598.

Davies, M. A. et al., 2003. Application of precision diamond machining to the manufacture of micro-photonics components. *Proceedings of SPIE ,* Volume 5183, pp. 94-108.

Dornfeld, D. A., 1990. Neural network sensor fusion for tool condition monitoring. *Annals of the CIRP,* Volume 39, pp. 101-105.

Dornfeld, D., Min, S. & Takeuchi, Y., 2006. Recent Advances in Mechanical Micromachining. *Annals of the CIRP,* Volume 55, pp. 745-768.

Dow, T. A., Miller, M. H. & Falter, P. J., 1991. Application of a fast tool servo for diamond turning of nonrotationally symmetric surfaces. *Precision Engineering,* 13(4), p. 243–250.

Drescher, J. & Dow, T. A., 1990. Tool force model development for diamond turning. *Precision Engineering,* 12(1), p. 29–35.

Duan, C., Cai, Y., Li, Y. & Wang, M., 2009. *Finite Element Simulation of Cutting Temperature Field during High Speed Machining Hardened Steel Based on ABAQUS.* s.l., s.n.

Ezugwu, E., Silva, R. D., Bonney, J. & Machado, Á., 2005. Evaluation of the performance of CBN tools when turning Ti–6Al–4V alloy with high pressure coolant supplies. *International Journal of Machine Tools & Manufacture,* Volume 45, p. 1009–1014.

Fang, F. Z. & Zhang, G. X., 2003. An experimental study of edge radius effect on cutting single crystal silicon. *The International Journal of Advanced Manufacturing Technology,* 22(9-10), pp. 703-707.

Fang, G. & Zeng, P., 2005. Three-dimensional thermo–elastic–plastic coupled FEM simulations for metal oblique cutting processes. *Journal of Materials Processing Technology,* Volume 168, p. 42–48.

Fang, N., Pai, P. S. & Edwards, N., 2012. Tool-Edge Wear and Wavelet Packet Transform Analysis in High-Speed Machining of Inconel 718. *Journal of Mechanical Engineering,* 58 (3), pp. 191-202.

François, D., Filippi, E. & Rivière-Lorphèvre, E., 2009. *Chip Formation and Minimum Chip Thickness in Micro-milling.* s.l., Proceedings of the 12th CIRP conference on modeling of machining operations, pp. 339-346.

Fratini, L. & Buffa, G., 2005. CDRX modelling in friction stir welding of aluminium alloys. *International Journal of Machine Tools & Manufacture,* 45(10), p. 1188–1194.

Gäbler, J. & Pleger, S., 2010. Precision and micro CVD diamond-coated grinding tools. *International Journal of Machine Tools and Manufacture,* 50(4), p. 420–424.

Gluche, P., Ertl, S. & Kohn, E., 2003. *DIAMOND CUTTING TOOL.* United States, Patent No. US 6,599,178 B1.

Hale, L. C., 1999. *Principles and techniques for designing precision machines,* Ph.D. Thesis: Massachusetts Institute of Technology.

Huang, P., Li, J., Sun, J. & Zhou, J., 2013. Vibration analysis in milling titanium alloy based on signal processing of cutting force. *The International Journal of Advanced Manufacturing Technology,* 64(5-8), pp. 613-621.

III, J. T. C. & Strenkowski, J. S., 1988. Finite element models of orthogonal cutting with application to single point diamond turning. *International Journal of Mechanical Sciences,* 30(12), p. 899–920.

Ikawa, N. & Shimada, S., 1985. Diamond tools for ultra-precision cutting. *Trans. JSME,* 456(50), p. 1321–1326.

IV, J. H. L. & V, J. H. L., 2012. *A Heat Transfer Textbook, 4th edition.* s.l.:Phlogiston. Press.

Kim, G.-H., Yoon, G.-S., Son, J.-I. & Cho, M.-W., 2012. Investigation on the Effect of Low Temperature Micro Cutting Process for Mold Core Material. *International Journal of Precision Engineering and Manufacturing,* Volume 13, pp. 783-788.

Kim, J.-D. & Kim, D. S., 1995. Theoretical analysis of micro-cutting characteristics in ultra-precision machining. *Journal of Materials Processing Technology,* 49(3–4), p. 387–398.

Kim, S.-G.et al., April. 9-11, 2008. *Analysis of dynamic characteristics and evaluation of dynamic stiffness of a 5-axis multi-tasking machine tool by using F.E.M and exciter test.* in KINTEX, Gyeonggi-do, Korea, International Conference on Smart Manufacturing Application.

Kwak, J.-S., 2006. Application of wavelet transform technique to detect tool failure in turning operations. *The International Journal of Advanced Manufacturing Technology ,* 28(11-12), pp. 1078-1083 .

Lai, X. et al., 2008. Modelling and analysis of micro scale milling considering size effect, micro cutter edge radius and minimum chip thickness. *International Journal of Machine Tools and Manufacture,* 48 (1), p. 1–14.

Lee, K. & Dornfeld, D. A., 2005. Micro-burr formation and minimization through process control. *Precision Engineering,* 29(2), p. 246–252.

Lee, W. B. & Cheung, B. C. F., 2003. *Surface Generation in Ultra-precision Diamond Turning: Modelling and Practices.* 1st ed. s.l.:John Wiley and Sons Ltd, United Kingdom.

Lee, W. B., Cheung, C. F. & To, S., 2002. A Microplasticity Analysis of Micro-Cutting Force Variation in Ultra-Precision Diamond Turning. *Journal of Manufacturing Science and Engineering,* 124(2), pp. 170-177 .

Leung, T., Lee, W. & Lu, X., 1998. Diamond turning of silicon substrates in ductile-regime. *Journal of Materials Processing Technology,* 73(1-3), pp. 42-48.

Li, H., Ibrahim, R. & Cheng, K., 2011. Design and principles of an innovative compliant fast tool servo for precision engineering. *The journal Mechanical Sciences ,* Volume 2, pp. 139-146.

Lin, C.-Y. & Chen, P.-Y., 2012 . Hysteresis compensation and high-performance tracking control of piezoelectric actuators. *Proceedings of the Institution of Mechanical Engineers, Part I: Journal of Systems and Control Engineering,* 226(8), pp. 1050-1059 .

Lin, J., 2001. Feature extraction of machine sound using wavelet and its application in fault diagnosis. *NDT & E International,* 34(1), p. 25–30.

Liu, K., 2005. *Process Modeling Of Micro-Cutting Including Strain Gradient Effects.* The thesis requirements for Doctor of Philosophy: Georgia Institute of Technology.

Liu, K. & Melkote, S. N., 2005. Material Strengthening Mechanisms and Their Contribution to Size Effect in Micro-Cutting. *Journal of Manufacturing Science and Engineering,* 128 (3), pp. 730-738.

Liu, K. & Melkote, S. N., 2007. Finite element analysis of the influence of tool edge radius on size effect in orthogonal micro-cutting process. *International Journal of Mechanical Sciences,* 49(5), p. 650–660.

Liu, X., DeVor, R. E. & Kapoor, S. G., 2006. An Analytical Model for the Prediction of Minimum Chip Thickness in Micromachining. *Journal of Manufacturing Science and Engineering, Transactions of the ASME,* 128(2), pp. 474-481.

Liu, X., DeVor, R., Kapoor, S. & Ehmann, K., 2004. The mechanics of machining at the microscale: Assessment of the current state of the science. *Journal of Manufacturing Science and Engineering, Transactions of the ASME,* 126(4), pp. 666-678.

Li, X., 2002 . A brief review: acoustic emission method for tool wear monitoring during turning. *International Journal of Machine Tools and Manufacture,* 42(2), p. 157–165.

Ikawa, N. et al., 1991. Ultraprecision Metal Cutting - The Past, the Present and the Future. *CIRP Annals - Manufacturing Technology,* 40(2), pp. 587-594.

Lo-A-Foe, T., Dautzenburg, J. & Van Der Wolf, A. C. H., 1988. *Cutting forces and their influences upon the surface integrity in single-point diamond turning.* Tokyo, Proceedings of the International congress for Ultra-precision Technology.

Lucca, D., Seo, Y. & Komanduri, R., 1993. Effect of Tool Edge Geometry on Energy Dissipation in Ultraprecision Machining. *CIRP Annals - Manufacturing Technology,* 42 (1), p. 83–86.

Lucca, D., Seo, Y., Rhorer, R. & Donaldson, R., 1994. Aspects of Surface Generation in Orthogonal Ultraprecision Machining. *CIRP Annals - Manufacturing Technology,* 43(1), p. 43–46.

Luo, X., Cheng, K., Webb, D. & Wardle, F., 2005. Design of ultraprecision machine tools with applications to manufacture of miniature and micro components. *Journal of Materials Processing Technology,* 167(2-3), pp. 515-528.

Luttrell, D. E., July 2010. *Innovations in ultra-precision machine tools: design and applications,* s.l.: Moore Nanotechnology Systems, LLC.

Lu, Z. & Yoneyama, T., 1999. Micro cutting in the micro lathe turning system. *International Journal of Machine Tools and Manufacture,* 39(7), p. 1171–1183.

Mamalis, A., HorvaÂth, M., Branis, A. & Manolakos, D., 2001. Finite element simulation of chip formation in orthogonal metal cutting. *Journal of Materials Processing Technology,* 110(1), pp. 19-27.

Manjunathaiah, J. & Endres, W. J., 2000. A Study of Apparent Negative Rake Angle and Its Effect on Shear Angle During Orthogonal Cutting with Edge-Radiused Tools. *TRANSACTIONS- NORTH AMERICAN MANUFACTURING RESEARCH INSTITUTION OF SME,* Volume 28, pp. 197-202.

Marusich, T. & Ortiz, M., 1995. Modelling and simulation of high-speed machining. *International journal for numerical methods in engineering,* 38(21), pp. 3675-3694.

Maycock, P., 1967. Thermal conductivity of silicon, germanium, III–V compounds and III–V alloys. *Solid-State Electronics,* 10(3), p. 161–168.

Merritt, H. E., 1965. Theory of Self-excited machine-tool chatter: contribution to machine-tool chatter research. *Journal of Manufacturing Science and Engineering,* 87(4), pp. 447-454 .

Michael J. Moran, H. N. S., 2006. *Fundamentals of Engineering Thermodynamics.* s.l.:John Wiley & Sons, Inc..

Misiti, M., Misiti, Y., Oppenheim, G. & Poggi, J.-M., 2000. *Wavelet Toolbox For Use with MATLAB,* s.l.: The MathWorks, Inc..

Miyamoto, I., Ezawa, T. & Nishimura, K., 1990 . Ion beam machining of single-point diamond tools for nano-precision turning. *Nanotechnology,* Volume 1, pp. 44-49.

Mohamed, M. F. A., 2006. *Multi-scale modelling of material behaviour in micro-cutting processes.* McMaster University, Canada: UMI Dissertations Publishing.

Moran, M. J. & Shapiro, H. N., 2006. *Fundamentals of Engineering Thermodynamics.* s.l.:John Wiley & Sons, Inc..

Moriwaki, T., 1989. Machinability of Copper in Ultra-Precision Micro Diamond Cutting. *CIRP Annals - Manufacturing Technology,* 38(1), p. 115–118.

Moriwaki, T., Horiuchi, A. & Okuda, K., 1990. Effect of Cutting Heat on Machining Accuracy in Ultra-Precision Diamond Turning. *CIRP Annals - Manufacturing Technology,* 39(1), pp. 81-84.

Nakasuji, T. et al., 1990. Diamond Turning of Brittle Materials for Optical Components. *CIRP Annals - Manufacturing Technology,* 39(1), p. 89–92.

Ng, C. K., Melkote, S. N., Rahman, M. & Kumar, A. S., 2006. Experimental study of micro- and nano-scale cutting of aluminum 7075-T6. *International Journal of Machine Tools and Manufacture,* 46(9), p. 929–936.

Nishiguchi, T., Maeda, Y., Masuda, M. & Sawa, M., 1988. Mechanism of Micro Chip Formation in Diamond Turning of Al-Mg Alloy. *CIRP Annals - Manufacturing Technology,* 37(1), p. 117–120.

Noh, Y. J., Nagashima, M., Arai, Y. & Gao, W., 2009. Fast Positioning of Cutting Tool by a Voice Coil Actuator for Micro-Lens Fabrication. *International Journal of Automation Technology,* 3(3), pp. 257-262.

Özel, T., 2006. The influence of friction models on finite element simulations of machining. *International Journal of Machine Tools and Manufacture,* 46(5), p. 518–530.

Özel, T. & Karpat, Y., 2007. Identification of constitutive material model parameters for high-strain rate metal cutting conditions using evolutionary computational algorithms. *Materials and Manufacturing Processes,* 22(5), p. 659–667.

Pal, S. et al., 2011. Tool wear monitoring and selection of optimum cutting conditions with progressive tool wear effect and input uncertainties. *Journal of Intelligent Manufacturing,* 22(4), p. 491–504.

Panusittikorn, W., 2010. *Error Compensation Using Inverse Actuator Dynamics,* PhD dissertation: the Graduate Faculty of North Carolina State University.

Patten, J., Gao, W. & Yasuto, K., 2005. Ductile regime nanomachining of single-crystal silicon carbide. *Journal of Manufacturing Science and Engineering, Transactions of the ASME,* 127(3), pp. 522-532.

Perret, R., 2007. *Power Electronics Semiconductor Devices.* s.l.:John Wiley & Sons.

Ramesh, R., Mannan, M. & Poo, A., 2000. Error compensation in machine tools — a review: Part I: geometric, cutting-force induced and fixture-dependent errors. *International Journal of Machine Tools and Manufacture,* 40(9), p. 1235–1256.

Rao, P. et al., 2014. Real-Time Identification of Incipient Surface Morphology Variations in Ultraprecision Machining Process. *Journal of Manufacturing Science and Engineering,* 136(2), pp. 021008-1-11.

Ravindra, H., Srinivasa, Y. & Krishnamurthy, R., 1993. Modelling of tool wear based on cutting forces in turning. *Wear,* 169 (1), pp. 25-32.

Rehorn, A. G., Jiang, J. & Orban, P. E., 2005. State-of-the-art methods and results in tool condition monitoring: a review. *The International Journal of Advanced Manufacturing Technology,* 26(7-8), pp. 693-710.

Rhorer, R. L. & Evans., C. J., 1995. Fabrication of optics by diamond turning. In: -, ed. *Handbook of Optics 1.* -: -, pp. -.

Riemer, O., 2011. *Advances in Ultra Precision Manufacturing.* -, Proc. Jpn. Soc. Precis. Eng.

Rupnowski, P. & Sopori, B., 2009. Strength of silicon wafers: fracture mechanics approach. *International Journal of Fracture,* 155(1), p. 67–74.

Scheffer, C. & Heyns, P. S., 2001. Wear Monitoring In Turning Operations Using Vibration And Strain Measurememts. *Mechanical Systems and Signal Processing,* 15(6), p. 1185–1202.

Shibata, T., Fujii, S., Makino, E. & Ikeda, M., 1996. Ductile-regime turning mechanism of single-crystal silicon. *Precision Engineering,* 18(2–3), p. 129–137.

Shimada, S. et al., 1992. Molecular Dynamics Analysis as Compared with Experimental Results of Micromachining. *CIRP Annals - Manufacturing Technology,* 41(1), pp. 117-120.

Shimada, S. et al., 1993. Feasibility Study on Ultimate Accuracy in Microcutting Using Molecular Dynamics Simulation. *CIRP Annals - Manufacturing Technology,* 42(1), pp. 91-94.

Sobhan, C. & Peterson, G., 2008. *Microscale and Nanoscale Heat Transfer: Fundamentals and Engineering Applications.* - ed. -: CRC Press.

Son, S. M., Lim, H. S. & Ahn, J. H., 2005. Effects of the friction coefficient on the minimum cutting thickness in micro cutting. *International Journal of Machine Tools and Manufacture,* 45(4–5), p. 529–535.

Suzuki, H., Moriwaki, T., Okino, T. & Ando, Y., 2006. Development of Ultrasonic Vibration Assisted Polishing Machine for Micro Aspheric Die and Mold. *CIRP Annals - Manufacturing Technology,* 55(1), p. 385–388.

Sze-Wei, G., Han-Seok, L., Rahman, M. & Watt, F., 2007. A fine tool servo system for global position error compensation for a miniature ultra-precision lathe. *International Journal of Machine Tools and Manufacture,* 47(7–8), p. 1302–1310.

Tansel, I. et al., 2000. Tool wear estimation in micro-machining.: Part I: tool usage–cutting force relationship. *International Journal of Machine Tools & Manufacture,* Volume 40, p. 599–608.

Tan, X., 2002. Comparisons of friction models in bulk metal forming. *Tribology International,* 35 (6), p. 385–393.

Teti, R., Jemielniak, K., O'Donnell, G. & Dornfeld, D., 2010. Advanced monitoring of machining operations. *CIRP Annals - Manufacturing Technology,* 59(2), p. 717–739.

Tian, Y., Shirinzadeh, B. & Zhang, D., 2009. A flexure-based mechanism and control methodology for ultra-precision turning operation. *Precision Engineering,* 33(2), p. 160–166.

Tönshoff, H. et al., 1990. Abrasive Machining of Silicon. *CIRP Annals - Manufacturing Technology,* 39(2), p. 621–635.

Venkatachalam, S., Li, X. & Liang, S. Y., 2009. Predictive modeling of transition undeformed chip thickness in ductile-regime micro-machining of single crystal brittle materials. *Journal of Materials Processing Technology,* 209(7), p. 3306–3319.

Volz, S., 2007. *Microscale and Nanoscale Heat Transfer. -* ed. -: Springer.

Wang, C. et al., 2014. Design of an instrumented smart cutting tool and its implementation and application perspectives. *Smart Materials and Structures,* 23(3), pp. 1-11.

Wang, L., Mehrabi, M. G. & Kannatey-Asibu, E., 1998. Tool wear monitoring in reconfigurable machining systems through Wavelet analysis. *Journal of Electronic Imaging ,* Volume XXIX, pp. 1017-9909.

Wu, T., 2012. *Tooling Performance in Micro Milling: Modelling, Simulation and Experimental Study.* PhD thesis: School of Engineering and Design, Brunel University.

Xiaoli, L., Yingxue, Y. & Zhejun, Y., 1997. On-line tool condition monitoring system with wavelet fuzzy neural network. *Journal of Intelligent Manufacturing,* 8(4), pp. 271-276.

Yang, K. et al., 2011. Tool edge radius effect on cutting temperature in micro-end-milling process. *The International Journal of Advanced Manufacturing Technology,* 52(9-12), pp. 905-912.

Yan, J., Syoji, K. & Tamaki, J., 2003. Some observations on the wear of diamond tools in ultra-precision cutting of single-crystal silicon. *Wear,* 255(7–12), p. 1380–1387.

Yan, J. et al., 2001. On the ductile machining of silicon for micro electro-mechanical systems (MEMS), opto-electronic and optical applications. *Materials Science and Engineering: A,* 297(1–2), p. 230–234.

Yigit, A. S. & Ulsoy, A. G., 2002. Dynamic stiffness evaluation for reconfigurable machine tools including weakly non-linear joint characteristics. *Proceedings of the Institution of Mechanical Engineers, Part B: Journal of Engineering Manufacture,* 216(1), pp. 87-101.

Zhao, X. & Bhushan, B., 1998. Material removal mechanisms of single-crystal silicon on nanoscale and at ultralow loads. *Wear,* 223(1–2), p. 66–78.

Zhou, J., Hayden, M. & Gao, X., 2013. An investigation of the strain rate and temperature effects on the plastic flow stress and ductile failure strain of aluminum alloys 5083-H116, 6082-T6 and a 5183 weld metal. *Proceedings of the Institution of Mechanical Engineers, Part C: Journal of Mechanical Engineering Science,* 227(5), pp. 883-895.

Zhou, L. & Cheng, K., 2009. Modelling and simulation of the dynamic cutting process and surface topography generation in nano/micro cutting. *International Journal of Nanomanufacturing,* 3(1-2), pp. 3-14.

Zong, W. J. et al., 2007. Finite element optimization of diamond tool geometry and cutting-process parameters based on surface residual stresses. *The International Journal of Advanced Manufacturing Technology,* 32(7-8), p. 666–674.

Zong, W. et al., 2006. FEM optimization of tool geometry based on the machined near surface's residual stresses generated in diamond turning. *Journal of Materials Processing Technology,* 180(1-3), p. 271–278.

Appendices

Appendix 1:
List of Publications Arising from the Research

1. W. Sawangsri, K. Cheng. "An investigation on Improved Theoretical Modelling for Nanometric Cutting Physics," *the 6th International Congress on Precision Machining (ICPM 2011)*, 13-15th September 2011, Liverpool, United Kingdom

2. W. Sawangsri, K. Cheng. "An experiment-based investigation on the partitioned distribution of cutting heat and cutting temperature in micro cutting," *the 9th International Conference on MicroManufacturing (ICOMM 2014)*, 25-28th March 2014, Singapore

3. W. Sawangsri, K. Cheng. "A novel approach to cutting force modelling in diamond turning and its correlation analysis on tool wear," *Euspen's 14th International Conference & Exhibition*, 2nd - 6th June 2014, Dubrovnik, Croatia

4. W. Sawangsri, K. Cheng. "An innovative approach to cutting force modelling in diamond turning and its correlation analysis with tool wear". *Proceedings of the Institution of Mechanical Engineers, Part B: Journal of Engineering Manufacture*, 2014 (Accepted)

5. W. Sawangsri, K. Cheng. "Investigation on partitioned distribution of cutting heat and cutting temperature in micro cutting". *Journal of Micro and Nano-Manufacturing , Transactions of the ASME*, 2014 (Submitted)

6. C. Wang, K. Cheng, N. Nelson, W. Sawangsri and R Rakowski. "Cutting force based analysis and correlative observations on the tool wear in diamond turning of single-crystal silicon". *Proceedings of the Institution of Mechanical Engineers, Part B: Journal of Engineering Manufacture*, 2014 (Accepted)

Appendix 2:

Summary of Facilities in the Research

Diamond turning machine test rig	1. 3D diamond turning machine 2. Fast tool servo
Diamond cutting tools	1. Diamond cutting tool with the edge radius 82 nm and nose radius 0.30 mm
Work materials	1. Aluminium alloy AA6082-T6 2. Titanium alloy Ti-6al-4V 3. Single crystal silicon
Instrument and metrology	1. Kistler Dynamometer MiniDyn 9256C2 with a charge amplifier 5070A 2. White light interferometer Zygo NewView 5000 3. Optris PI160 thermal imager with 120 Hz frame rate 4. Microscope Axio Scope.A1 5. Optical microscope TESA VISIO-200

Appendix 3:

Technical Specifications of Zygo NewView 5000

System Overview

Zygo NewView 5000

Tool Overview:

The Zygo NewView 5000 is a non-contact 3D surface profiler that uses scanning white light interferometry to image and measure the microstructure and topography of surfaces. It provides graphic images and high-resolution numerical analysis to accurately characterize the surface structure of test parts.

Tool Capabilities/Limitations:

- Objectives: 5x, 10x, 50x
- Vertical Resolution: 0.1-20nm (FDA resolution setting dependent)
- Lateral Resolution Range: 0.64 – 2.6µm (objective dependent)
- Max Vertical Step Height: 5mm
- Vertical scan rate: ≤ 10µm/sec
- Sample specifications:
    - Type: opaque and transparent surfaces
    - Max Roughness: ≤ 100µm Rp
    - Reflectivity: 4-100%
    - Max Sample Thickness: 104mm
    - Note: If your sample has surfaces with dissimilar optical properties, the accuracy of step height measurements from one material to the other may be degraded. The dissimilar optical properties cause relative phase shift error in the measured vertical heights of the dissimilar materials.

Appendix 4:
Technical Specifications of Kistler Dynamometer MiniDyn 9256C2 and its Calibration Certificate

Technical Data

KISTLER
measure. analyze. innovate.

8. Technical Data

Please note that all technical data and all additional information in this section my be altered at any time without prior notice.

8.1 MiniDyn Type 9256C1 and Type 9256C2

Measuring range	F_x, F_y, F_z	N	–250 … 250
Type 9256C1	M_x, M_z	N·m	–8 … 8
Type 9256C2	M_x, M_z	N·m	–11 … 11
Calibrated measuring range			
100 %	F_x, F_y, F_z	N	0 … 250
10 %	F_x, F_y, F_z	N	0 … 25
Overload	F_x, F_y, F_z	N	–300/300
Threshold		N	<0,002
Sensitivity	F_x, F_z	pC/N	≈–26
	F_y	PC/N	≈–13
Linearity, all ranges		%FSO	≤±0,4
Hysteresis, all ranges		%FSO	≤0,5
Overload		%	≤±2
Rigidity	c_x, c_z	N/μm	>250
	c_y	N/μm	>300
Natural frequency (mounted on rigid base)			
Type 9256C1	f_n (x)	kHz	≈5,1
	f_n (y)	kHz	≈5,5
	f_n (z)	kHz	≈5,6
Type 9256C2	f_n (x)	kHz	≈4,0
	f_n (y)	kHz	≈4,8
	f_n (z)	kHz	≈4,6
Operating temperature range		°C	0 … 70
Insulation resistance		Ω	$>10^{13}$
Ground isolated		Ω	$>10^{8}$
Degree of protection EN60529 (with connecting cable Type 1696A5/1697A5)			IP67
Weight Dynamometer	Type 9256C1/C2	kg	0,75/0,87
Top plate	Type 9256C1/C2	kg	0,24/0,36
Clamping area Type 9256C1		mm	39x80
Type 9256C2		mm	55x80

Kalibrierschein
Calibration Certificate

Type Kistler 9256C2   Serial No. 4277565

Kalibriert durch Calibration Technician	Datum Date	
K. Ta	15. Jun. 2012	

Referenzgeräte Reference Equipment	Typ Type	Serien-Nr. Serial No.
Gebrauchsnormal Working Standard	Kistler 9251A Kistler 9252A Kistler 9252A	446442 517947 550683
Ladungskalibrator Charge Calibrator	Kistler 5395A	441991

Umgebungstemperatur Ambient Temperature °C	Relative Feuchte Relative Humidity %
24	53

Messergebnisse Results of Measurement

Kalibrierter Bereich Calibrated Range N	Empfindlichkeit Sensitivity pC / N	Linearität Linearity $\leq \pm$ %FSO	Übersprechen Cross talk %		%
Fx 0 … 250	-25,37	0,06	$Fx \rightarrow Fy$ 0,5	$Fx \rightarrow Fz$ -0,5	
Fx 0 … 25	-25,31	0,03	$Fx \rightarrow Fy$ 0,5	$Fx \rightarrow Fz$ -0,4	
Fy 0 … 250	-12,72	0,11	$Fy \rightarrow Fx$ 0,5	$Fy \rightarrow Fz$ 0,3	
Fy 0 … 25	-12,67	0,06	$Fy \rightarrow Fx$ 0,7	$Fy \rightarrow Fz$ 0,1	
Fz 0 … 250	-25,67	0,07	$Fz \rightarrow Fx$ -0,6	$Fz \rightarrow Fy$ 0,8	
Fz 0 … 25	-25,60	0,07	$Fz \rightarrow Fx$ -0,8	$Fz \rightarrow Fy$ 0,7	

Messverfahren Measurement Procedure	Kontinuierliche Kalibrierung, Vergleichsverfahren Continuous Calibration, Comparison Method

Kistler betreibt die SCS Kalibrierstelle Nr. 049, akkreditiert nach ISO 17025. SCS Kalibrierzertifikate sind auf Bestellung erhältlich.
Kistler operates the SCS Calibration Laboratory No. 049, which is accredited per ISO 17025. SCS Calibration Certificates are available on request.

Bestätigung Confirmation

Das oben durch die Serienummer identizierte Gerät entspricht der Vereinbarung der Bestellung und hält die Herstelltoleranzen gemäss den Spezifikationen der Datenblätter ein. Dieses Dokument erfüllt die Anforderungen von EN 10204 Abnahmeprüfzeugnis "3.1". Alle Messmittel sind auf nationale Normale rückverfolgbar. Das Kistler Qualitätsmanagement System ist nach ISO 9001 zertifiziert. Dieses Dokument ist ohne Unterschrift gültig.
The equipment mentioned above and identified by Serial Number complies with the agreement of the order and meets the manufacturing tolerances specified in the data sheets. This document fulfils the requirements of EN 10204 Inspection Certificate "3.1". All measuring devices are traceable to national standards. The Kistler Quality Management System is certified per ISO 9001. This document is valid without a signature.
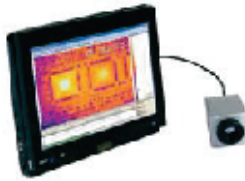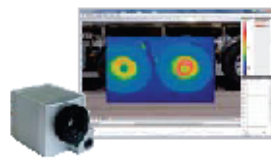
Appendix 5:

Technical Specifications of the Optris PI160 Thermal Imager

Technical data of Optris infrared cameras

Basis model	PI 160	PI 200 / PI 230
Type	IR	BI-SPECTRAL
Scope of supply	USB camera incl. 1 lens, USB cable (1 m), table tripod, PIF cable incl. terminal block (1 m), software package optris PI Connect, aluminum case	USB camera with 1 lens and BI-SPECTRAL technology, USB cable (1 m), table tripod, focussing tool, PIF cable incl. terminal block (1 m), software package optris PI Connect, aluminum case
Detector	FPA, uncooled (25 µm x 25 µm)	FPA, uncooled (25 µm x 25 µm)
Optical resolution	160 x 120 pixel	160 x 120 pixel
Spectral range	7.5 - 13 µm	7.5 - 13 µm
Temperature ranges	-20°C...100°C, 0°C...250°C, 150°C...900°C, additional range: 200°C...1500°C (option)*	-20°C...100°C, 0°C...250°C, 150°C...900°C, additional range: 200°C...1500°C (option)*
Frame rate	120 Hz	128 Hz***
Optics (FOV)	23° x 17° FOV / f = 10 mm or 6° x 5° FOV / f = 35.5 mm or 41° x 31° FOV / f = 5.7 mm or 72° x 52° FOV / f = 3.3 mm	23° x 17° FOV** / f = 10 mm or 6° x 5° FOV / f = 35.5 mm or 41° x 31° FOV** / f = 5.7 mm or 72° x 52° FOV / f = 3.3 mm
Thermal sensitivity (NETD)	0.08 K with 23° x 17° FOV / F = 0,8 0.3 K with 6° x 5° FOV / F = 1,6 0.1 K with 41° x 31° FOV and 72° x 52° FOV / F = 1	0.08 K with 23° x 17° FOV / F = 0,8 0.3 K with 6° x 5° FOV / F = 1,6 0.1 K with 41° x 31° FOV and 72° x 52° FOV / F = 1
Option for visual camera (only for BI-SPECTRAL camera)	-	Optical resolution: 640 x 480 Pixel, Frame rate: 32 Hz*** Optics (FOV): 54° x 40° (PI 200), 30° x 23° (PI 230)
Accuracy	±2°C or ±2%	±2°C or ±2%
PC interface	USB 2.0	USB 2.0
Process interface (PIF)		
Standard PIF	0-10V input, digital input (max. 24V), 0-10V output	0-10V input, digital input (max. 24V), 0-10V output
Industrial PIF	2x 0-10V inputs, digital input (max. 24V), 3x 0-10V outputs, 3x relay (0-30V/ 400mA), fail safe relay	2x 0-10V inputs, digital input (max. 24V), 3x 0-10V outputs, 3x relay (0-30V/ 400mA), fail safe relay
Ambient temperature (T$_{Amb}$)	0°C...50°C	0°C...50°C
Storage temperature	-40°C...70°C	-40°C...70°C
Relative humidity	20 - 80%, non condensing	20 - 80%, non condensing
Enclosure (size / rating)	45 mm x 45 mm x 62 mm / IP 67 (NEMA 4)	45 mm x 45 mm x 62 mm / IP 67 (NEMA 4)
Weight	195 g, incl. lens	215 g, incl. lens
Shock / vibration	25G, IEC 68-2-29 / 2G, IEC 68-2-6	25G, IEC 68-2-29 / 2G, IEC 68-2-6
Tripod mount	1/4-20 UNC	1/4-20 UNC
Power supply	USB powered	USB powered

The optris PI 160 / PI 200 as Thermal Analysis Package

- Infrared camera optris PI 160 or PI 200
- 3 lenses (23°, 6°, 41°) incl. calibration certificate
- USB cable (1 m and 10 m)
- Table tripod (20 - 63 cm)
- PIF cable with terminal block (1 m)
- Software package optris PI Connect
- Aluminum case
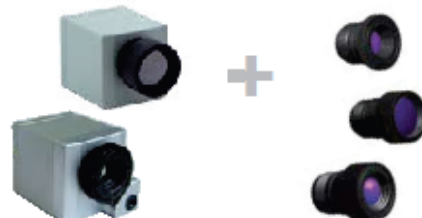
* The additional measurement range is not available for 72° HFOV optics
** For ideal combination of IR and VIS image, a 41° HFOV lens is recommended (optris PI 200). For the PI 230, a 23° HFOV lens is recommended.
*** The following options can be set: Option 1 (IR with 96 Hz at 160 x 120 px; VIS with 32 Hz at 640 x 480 px)
                                        Option 2 (IR with 128 Hz at 160 x 120 px; VIS with 32 Hz at 596 x 447 px)

6

Appendix 6:

Technical Specifications of Microscope Axio Scope.A1

2.3 Technical Data

Dimensions (width x depth x height)
Microscope stand Axio Scope.A1 (no DL illumination) .... approx. 240 mm x 340 mm x 365 mm
Stand column Vario 380 mm .... approx. 460 mm x 390 mm x 465 mm
Stand column Vario 560 mm .... approx. 460 mm x 390 mm x 645 mm

Mass
Microscope stand Axio Scope.A1 (depending on variant and accessories) .... approx. 14 to 20 kg
Stand column Vario .... approx. 19 kg

Environmental conditions
Transport (in packaging):
    Permissible environment temperature .... -40 to +70 °C
Storage:
    Permissible environment temperature .... +10 to +40 °C
    Permissible humidity (no condensation) .... max. 75 % at 35 °C
Operation:
    Permissible environment temperature .... -10 to +40 °C
    Permissible relative humidity (no condensation) .... max. 75 % at 35 °C
    Height of application .... max. 2000 m
    Air pressure .... 800 hPa to 1060 hPa
    Pollution level 2

Operational data
Range of application .... indoor
Protection class I
Protection type .... IP 20
Electrical security .... according to DIN EN 61010-1 (IEC 61010-1)
.... In consideration of CSA and UL regulations
Overvoltage category II
Radio interference suppression .... according to EN 55011 class B
Immunity .... according to DIN EN 61326
Voltage range .... 100 to 240 V ±10 %, no voltage adjustment is necessary
Power frequency .... 50/60 Hz
Power input Axio Scope.A1 with internal power supply unit .... 110 VA
Power input Axio Scope.A1 with auxiliary power supply unit 12 V DC 100 W .... 220 VA

Transformer mbq52ac-z for HBO 50
Range of application .... indoor
Protection class I
Protection type .... IP 20
Switchable voltage range .... 100, 110, 120, 127 VAC and 230, 240 VAC
Switchable power frequency .... 50 and 60 Hz
Power input with HBO 50 in operation .... max. 350 VA

Transformer HBO 100 W

Range of application ....indoor
Protection class I
Protection type .... IP 20
Voltage .... 100 VAC ... 240 VAC
Power frequency ....50 ... 60 Hz
Power input with HBO 103 in operation .... 155 VA

Fuses according to IEC 127

Microscope stand Axio Scope.A1 for LED illumination in transmitted light .... 2x T 3.15 A/H, 5x20 mm
Microscope stand Axio Scope.A1 for HAL 50 illumination in transmitted light ...... 2x T 3.15 A/H, 5x20 mm
Transformer mbq52ac-z for HBO 50...100 V, 127 V: 2x T 4 A
....220 V - 240 V: 2x T 2.5 A
Transformer HBO 100 W ....T 2.0 A/H, 5x20 mm
Auxiliary power supply unit 12 V DC 100 W .... 2x T 5.0 A/H, 5x20 mm

Light sources

LED illumination DL
    Power input ....7 W
Halogen lamp .... 12 V / 50 W
    Light source control ....infinitely variable from approx. 3 to 12 V
Halogen lamp .... 12 V / 100 W
    Light source control ....infinitely variable from approx. 3 to 12 V
Mercury vapor short arc lamp ....HBO 50
    Power input for HBO 50...50 W
Mercury vapor short arc lamp ....HBO 103 W/2
    Power input for HBO 103 W/2 ....100 W
Illumination system Colibri
    Power input..70 W

Axio Scope.A1:

Stand with manual stage focusing
    Rough drive .... approx. 4 mm / rotation
    Fine drive .... approx. 0.4 mm / rotation; approx. 4 µm mark distance
    Lift range .... approx. 25 mm
    Vertical stop...mechanically variable
Condenser 0.9/1.25 H with optional
    Modulator disk ....for bright field, dark field and
    ....phase-contrast 1, 2, 3 or PlasDIC

Manual objective change ....via nosepiece, 6-fold H, M27
Manual reflector module change ....via reflector slider 2-fold,
....reflector turret 4-fold or 6-fold

Appendix 7:

Part of LabView Programming

(1) Cutting force data acquisition associated with wavelet transform analysis and its standard deviation

(a) Spatial aspect analysis: Radial force analysis

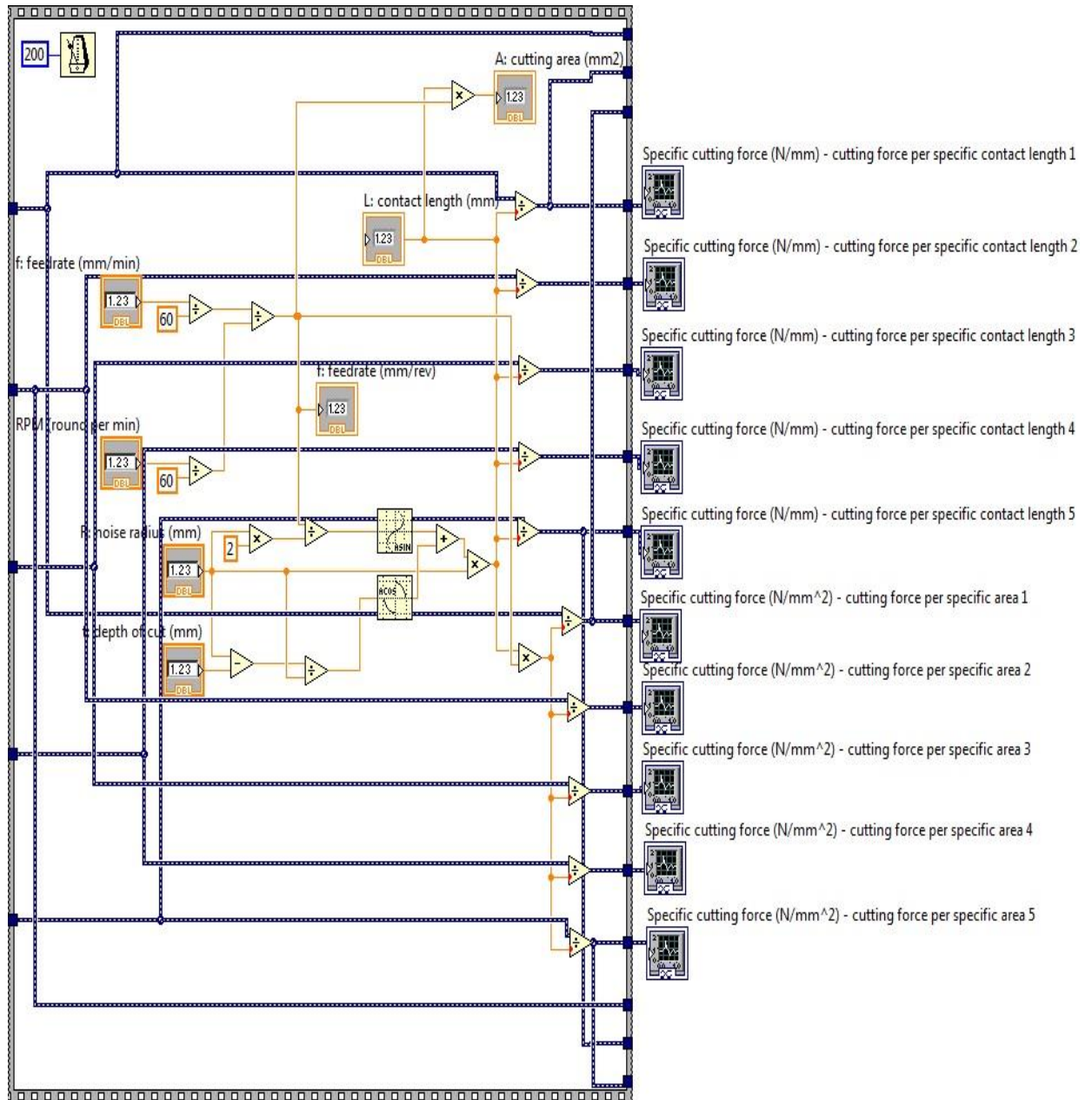(b) Spatial aspect analysis: Cutting force analysis

(1.a) Radial force analysis: the special aspect analysis using wavelet transform technique associated with standard deviation

(2) Cutting force modelling: amplitude and spatial aspects

(a) Specific cutting force calculation and analysis
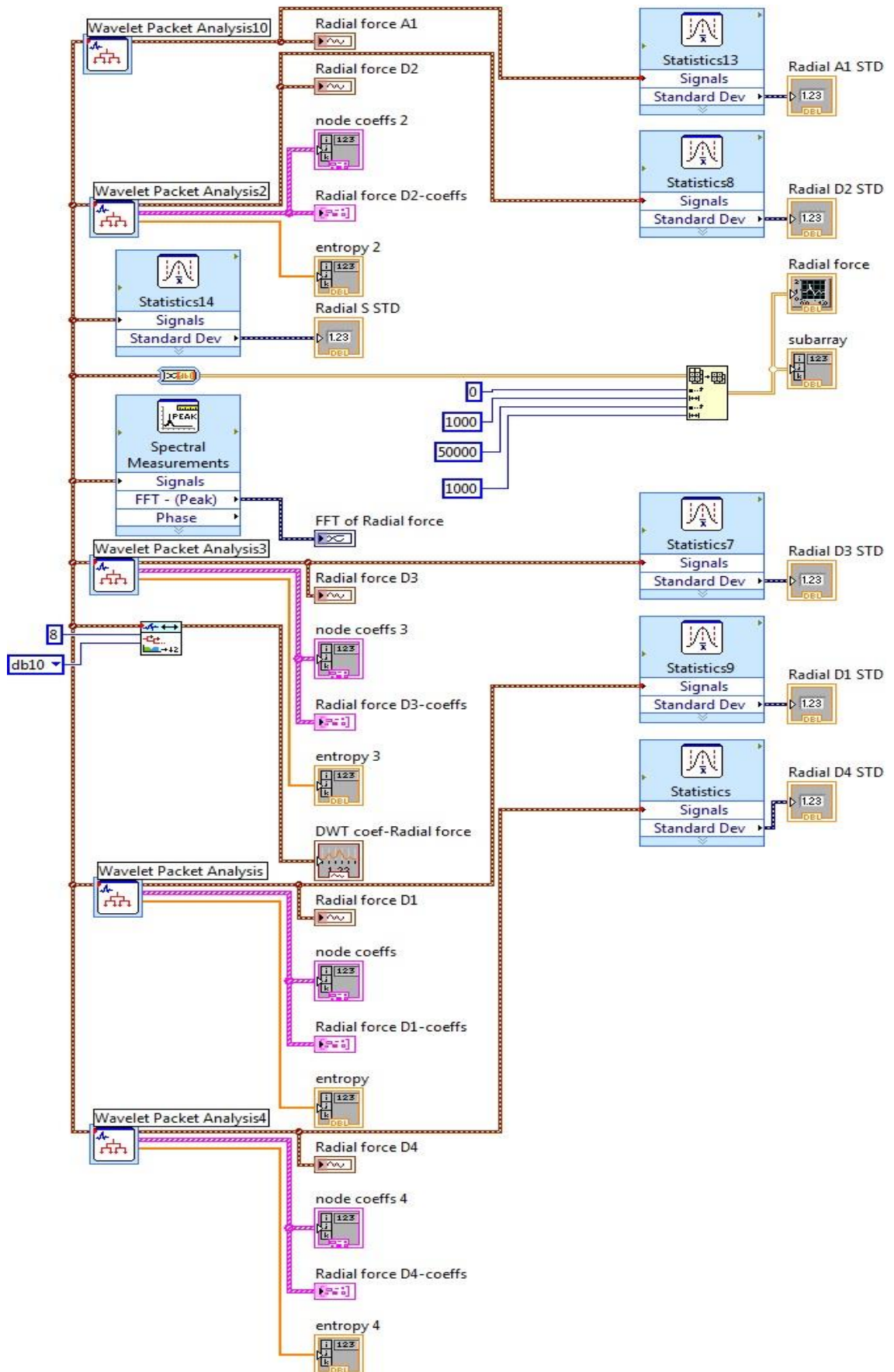
(b) Detail coefficients and reconstructed signals analysis
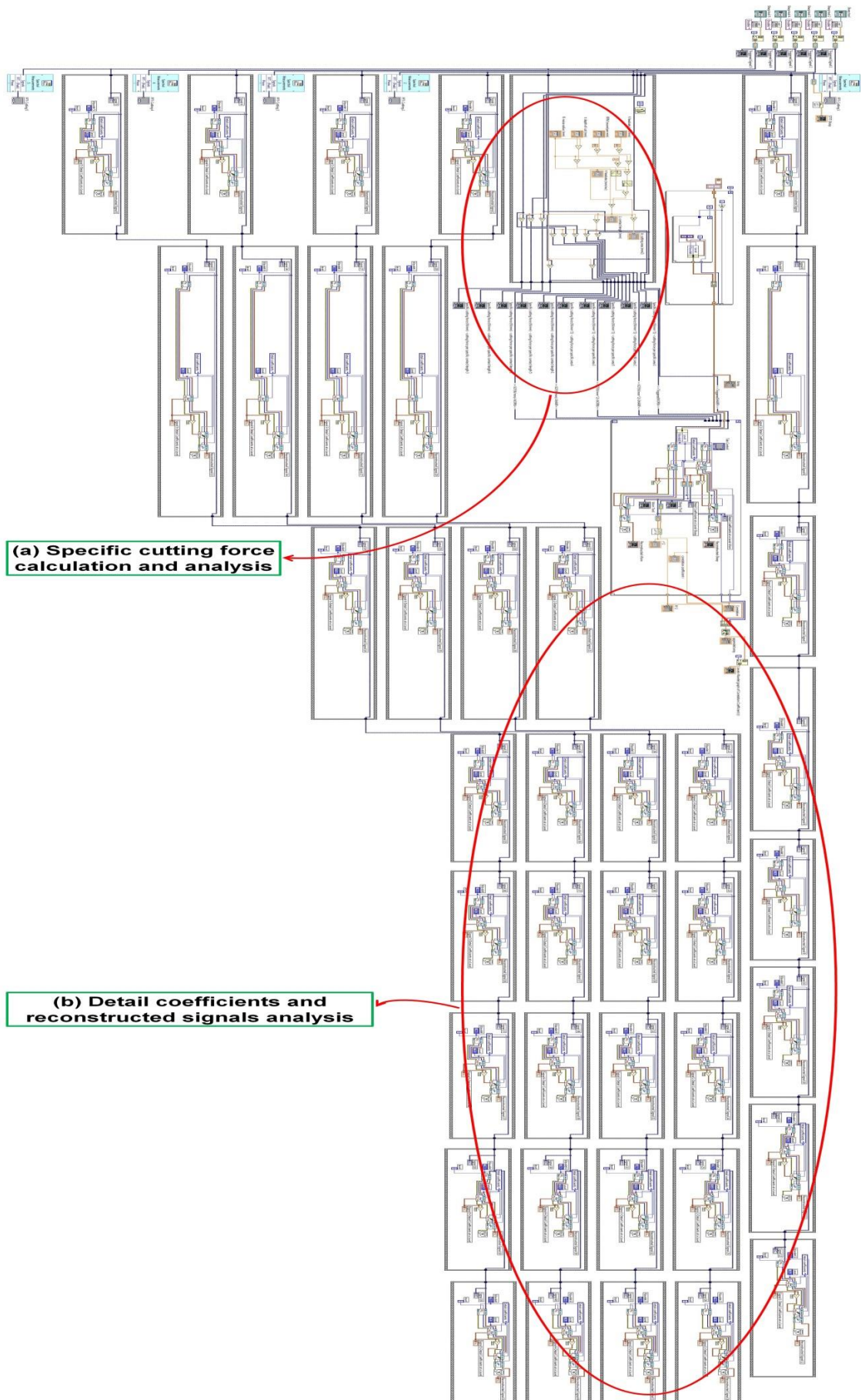
(2.a) Specific cutting force calculation and analysis: amplitude aspect analysis

)